

Department of Electrical, Electronic, and Information Engineering "Guglielmo Marconi"- DEI

SECOND CYCLE DEGREE IN BIOMEDICAL ENGINEERING

Curriculum: Biomedical Engineering for Neuroscience

Class: LM-21

THESIS TITLE:

Modeling Neuroplasticity in Cortical and Hippocampal Microcircuits: Toward Improved Understanding of Epilepsy

Graduation Thesis in

Neural Systems

Supervisor: Candidate:

Prof. Mauro Ursino Fateme Karimi

Co-Supervisor: Co-Supervisor:

Dr. Mariam Alharrach Linda Iris Joseph Tomy

Academic Year 2024–2025 Session 20/11/2025

Contents

A	ckno	wledge	ements	iv
List of Abbreviations				
A	bstra	ıct		vii
In	trod	uction		viii
1	Sta	te of t	he Art and Theoretical Principles	1
	1.1	Introd	luction	. 1
	1.2	Epilep	psy	. 1
		1.2.1	Definition of Epilepsy	. 1
			1.2.1.1 Seizures: definition and types	. 2
			1.2.1.2 Types of Epilepsy	. 3
		1.2.2	Electroencephalography in Epilepsy Evaluation	. 3
			1.2.2.1 EEG Recording Modalities	. 4
		1.2.3	Drug-Resistant Epilepsy and Treatment	. 5
			1.2.3.1 Resective epilepsy surgery	. 6
			1.2.3.2 Neuromodulation	. 6
		1.2.4	The GALVANI Project Approach to tDCS and Epilepsy	. 8
	1.3	Neuro	pplasticity	. 8
		1.3.1	Neuronal and Synaptic Structure	. 8
			1.3.1.1 Neurons	. 8
			1.3.1.2 Synapses	. 9
			1.3.1.3 Synaptic Transmission	. 10
		1.3.2	Neuroplasticity: Definition and Principles	. 11
			1.3.2.1 Long-Term Potentiation and Depression	. 12
			1.3.2.2 Spike timing dependent plasticity (STDP)	. 13
	1.4	Comp	outational Neuroscience and Modeling	. 13
		1.4.1	Hodgkin-Huxley Formalism	. 13
		1.4.2	Neural Networks Modeling	. 14
			1.4.2.1 Microcircuit Model of the Hippocampus	. 14
			1.4.2.2 Microcircuit model of the Neocortex: NeoCoMM Model	. 17
		1.4.3	Computational Modeling of Neural Plasticity	. 20
			1.4.3.1 Shouval Model of Calcium-Dependent Plasticity	
			1.4.3.2 Brunel Model of Spike-Timing Dependent Plasticity (STD	
	1 5	Proble	em Statement and Objectives	2/

1.5.2 Specific Thesis Objectives 2 Modeling neuroplasticity in multicompartment neuron models 2.1 Introduction 2.2 PC Model 2.2.1 Calcium Dynamics 2.2.2 Synaptic Dynamics and NMDA Current 2.2.3 Numerical Integration and Extensions 2.3 Implemented Neuroplasticity Models: Modifications to the PC Model 2.3.1 Main modification to the PC models 2.3.1.1 Modified Ca Dynamics 2.3.1.2 Modified NMDA Current 2.3.1.3 Synaptic Efficacy Variable (W) 2.3.2 Shouval Neuroplasticity Model 2.3.3 Hybrid Neuroplasticity Model 2.3.4 Epileptogenic Plasticity Parameterization 2.4 Testing Framework 2.4.1 Network of Three Cells 2.4.2 Results 2.4.2.1 Simulating LTD and LTP: Shouval Model 2.4.3.2 STDP Testing in Two-Cell Networks 2.4.3.1 Shouval Model 2.4.3.2 Hybrid Model 2.4.3.2 Hybrid Model			1.5.1	Research Gap and Motivation				
2.1 Introduction 2.2 PC Model 2.2.1 Calcium Dynamics 2.2.2 Synaptic Dynamics and NMDA Current 2.2.3 Numerical Integration and Extensions 2.3 Implemented Neuroplasticity Models: Modifications to the PC Model 2.3.1 Main modification to the PC models 2.3.1.1 Modified Ca Dynamics 2.3.1.2 Modified NMDA Current 2.3.1.3 Synaptic Efficacy Variable (W) 2.3.2 Shouval Neuroplasticity Model 2.3.4 Epileptogenic Plasticity Model 2.3.4 Epileptogenic Plasticity Parameterization 2.4 Testing Framework 2.4.1 Network of Three Cells 2.4.2 Results 2.4.2.1 Simulating LTD and LTP: Shouval Model 2.4.3.2 STDP Testing in Two-Cell Networks 2.4.3.1 Shouval Model 2.4.3.2 Hybrid Model			1.5.2	Specific Thesis Objectives				
2.1 Introduction 2.2 PC Model 2.2.1 Calcium Dynamics 2.2.2 Synaptic Dynamics and NMDA Current 2.2.3 Numerical Integration and Extensions 2.3 Implemented Neuroplasticity Models: Modifications to the PC Model 2.3.1 Main modification to the PC models 2.3.1.1 Modified Ca Dynamics 2.3.1.2 Modified NMDA Current 2.3.1.3 Synaptic Efficacy Variable (W) 2.3.2 Shouval Neuroplasticity Model 2.3.4 Epileptogenic Plasticity Model 2.3.4 Epileptogenic Plasticity Parameterization 2.4 Testing Framework 2.4.1 Network of Three Cells 2.4.2 Results 2.4.2.1 Simulating LTD and LTP: Shouval Model 2.4.3.2 STDP Testing in Two-Cell Networks 2.4.3.1 Shouval Model 2.4.3.2 Hybrid Model	2	Modeling neuroplasticity in multicompartment neuron models						
2.2.1 Calcium Dynamics 2.2.2 Synaptic Dynamics and NMDA Current 2.2.3 Numerical Integration and Extensions 2.3 Implemented Neuroplasticity Models: Modifications to the PC Model 2.3.1 Main modification to the PC models 2.3.1.1 Modified Ca Dynamics 2.3.1.2 Modified NMDA Current 2.3.1.3 Synaptic Efficacy Variable (W) 2.3.2 Shouval Neuroplasticity Model 2.3.4 Epileptogenic Plasticity Model 2.3.4 Epileptogenic Plasticity Parameterization 2.4 Testing Framework 2.4.1 Network of Three Cells 2.4.2 Results 2.4.2.1 Simulating LTD and LTP: Shouval Model 2.4.2.2 Simulating LTP and LTD: Hybrid Model 2.4.3 STDP Testing in Two-Cell Networks 2.4.3.1 Shouval Model 2.4.3.2 Hybrid Model			_					
2.2.2 Synaptic Dynamics and NMDA Current 2.2.3 Numerical Integration and Extensions 2.3 Implemented Neuroplasticity Models: Modifications to the PC Model 2.3.1 Main modification to the PC models 2.3.1.1 Modified Ca Dynamics 2.3.1.2 Modified NMDA Current 2.3.1.3 Synaptic Efficacy Variable (W) 2.3.2 Shouval Neuroplasticity Model 2.3.4 Epileptogenic Plasticity Parameterization 2.4 Testing Framework 2.4.1 Network of Three Cells 2.4.2 Results 2.4.2.1 Simulating LTD and LTP: Shouval Model 2.4.2.2 Simulating LTP and LTD: Hybrid Model 2.4.3 STDP Testing in Two-Cell Networks 2.4.3.1 Shouval Model 2.4.3.2 Hybrid Model		2.2	РС М	[odel				
2.2.3 Numerical Integration and Extensions 2.3 Implemented Neuroplasticity Models: Modifications to the PC Model 2.3.1 Main modification to the PC models 2.3.1.1 Modified Ca Dynamics 2.3.1.2 Modified NMDA Current 2.3.1.3 Synaptic Efficacy Variable (W) 2.3.2 Shouval Neuroplasticity Model 2.3.3 Hybrid Neuroplasticity Model 2.3.4 Epileptogenic Plasticity Parameterization 2.4 Testing Framework 2.4.1 Network of Three Cells 2.4.2 Results 2.4.2.1 Simulating LTD and LTP: Shouval Model 2.4.2.2 Simulating LTD and LTD: Hybrid Model 2.4.3 STDP Testing in Two-Cell Networks 2.4.3.1 Shouval Model 2.4.3.2 Hybrid Model			2.2.1	Calcium Dynamics				
2.3 Implemented Neuroplasticity Models: Modifications to the PC Model 2.3.1 Main modification to the PC models 2.3.1.1 Modified Ca Dynamics 2.3.1.2 Modified NMDA Current 2.3.1.3 Synaptic Efficacy Variable (W) 2.3.2 Shouval Neuroplasticity Model 2.3.3 Hybrid Neuroplasticity Model 2.3.4 Epileptogenic Plasticity Parameterization 2.4 Testing Framework 2.4.1 Network of Three Cells 2.4.2 Results 2.4.2 Results 2.4.2.2 Simulating LTD and LTP: Shouval Model 2.4.2.3 STDP Testing in Two-Cell Networks 2.4.3.1 Shouval Model 2.4.3.2 Hybrid Model			2.2.2	Synaptic Dynamics and NMDA Current				
2.3.1 Main modification to the PC models 2.3.1.1 Modified Ca Dynamics 2.3.1.2 Modified NMDA Current 2.3.1.3 Synaptic Efficacy Variable (W) 2.3.2 Shouval Neuroplasticity Model 2.3.3 Hybrid Neuroplasticity Model 2.3.4 Epileptogenic Plasticity Parameterization 2.4 Testing Framework 2.4.1 Network of Three Cells 2.4.2 Results 2.4.2.1 Simulating LTD and LTP: Shouval Model 2.4.2.2 Simulating LTP and LTD: Hybrid Model 2.4.3.1 Shouval Model 2.4.3.1 Shouval Model 2.4.3.2 Hybrid Model			2.2.3	Numerical Integration and Extensions				
2.3.1.1 Modified Ca Dynamics 2.3.1.2 Modified NMDA Current 2.3.1.3 Synaptic Efficacy Variable (W) 2.3.2 Shouval Neuroplasticity Model 2.3.3 Hybrid Neuroplasticity Model 2.3.4 Epileptogenic Plasticity Parameterization 2.4 Testing Framework 2.4.1 Network of Three Cells 2.4.2 Results 2.4.2.1 Simulating LTD and LTP: Shouval Model 2.4.2.2 Simulating LTD and LTD: Hybrid Model 2.4.3.1 Shouval Model 2.4.3.1 Shouval Model 2.4.3.2 Hybrid Model		mented Neuroplasticity Models: Modifications to the PC Model						
2.3.1.2 Modified NMDA Current 2.3.1.3 Synaptic Efficacy Variable (W) 2.3.2 Shouval Neuroplasticity Model 2.3.3 Hybrid Neuroplasticity Model 2.3.4 Epileptogenic Plasticity Parameterization 2.4 Testing Framework 2.4.1 Network of Three Cells 2.4.2 Results 2.4.2.1 Simulating LTD and LTP: Shouval Model 2.4.2.2 Simulating LTD and LTD: Hybrid Model 2.4.3.1 Shouval Model 2.4.3.1 Shouval Model 2.4.3.2 Hybrid Model			2.3.1	Main modification to the PC models				
2.3.1.3 Synaptic Efficacy Variable (W) 2.3.2 Shouval Neuroplasticity Model 2.3.3 Hybrid Neuroplasticity Model 2.3.4 Epileptogenic Plasticity Parameterization 2.4 Testing Framework 2.4.1 Network of Three Cells 2.4.2 Results 2.4.2.1 Simulating LTD and LTP: Shouval Model 2.4.2.2 Simulating LTP and LTD: Hybrid Model 2.4.3.1 Shouval Model 2.4.3.1 Shouval Model 2.4.3.2 Hybrid Model				2.3.1.1 Modified Ca Dynamics				
2.3.2 Shouval Neuroplasticity Model 2.3.3 Hybrid Neuroplasticity Model 2.3.4 Epileptogenic Plasticity Parameterization 2.4 Testing Framework 2.4.1 Network of Three Cells 2.4.2 Results 2.4.2.1 Simulating LTD and LTP: Shouval Model 2.4.2.2 Simulating LTP and LTD: Hybrid Model 2.4.3.1 Shouval Model 2.4.3.1 Shouval Model 2.4.3.2 Hybrid Model				2.3.1.2 Modified NMDA Current				
2.3.3 Hybrid Neuroplasticity Model 2.3.4 Epileptogenic Plasticity Parameterization 2.4 Testing Framework 2.4.1 Network of Three Cells 2.4.2 Results 2.4.2.1 Simulating LTD and LTP: Shouval Model 2.4.2.2 Simulating LTP and LTD: Hybrid Model 2.4.3.1 Shouval Model 2.4.3.1 Shouval Model 2.4.3.2 Hybrid Model				2.3.1.3 Synaptic Efficacy Variable (W)				
2.3.4 Epileptogenic Plasticity Parameterization			2.3.2	Shouval Neuroplasticity Model				
2.4 Testing Framework 2.4.1 Network of Three Cells 2.4.2 Results 2.4.2.1 Simulating LTD and LTP: Shouval Model 2.4.2.2 Simulating LTP and LTD: Hybrid Model 2.4.3 STDP Testing in Two-Cell Networks 2.4.3.1 Shouval Model 2.4.3.2 Hybrid Model			2.3.3	Hybrid Neuroplasticity Model				
2.4.1 Network of Three Cells			2.3.4	Epileptogenic Plasticity Parameterization				
2.4.2 Results		2.4	Testin	ng Framework				
2.4.2.1 Simulating LTD and LTP: Shouval Model			2.4.1	Network of Three Cells				
2.4.2.2 Simulating LTP and LTD: Hybrid Model			2.4.2	Results				
2.4.3 STDP Testing in Two-Cell Networks								
2.4.3.1 Shouval Model				2.4.2.2 Simulating LTP and LTD: Hybrid Model				
2.4.3.2 Hybrid Model			2.4.3	STDP Testing in Two-Cell Networks				
·				2.4.3.1 Shouval Model				
2.5 Discussion				2.4.3.2 Hybrid Model				
		2.5	Discus	ssion				
		$\mathbf{E}\mathbf{p}\mathbf{i}$	${f leptifo}$	rm Dynamics in the Hippocampal Network				
Epileptiform Dynamics in the Hippocampal Network		3.1	Introd	luction				
		3.2	Netwo	ork Construction and Parameter Modulation Toward Epileptic States				
3.1 Introduction			3.2.1	Methods to Induce Epileptic Activity: Establishing Excitation/Inhi-				
3.1 Introduction				bition Imbalance				
 3.1 Introduction				3.2.1.1 Modification of Cellular and Synaptic Parameters				
 3.1 Introduction				3.2.1.2 External Stimulation Protocol				
3.1 Introduction				3.2.1.3 Inclusion of Neuroplasticity Parameters				
3.1 Introduction			3.2.2	Simulation Protocols				
3.1 Introduction		3.3	Result	ts				
3.1 Introduction			3.3.1	Network Firing Patterns				
3.1 Introduction			3.3.2	Analysis of Cellular and Population Activity				

		v	51
		v	53
			56
	3.4	Discussion	59
4	Mo	deling of Neuroplasticity in the Neocortical Network	61
	4.1	Introduction	61
	4.2	Network Model and Epileptic State Induction	61
		4.2.1 Network Model	61
		4.2.2 Epileptic State Induction	61
		4.2.2.1 Inclusion of Hybrid plasticity model's Parameters	62
	4.3	Analysis of Network Dynamics and Plasticity Influence	63
		4.3.1 Cellular and Population Activity Analysis:	63
		4.3.1.1 Synaptic efficacy evolution	63
		4.3.1.2 Cellular Activity Analysis:	64
		4.3.1.3 Local Field Potential Analysis	67
	4.4	Modeling of tES in the NeoCoMM Framework	68
		4.4.1 Computation of Single-Cell Polarization Lengths	68
		4.4.2 Implementation of tES in NeoCoMM	70
		4.4.3 Entrainment Analysis	70
		4.4.4 Integration with the Plasticity-Enabled NeoCoMM	71
		4.4.5 Results	71
		4.4.5.1 tACS Impact on Physiological Cortical Oscillations	71
		4.4.5.2 tDCS Impact on Epileptic Events	72
	4.5	Discussion	75
5	Dis	cussion and Conclusion	7 6
	5.1	Discussion	76
	5.2	Implications and Future Work	79
	5.3	Conclusion	80
	5.4	Funding Acknowledgement	80
Sι	ıpple	ementary Materials	81

Acknowledgements

I would like to thank Prof. Fabrice Wendling for the opportunity to conduct this Master's thesis as part of the GALVANI project at LTSI, University of Rennes. I am especially grateful to Dr. Mariam Al Harrach and Linda Iris Joseph Tomy for their invaluable guidance and support during my internship. Their advice and help, both scientific and personal, were essential to the success of this work.

I am very grateful to Prof. Mauro Ursino for introducing me to the field of computational neuroscience and for his valuable supervision and insightful advice throughout my research journey. His mentorship has greatly shaped my understanding and appreciation of this field.

I warmly thank Dr. Maxime Yochum for his help with the technical and coding aspects of my project, and for his constant availability and patience. My appreciation extends to all members of the Cynetiks team for their kindness, collaboration, and willingness to help, which created a truly welcoming and supportive environment.

A heartfelt thank you to my friends, whose encouragement and companionship have been a great source of strength throughout my studies. Above all, I am deeply grateful to my family for their endless love, patience, and support from afar; their faith in me has been the foundation of all my achievements.

Finally, I would like to thank the University of Bologna and Italy for giving me the opportunity to pursue my Master's degree in Biomedical Engineering and for an enriching academic and cultural experience.

List of Abbreviations

Acronym	Full Term
AIS	Axon Initial Segment
AMPA / AMPAR	α -Amino-3-hydroxy-5-methyl-4-isoxazole propionic acid / Receptor
AP	Action Potential
BAS	Basket Cell Interneuron
BIS	Bistratified Cell Interneuron
BPC	Bipolar Pyramidal Cell
BC	Basket Cell (Interneuron subtype)
BiC	Bipolar Cell (Interneuron subtype)
CA1	Cornu Ammonis Area 1
CA3	Cornu Ammonis Area 3
ChC	Chandelier Cell
CNS	Central Nervous System
Cm	Membrane Capacitance
DBS	Deep Brain Stimulation
DC	Distant Cortex
DRE	Drug-Resistant Epilepsy
E/I	Excitatory/Inhibitory
EEG	Electroencephalography
EGABA	GABA Reversal Potential
ERC	European Research Council
EPSP	Excitatory Postsynaptic Potential
FR	Firing Rate
GABA / GABAR	Gamma-Aminobutyric Acid / GABA Receptor
GLUT	Glutamate
GUI	Graphical User Interface
H-H	Hodgkin-Huxley
Hz	Hertz
IAHP	After-Hyperpolarization Potassium Current
Ih	Hyperpolarization-Activated Cation Current
ILAE	International League Against Epilepsy
${ m Im}$	Muscarinic Potassium Current
IN	Interneuron
INa	Sodium Current
IPSP	Inhibitory Postsynaptic Potential
IPC	Inverted Pyramidal Cell
IES	Interictal Epileptiform Spike
IKA	Fast Inactivating Potassium Current
IKDR	Potassium Delayed Rectifier Current

Acronym	Full Term
ICaL / ICaT / ICaR	L-type / T-type / R-type Calcium Currents
LFP	Local Field Potential
LTD	Long-Term Depression
LTP	Long-Term Potentiation
LTSI	Laboratoire Traitement du Signal et de l'Image
mA	Milliampere
$\mathrm{mS/cm^2}$	Millisiemens per Square Centimeter
mV	Millivolt
NeoCoMM	Neocortical Computational Model
NGF	Neurogliaform Cell
NMDA / NMDAR	N-Methyl-D-Aspartate / NMDA Receptor
PC	Pyramidal Cell
PLV	Phase Locking Value
PSD	Power Spectral Density
PV+	Parvalbumin-Positive Interneuron
RNS	Responsive Neurostimulation
RLN+	Reelin-Positive Interneuron
SOM	Somatostatin Interneuron
SST+	Somatostatin-Positive Interneuron
SS	Spiny Stellate Cell
STDP	Spike-Timing-Dependent Plasticity
SW / DSW	Spike-and-Wave / Double Spike-and-Wave
tACS	Transcranial Alternating Current Stimulation
tCS	Transcranial Current Stimulation
tDCS	Transcranial Direct Current Stimulation
tES	Transcranial Electrical Stimulation
TPC / TTPC	Tufted Pyramidal Cell
UTPC	Untufted Pyramidal Cell
VNS	Vagus Nerve Stimulation
VIP+	Vasoactive Intestinal Peptide-Positive Interneuron
VDCC	Voltage-Dependent Calcium Channel
W	Synaptic Weight / Efficacy Variable
$\mu A/cm^2$	Microampere per Square Centimeter

Abstract

This study was conducted within the framework of the GALVANI project, which aims to develop computational and experimental tools to optimize non-invasive brain stimulation strategies for drug-resistant epilepsy (DRE). The work focused on integrating biologically realistic neuroplasticity mechanisms into existing detailed computational models of hippocampal and neocortical microcircuits to examine how synaptic plasticity contributes to epileptiform dynamics and influences the effects of transcranial electrical stimulation (tES). Two calcium-dependent plasticity models (Shouval and Brunel) were implemented and combined into a novel Hybrid model that merges the continuous calcium dependence of Shouval's model with the stabilizing bistability of Brunel's framework. Validation in small networks reproduced canonical long-term potentiation (LTP), long-term depression (LTD), and the triphasic spike-timing-dependent plasticity (STDP) profile, demonstrating how parameter shifts can induce an epileptogenic bias toward potentiation. These models were then applied to large-scale hippocampal CA1 and neocortical networks. To simulate epileptiform activity, single-cell and network parameters were systematically adjusted to induce a hyperexcitable state capable of generating interictal epileptiform spikes (IESs). In the hippocampal model, Shouval's plasticity model increased pyramidal firing rates (FRs) and high-frequency activities, leading to excessive excitation, whereas the Hybrid model produced a moderate FR increase and preserved IES morphology. In the neocortical model, hybrid plasticity similarly enhanced excitability but preserved rhythmic organization. Preliminary tES simulations revealed that cathodal tDCS stimulation produced mild potentiation, while anodal tDCS led to slight synaptic depression. These findings demonstrate that calcium-dependent plasticity critically shapes network excitability and may alter responses to tES. The implemented plasticity framework provides a mechanistic foundation for studying synaptic adaptation and tES modulation, supporting the GALVANI project's overarching goal of developing personalized neuromodulation strategies for epilepsy.

Introduction

Epilepsy is a chronic neurological disorder of the central nervous system (CNS) characterized by spontaneous recurrent seizures, often resulting from an imbalance between excitatory and inhibitory synaptic activity. This imbalance leads to hypersynchronous neuronal discharges that may begin focally and spread to involve broader networks [1]. Despite major advances in pharmacological treatments, about 30–40% of patients develop drug-resistant epilepsy (DRE), for whom standard therapies fail and surgical options are often limited [2]. In this context, non-invasive neuromodulation techniques, such as transcranial electrical stimulation (tES), have emerged as promising alternatives. tES applies low-intensity, controlled electrical currents (approximately 1 mA and < 2 mA) to the scalp to modulate cortical excitability and reduce seizure frequency [3]. While early studies support its safety and therapeutic potential, the mechanisms of action remain poorly understood, especially with respect to long-term effects and interindividual variability[4]. To address these challenges, the GALVANI project (ERC Synergy Galvani, 2020–2027) was initiated to develop computational models aimed at studying the effects of tES on epileptic brain activity. The project seeks to optimize stimulation parameters and personalize treatment protocols by understanding how low-level electric fields interact with individual brain anatomy and physiology. Led by Inserm-LTSI, the project employs biophysically detailed microcircuit models of the neocortex [5] and hippocampus [6] to study seizure dynamics and to inform precision neuromodulation strategies. A critical feature still missing in these microscale models is neuronal plasticity, the dynamic adaptation of synaptic strength based on neural activity. Plasticity plays a dual role in epilepsy: it can contribute to both the development of hyperexcitable networks and their potential recovery through neuromodulation[7]. Understanding how plasticity shapes network behavior is essential for predicting and optimizing long-term responses to interventions like tES. The objective of this thesis is to address this gap by modeling neuroplasticity and integrating plasticity mechanisms into existing single-neuron and network models. Specifically, this work focuses on implementing biologically realistic plasticity models (Shouval[8] and Brunel[9]) within detailed simulations of hippocampal and neocortical microcircuits. Through this integration, we aim to explore how plasticity alters epileptogenic dynamics and how it might modulate the efficacy of tES in suppressing seizure activity. Ultimately, this work contributes to the GALVANI project's goal of developing mechanistically grounded, patient-specific neuromodulation strategies for epilepsy. This thesis is divided in 5 chapters:

Chapter 1 - State of the Art and Theoretical Principles: Provides background on

epilepsy, including its classification, drug-resistant epilepsy (DRE), treatments such as non-invasive brain stimulation, as well as the core principles of neuroplasticity and its mechanisms (LTP, LTD, STDP). Moreover, foundational computational models, including Hodgkin-Huxley (H-H), hippocampus, and neocortex, used in this study are introduced, together with a detailed description of the two foundational calcium-dependent plasticity models (those proposed by Shouval and Brunel) that serve as the basis for the work developed in later chapters.

Chapter 2– Modeling Neuroplasticity in Multicompartment Neuron Models: focuses on the single-neuron implementation of the calcium-dependent plasticity mechanisms. It describes the adaptation of the Shouval[8] and the novel Hybrid plasticity models to the single pyramidal cell (PC) models. The chapter also presents the validation of these mechanisms in small networks, demonstrating their ability to reproduce classical plasticity phenomena such as LTP, LTD, and STDP.

Chapter 3 – Investigating the Impact of Calcium-Dependent Plasticity Models on Epileptiform Dynamics in the Hippocampal Network: extends these plasticity implementations to a large-scale hippocampal CA1 network. It details the parameter adjustments used to induce an epileptic state and analyzes the effects of the implemented plasticity models on network behavior, including PC firing rates and analysis of local field potentials (LFPs) under both baseline and plasticity conditions.

Chapter 4 – Modeling Neuroplasticity in the Neocortical Network (NeoCoMM): addresses the integration of the plasticity mechanisms into the neocortical computational model (NeoCoMM). It examines how plasticity shapes cortical network activity and describes the preliminary simulations of tES, including tDCS and tACS, to investigate how the presence of plasticity modulates the response of cortical circuits to external electric fields.

Chapters 5 – Discussion and Conclusion: Summarize key findings, discuss their limitations and significance, and propose directions for future research.

Chapter 1

State of the Art and Theoretical Principles

1.1 Introduction

This chapter provides the theoretical and scientific background relevant to the project, laying the foundation for the modeling work described in subsequent chapters. It begins with an overview of epilepsy, including its clinical classification, treatment challenges, and surgical options. The next section introduces the concept of neuroplasticity, focusing on synaptic mechanisms such as long-term potentiation (LTP) and depression (LTD) that are particularly relevant to the development and progression of epilepsy. The chapter then discusses computational approaches to modeling neural activity, including single-cell and network-level models as well as synaptic plasticity. Finally, we articulate the problem this thesis addresses and define the objectives pursued.

1.2 Epilepsy

1.2.1 Definition of Epilepsy

Epilepsy is a neurological disorder characterized by recurrent seizures and their significant cognitive, psychological, and social impact on patients. It is considered one of the most common brain conditions, affecting approximately 70 million people worldwide[10]. Epilepsy is characterised by a lasting predisposition to generate spontaneous epileptic seizures and has numerous neurobiological, cognitive, and psychosocial consequences [11]. The global prevalence rate is estimated at 7.60 cases per 1,000 individuals, with an annual cumulative incidence of 67.8 cases per 100,000 person-years, ranking it as the second most burdensome neurologic disorder worldwide. [12]

According to the International League Against Epilepsy (ILAE), epilepsy is defined by any of the following conditions:

• At least two unprovoked (or reflex) seizures occurring more than 24 hours apart.

- One unprovoked (or reflex) seizure and a probability of further seizures (at least 60%) occurring over the next 10 years, similar to the general recurrence risk after two unprovoked seizures.
- Diagnosis of an epilepsy syndrome[11].

Too often, people are categorised as simply having epilepsy whereas the diagnosis should be as specific and as precise as possible. Classification is made at three levels: **seizure type**, **epilepsy type**, and **syndrome** as shown in Figure 1.1. At each stage, cause and comorbidities should be identified as these might have important therapeutic implications. The causes are divided into six categories: genetic, structural, metabolic, infectious, immune, and unknown.[13]

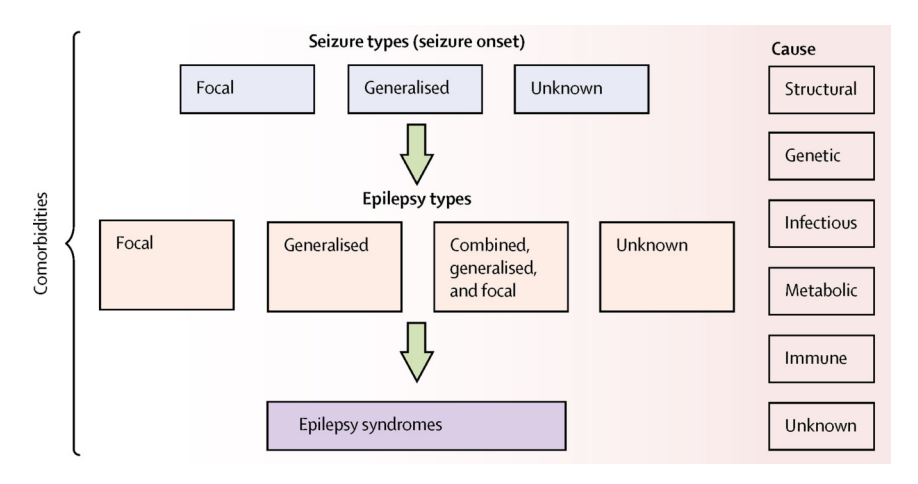


Figure 1.1: The International League Against Epilepsy framework for the classification of epilepsies [13].

1.2.1.1 Seizures: definition and types

An epileptic seizure is conceptually defined as "a transient occurrence of signs and/or symptoms due to abnormal excessive or synchronous neuronal activity in the brain" [14]. This sudden, intense burst of brain activity is termed a *paroxysmal discharge*.

Seizures are classified based on their anatomical onset, level of awareness, and motor or non-motor manifestations into three principal categories [13]. Focal seizures arise within one cerebral hemisphere, may involve cortical or subcortical networks, and are frequently described according to the lobe of origin (e.g., frontal or temporal) [15, 16]. They are further divided into focal aware seizures, in which consciousness is preserved and symptoms may include sensory phenomena or focal motor activity, and focal impaired awareness seizures, which disrupt consciousness and are often followed by postictal amnesia [17] (Figure 1.2).

Generalized seizures, in contrast, result from aberrant neuronal activity engaging both hemispheres at onset, leading to loss of consciousness and widespread motor manifestations;

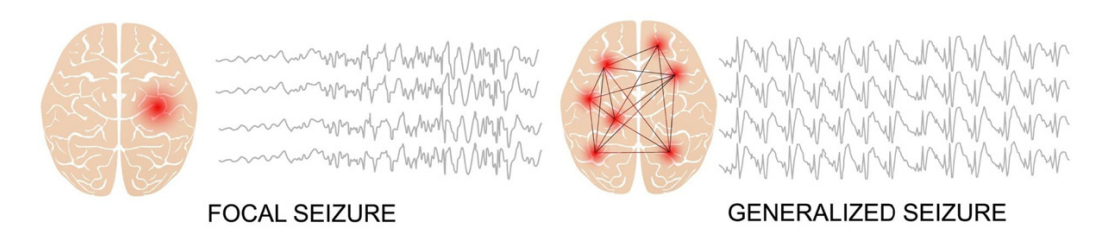


Figure 1.2: Different types of focal seizures

the ILAE categorizes these into motor (e.g., tonic-clonic, myoclonic, atonic) and non-motor (e.g., absence, atypical, eyelid myoclonia) subtypes [16, 18]. Seizures with insufficient information for classification are designated as of unknown onset [15].

1.2.1.2 Types of Epilepsy

After classification of seizure type, the clinician identifies the patient's epilepsy type which is broader in scope than is the seizure classification, and considers the possibility of having multiple seizure types, and incorporates information about the overall clinical picture, imaging, genetics, laboratory tests, prognoses, and comorbidities[19]. It can be classified into four categories depending on the seizure type: **focal**, **generalized**, **combined generalized** and **focal**, and **unknown**, as illustrated in Figure 1.1.

Generalized epilepsies consist of abnormal brain activity involving both hemispheres at the onset. People with generalized epilepsy may experience tonic-clonic seizures, absence seizures, myoclonic seizures, or atonic seizures.

Focal epilepsies involve seizures with a localized origin, which may then spread to other brain regions. People with focal epilepsy may have focal aware seizures or focal seizures with impaired awareness.

The **combined generalized and focal** category is used for individuals presenting with both seizure types.

The **unknown** category is applied when a patient is diagnosed with epilepsy but, due to insufficient data, the clinician is unable to classify the type of epilepsy [20, 21].

In this work, we will mainly focus on focal epilepsy.

1.2.2 Electroencephalography in Epilepsy Evaluation

Electroencephalography (EEG) is one of the most important and widely used ancillary tests in the diagnosis of epilepsy. EEG signals are generated by cortical neuronal postsynaptic potentials, providing real-time assessment of cerebral physiological function. Clinicians rely heavily on EEG patterns to identify, classify, quantify, and localize seizures [22]. For example, a focal interictal spike suggests focal epilepsy (such as temporal lobe epilepsy),

whereas a generalized spike-wave complex is more consistent with generalized epilepsy syndromes (such as idiopathic generalized epilepsy) [23].

EEG abnormalities associated with epilepsy include focal spikes, generalized spikes, spike-wave complexes, and seizures with focal onset, as illustrated in Figure 1.3.[22]

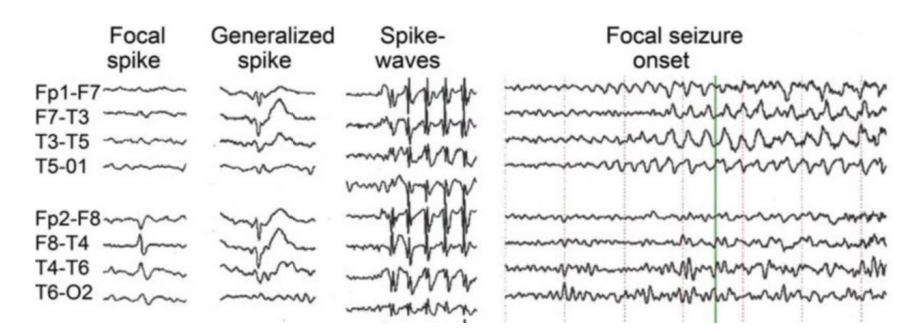


Figure 1.3: Common epileptiform EEG patterns: focal spikes, generalized spikes, spike-wave complexes, and seizures with focal onset [11].

Epileptic EEG signals can be classified into four main temporal categories: **preictal**, **ictal (seizure)**, **postictal**, and **interictal**. The preictal phase corresponds to the period before seizure onset (lasting approximately 50 minutes to one hour). The ictal phase marks the occurrence of the seizure itself. The postictal phase immediately follows the seizure, lasting around 5 to 30 minutes [24], and the interictal phase corresponds to the time between seizures (Figure 1.4) [25].

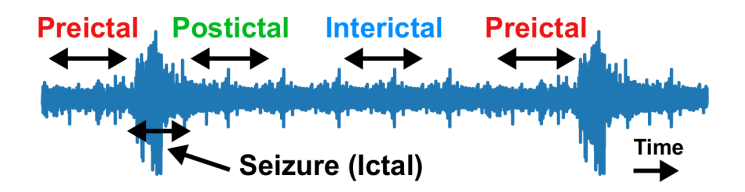


Figure 1.4: Various phases of EEG activity in epileptic patients: preictal, ictal (seizure), postictal, and interictal stages[25].

Interictal epileptiform discharges are sharply contoured waveforms that stand out from background activity, with spikes and sharp waves being the most common forms[26]. In both experimental and human focal epilepsies, these discharges appear as high-amplitude (> 50 μ V) fast EEG transients, called interictal spikes (ISs), usually followed by a slow wave lasting several hundred milliseconds [27].

1.2.2.1 EEG Recording Modalities

EEG can be recorded using two main modalities:

Scalp EEG (sEEG) Scalp EEG is noninvasive and uses electrodes placed on the scalp (Figure 1.5a). It is relatively easy to perform, covers a larger cortical surface, and is suitable for routine evaluations. However, sEEG has limitations such as lower spatial resolution, susceptibility to motion artifacts, and limited utility for long-term monitoring. [25].

Intracranial EEG (iEEG) Intracranial EEG uses invasive electrodes placed directly on the brain (Figure 1.5b). Intracranial EEG recording mainly involves two techniques:

- **Depth electrodes:** implantation uses multiple electrodes stereotactically implanted into the brain parenchyma via small screws fixed to the skull. This stereo-EEG technique allows recording from both deep and superficial areas.
- Subdural electrodes (strips and grids): placed directly on the brain surface, covering larger cortical areas. iEEG is typically reserved for presurgical evaluation in patients with refractory epilepsy. Subdural strips can be placed through simple burn holes, whereas grids require a craniotomy and can record from a larger area of contiguous cortex[25, 28].

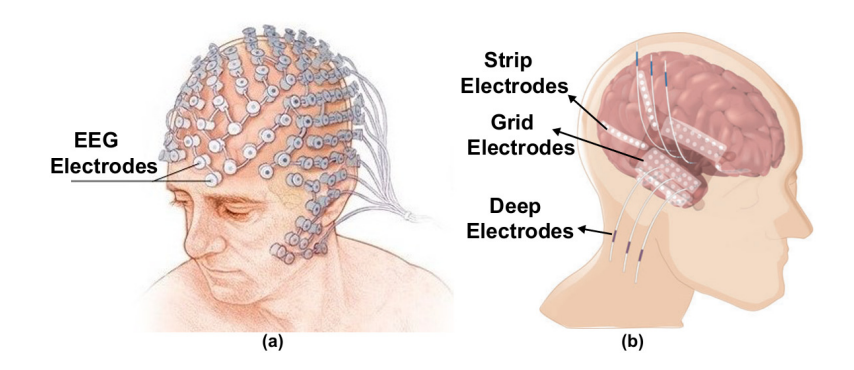


Figure 1.5: Placement of electrodes in EEG recording: (a) scalp EEG (sEEG) with electrodes on the scalp, and (b) intracranial EEG (iEEG) with subdural or depth electrodes placed directly on the brain [25].

1.2.3 Drug-Resistant Epilepsy and Treatment

The treatment of epilepsy is primarily based on anti-seizure medications (ASMs), with about two-thirds of patients achieving seizure freedom. The remaining third of patients are considered to have drug-resistant epilepsy (DRE) and are eligible for alternative treatments, such as epilepsy surgery (i.e., surgical resection, disconnection, and neurostimulation) and non-pharmacological therapies (e.g., ketogenic diet) [29].

To establish a common terminology, the ILAE in 2010 defined DRE as "failure of adequate trials of two tolerated, appropriately chosen and used antiepileptic drug schedules (whether as monotherapies or in combination) to achieve sustained seizure freedom" [30]. This definition encompasses underlying pathogenic factors leading to structural and neurobiochemical changes, often resulting in cognitive, psychiatric, and psychosocial disturbances [30, 31].

1.2.3.1 Resective epilepsy surgery

Surgical treatment is the most cost-effective approach for patients with drug-resistant focal epilepsy when a clearly defined epileptogenic zone can be resected or disconnected [32]. The epileptogenic zone is a theoretical construct, defined as the minimum amount of cortex that must be resected to give seizure freedom[28]. Despite sophisticated presurgical methods, surgery is not always feasible or successful. Even when feasible, resection surgery carries risks such as post-surgical complications, cognitive deficits, and psychosis, and does not guarantee seizure freedom [32].

Consequently, alternative or complementary therapeutic strategies are increasingly utilized. One promising treatment is neuromodulation, which is premised upon the electrical circuit model of neural function and uses direct or induced electrical currents to modulate network activity. Neuromodulation aims to restore the excitatory/inhibitory balance in patients with DRE who are not eligible for surgery or whose epileptogenic zone cannot be localized [29].

1.2.3.2 Neuromodulation

Neuromodulation can be devided into two main categories invasive and non-invasive.

Invasive Neuromodulation:

- Vagus Nerve Stimulation (VNS): Involves an implanted electrode around the left vagus nerve and a sub-clavicular generator. VNS reduces seizure frequency and improves long-term quality of life but carries surgical risks and side effects.
- Responsive Neurostimulation (RNS): Detects ongoing epileptiform activity with implanted electrodes and delivers stimulation in a closed-loop manner.
- Deep Brain Stimulation (DBS): Delivers chronic, intermittent pulse-trains via intracerebral electrodes.

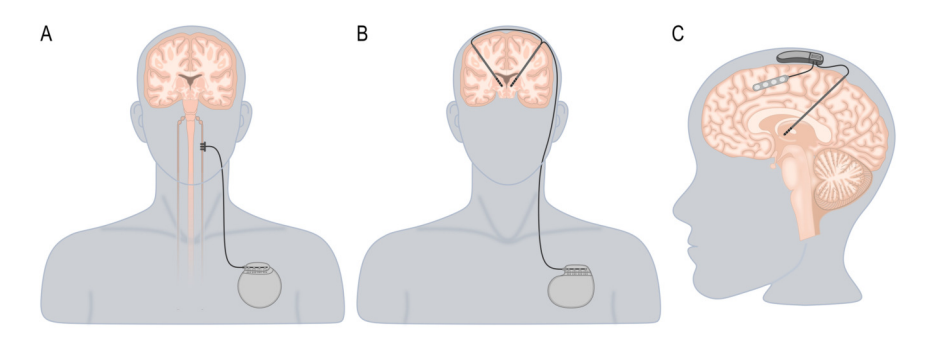


Figure 1.6: Illustration of invasive neuromodulation therapies. A. The vagus nerve stimulation device comprises an electrode with three helical contacts connected to a subclavicular implantable pulse generator. B. The deep brain stimulation system comprises depth electrodes connected to a subclavicular implantable pulse generator. C. The responsive neurostimulation device comprises depth electrodes, cortical strips, and a cranial implantable pulse generator. figure adapted from [29].

Non-invasive Neuromodulation: Transcranial Electrical Stimulation (tES) is a non-invasive neuromodulation technique designed to modulate brain activity by delivering low-intensity electrical currents, typically between 1 and 2 mA, through electrodes placed on the scalp as shown in Figure 1.7. Two main forms are [33]:

- Transcranial Direct Current Stimulation (tDCS): This technique uses a constant and unidirectional electrical current flowing from an anodal electrode to a cathodal one.
- Transcranial Alternating Current Stimulation (tACS): involves an applied electrical current that changes sinusoidally over time.

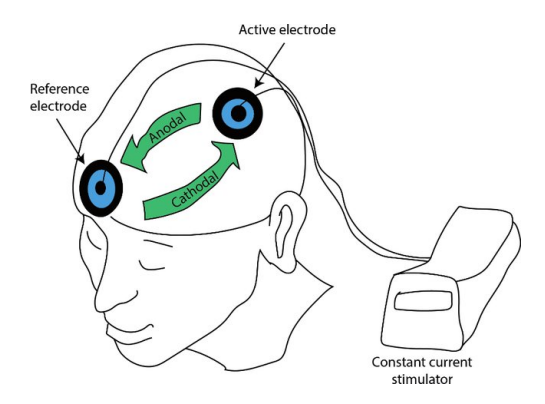


Figure 1.7: tDCS delivers continuous low current stimulation by applying a positive (anodal) or negative (cathodal) current via paired electrodes over the scalp[34].

In the context of epilepsy, Clinical studies have demonstrated that tES is generally safe and can induce clinically relevant improvements in seizure frequency and network activity in epileptic patients. Recent evidence suggests that tDCS may act by modulating functional brain networks rather than solely affecting the local cortical area, influencing connectivity patterns and potentially reducing pathological hyperexcitability.[3]

1.2.4 The GALVANI Project Approach to tDCS and Epilepsy

Despite its therapeutic potential, tES has several limitations. The precise mechanisms underlying its effects on epileptic brain activity remain poorly understood [35]. Moreover, clinical data, especially for tACS, are limited, with few trials involving sufficient patient numbers to draw robust conclusions[3].

These challenges highlight the need for computational models in tES research. Computational modeling can predict how electrical currents distribute across individual brains, optimize stimulation parameters, and personalize protocols for maximum efficacy. In this context, the GALVANI project (ERC Synergy, 2020–2027) was initiated to develop computational models aimed at studying the effects of tES on epileptic brain activity. The project seeks to optimize stimulation parameters and personalize treatment protocols by understanding how low-level electric fields interact with individual brain anatomy and physiology.

Computational modeling is crucial for predicting current distribution, guiding electrode placement, and determining optimal session timing. Importantly, to make microscale models realistic and neuro-inspired, neuroplasticity mechanisms need to be incorporated, ensuring that cellular and network responses to stimulation reflect the adaptive properties of the epileptic brain.

1.3 Neuroplasticity

1.3.1 Neuronal and Synaptic Structure

1.3.1.1 Neurons

Neurons are the fundamental building blocks of the nervous system. They are highly specialized cells capable of transmitting electrical and chemical signals to coordinate physiological and cognitive functions [36]. Neurons communicate via a combination of electrical impulses and chemical neurotransmitters. Electrical signals, called Action Potentials (APs), travel along the axon of a neuron. When they reach the axon terminal, they trigger the release of neurotransmitters into the synapse. These chemicals then interact with receptors on the postsynaptic neuron, converting the signal back into an electrical impulse. Structurally, a neuron consists of three main parts as portrayed in Figure 1.8 [36]:

• **Dendrites:** These are branched projections that receive incoming signals from other neurons. They integrate signals spatially (combining inputs from different synapses)

and temporally (combining inputs in rapid succession at the same synapse). This integration is essential for determining whether an AP is generated.

- Cell Body (Soma): The soma contains the nucleus and other organelles. It serves as the metabolic hub of the neuron and integrates inputs from the dendrites.
- Axon: This is a long, cylindrical projection that transmits APs away from the soma. The axon hillock, where the axon originates, is the site of AP initiation. Once an AP is generated, it propagates along the axon without loss of strength due to its regenerative nature. Microtubules within the axon facilitate intracellular transport, including the delivery of neurotransmitters from the soma to the presynaptic terminal.

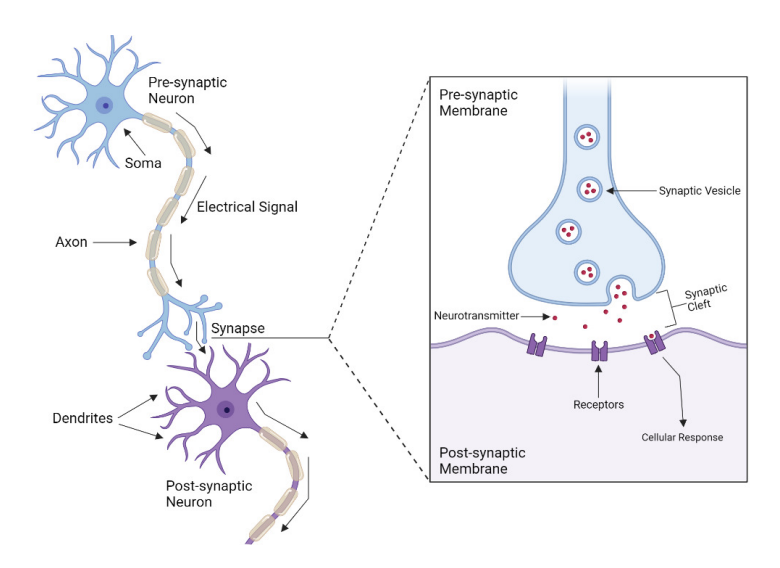


Figure 1.8: The figure illustrates the structural components of the neuron and the synapse adapted from [37].

1.3.1.2 Synapses

Synapses are the junctions where neurons communicate with each other. The human brain contains approximately 86 billion neurons, each forming thousands of synaptic connections [38]. Synapses can occur between different parts of neurons. A typical synapse consists of three components as shown in Figure 1.8:

- Presynaptic Terminal: Located at the end of the axon, this structure contains synaptic vesicles filled with neurotransmitters. When an AP arrives, voltage-gated calcium channels open, triggering the release of neurotransmitters into the synaptic cleft.
- Synaptic Cleft: This is a small gap between the presynaptic and postsynaptic terminals. Neurotransmitters diffuse rapidly across this cleft, within microseconds.

• Postsynaptic Terminal: This contains receptors that bind the neurotransmitters. The activation of these receptors alters the postsynaptic membrane potential, leading to either excitatory postsynaptic potentials (EPSPs) or inhibitory postsynaptic potentials (IPSPs).

Synaptic structure is tightly regulated and highly plastic. The type and density of receptors, the strength of neurotransmitter release, and the spatial arrangement of preand postsynaptic membranes all contribute to synaptic efficacy and plasticity[36].

1.3.1.3 Synaptic Transmission

Synaptic transmission in the central nervous system (CNS) relies on the precise release and detection of chemical messengers known as neurotransmitters. These molecules are essential for neuron-to-neuron communication and for modulating the strength of synaptic connections, a key mechanism in neuroplasticity [39]. Figure 1.9 illustrates the Sequence of Events During Synaptic Transmission.

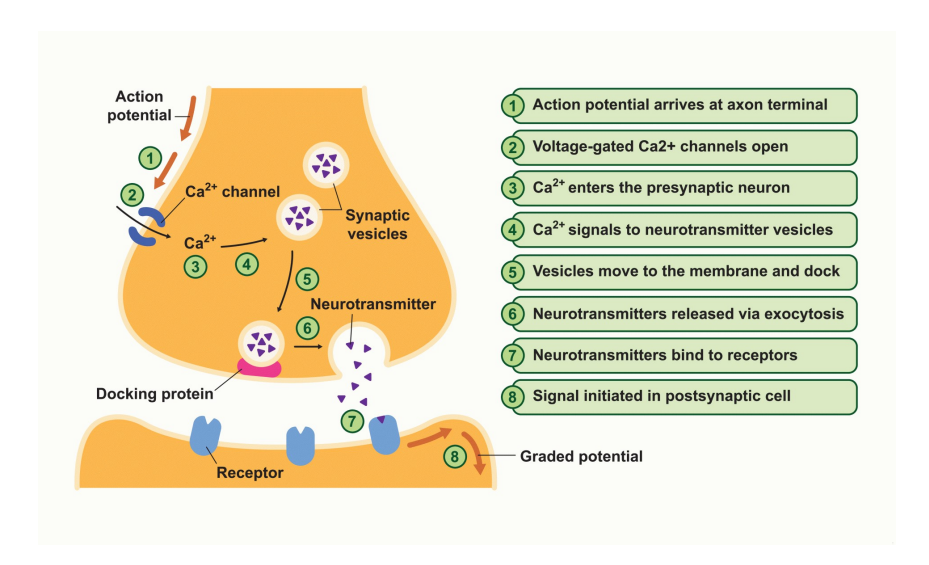


Figure 1.9: This picture illustrates the sequence of events During synaptic transmission[40].

The two most prominent neurotransmitters in the CNS are:

- Glutamate, the primary excitatory neurotransmitter, and
- Gamma-aminobutyric acid (GABA), the main inhibitory neurotransmitter.

A tightly regulated balance between excitation (via glutamate) and inhibition (via GABA) is critical for maintaining normal brain function, preventing excessive neuronal activity, and enabling plastic adaptations of neural circuits [41].

Glutamate and Excitatory Transmission At excitatory synapses, L-glutamate is released from the presynaptic terminal into the synaptic cleft, where it binds to glutamate receptors on the postsynaptic membrane. These receptors include:

- α-amino-3-hydroxy-5-methyl-4-isoxazolepropionic acid Receptors (AMPARs): These mediate fast, short-lived excitatory synaptic responses. Upon glutamate binding, AMPARs rapidly open to allow Na⁺ influx, leading to brief excitatory postsynaptic potentials (EPSPs). This is the primary mechanism for baseline excitatory transmission.
- N-methyl-D-aspartate (NMDA) Receptors (NMDARs): These receptors play a central role in synaptic plasticity rather than in baseline synaptic transmission. NMDARs are unique in that they are both ligand-gated and voltage-dependent. At resting membrane potentials, the NMDAR channel pore is blocked by Mg²⁺ ions. When AMPAR-mediated depolarization is sufficient, the Mg²⁺ block is removed, enabling Ca²⁺ influx through the NMDA channel.

This dual requirement, "glutamate binding and postsynaptic depolarization", makes NMDARs highly effective coincidence detectors, crucial for activity-dependent plasticity. The calcium influx they mediate initiates intracellular signaling cascades that can lead to LTP or LTD, depending on the timing and frequency of synaptic activity[42, 43].

GABA and Inhibitory Transmission In contrast, GABA mediates inhibition primarily through GABA receptors, which are ligand-gated chloride channels. When GABA binds to these receptors, Cl⁻ ions enter the postsynaptic neuron, causing hyperpolarization of the membrane and generating inhibitory postsynaptic potentials (IPSPs). This inhibitory mechanism counterbalances excitatory activity and is essential for controlling neural excitability, preventing runaway excitation, and shaping synaptic plasticity [44].

1.3.2 Neuroplasticity: Definition and Principles

Neuroplasticity, also referred to as neural plasticity or brain plasticity, is the capacity of the nervous system to change its structure and function in response to intrinsic or extrinsic stimuli. It involves dynamic processes such as the formation of new synapses, the elimination of old connections, and the modulation of existing synaptic strength. A widely accepted definition is:

"The ability of the nervous system to change its activity in response to intrinsic or extrinsic stimuli by reorganizing its structure, functions, or connections" [45]. This biological

property is essential for learning, memory, adaptation to new experiences, recovery after injury, and the maintenance of functional brain networks throughout life.

1.3.2.1 Long-Term Potentiation and Depression

LTP and LTD are activity-dependent, long-lasting changes in synaptic strength and are considered cellular correlates of learning and memory. Both are primarily mediated by NMDARs and the resulting postsynaptic calcium influx.

- LTP is triggered by strong NMDAR activation and large calcium influx, usually when pre- and postsynaptic neurons fire together. This depolarization relieves the Mg²⁺ block of NMDARs. High-frequency stimulation or spike-timing, where presynaptic spikes precede postsynaptic spikes, typically induces LTP.
- LTD arises from modest NMDAR activation and smaller calcium influx, often due to low-frequency presynaptic stimulation or spike-timing where postsynaptic spikes precede presynaptic spikes.

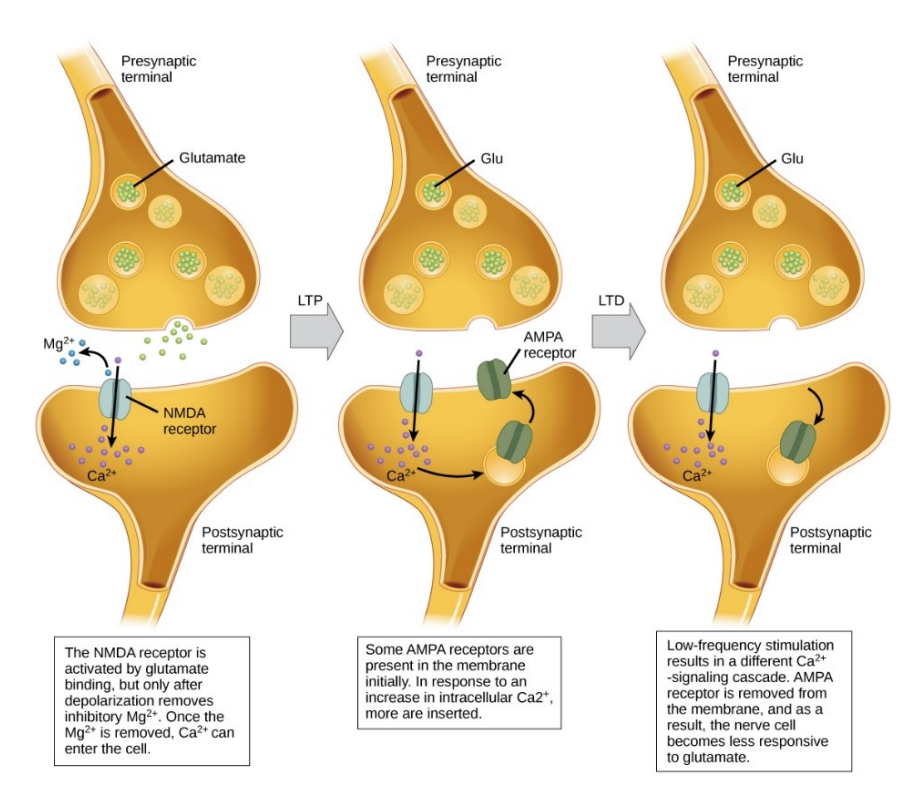


Figure 1.10: Schematic of the LTP and LTD processes based on calcium influx through NMDA receptors. Adapted from [46]

These processes, portrayed by Figure 1.10 show that the magnitude and timing of post-synaptic calcium signals determine whether synaptic strength increases (LTP) or decreases (LTD), linking specific activity patterns to lasting synaptic modifications. LTP and LTD

are fundamental for synaptic plasticity, learning, memory formation, and network adaptation [47].

1.3.2.2 Spike timing dependent plasticity (STDP)

STDP is a fundamental form of synaptic plasticity where the precise temporal interval and order between presynaptic and postsynaptic APs dictate the sign and magnitude of long-term synaptic change. This concept traces back to Donald Hebb's 1949 theory [48], "cells that fire together, wire together," and was experimentally quantified by studies like Bi and Poo (1998) [49]. In its classical form, causal pairings (presynaptic spike shortly before postsynaptic spike) lead to LTP, strengthening the synapse. Anticausal pairings (postsynaptic spike before presynaptic spike) result in LTD, weakening the synapse, reflecting that the presynaptic input did not cause the postsynaptic activity. While spike timing is central, other factors such as firing rate, synaptic cooperativity (the interaction between multiple nearby synapses), and dendritic location can modulate STDP [50].

1.4 Computational Neuroscience and Modeling

Computational models provide a framework for exploring hypotheses that are difficult to test experimentally. They enable simulation of neural dynamics at various scales:

- **Single-cell models:** such as Hodgkin-Huxley, describe ionic mechanisms underlying APs.
- Network models: integrate multiple neurons and synapses to simulate emergent properties.

Computational modeling helps in understanding how local mechanisms scale up to system-level behavior, including seizure generation and propagation.

1.4.1 Hodgkin-Huxley Formalism

The Hodgkin-Huxley (HH) formalism [51], is a foundational framework for modeling the electrical behavior of single neurons. Developed in 1952 by Alan Hodgkin and Andrew Huxley through experiments on the squid giant axon, the model describes how APs are generated and propagated via voltage-dependent ion conductances.

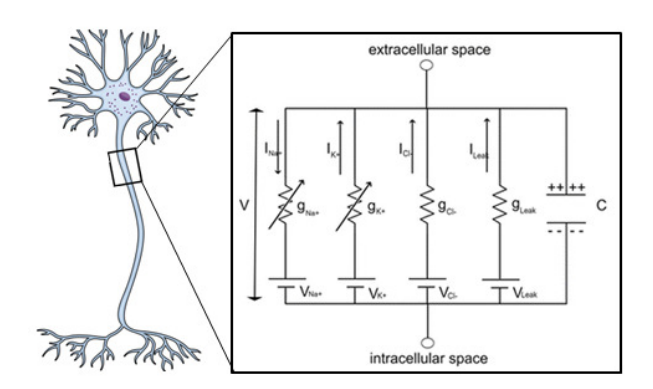


Figure 1.11: Hodgkin-Huxley Model circuit representation of the neuronal membrane. The circuit consists of a capacitor cell generating capacitive current and ion flow across the cell membrane, generating the ionic current. Ion channels and ionic currents cause an acquisition of net charge in the extracellular and a depletion of charge in the intracellular space. This leads to a potential difference, V, across the neuronal membrane. [52]

In the HH model, the neuronal membrane is treated as an electrical circuit consisting of a capacitor (representing the membrane capacitance) and variable conductances for sodium (Na⁺), potassium (K⁺), and leak currents (Figure 1.11). These conductances are described using differential equations that capture the gating dynamics of ion channels in response to changes in membrane voltage.

The basic membrane equation is:

$$C_m \frac{dV}{dt} = -g_{Na} m^3 h(V - E_{Na}) - g_K n^4 (V - E_K) - g_L (V - E_L) + I_{ext}$$
 (1.1)

where V is the membrane potential, C_m is the membrane capacitance, g_{Na} , g_K , and g_L are the maximum conductances for Na⁺, K⁺, and leak channels, respectively, E_{Na} , E_K , and E_L are the respective reversal potentials, m, h, and n are the gating variables representing channel activation and inactivation, and I_{ext} is an external input current.

This formalism allows for a biophysically accurate simulation of APs and is widely used as the basis for more complex single-neuron and network models in computational neuroscience.

1.4.2 Neural Networks Modeling

In this section, we will present the two neuroinspired computational models used in this work.

1.4.2.1 Microcircuit Model of the Hippocampus

This model is a neuroinspired microscale model of the hippocampus CA1 subfield [6, 53]. It is a biologically inspired neural network that can simulate realistic interictal events

recorded via iEEG depth electrodes. This model provides the ability to explain underlying mechanisms for the generation of epileptic events such as Interictal Epileptic Spikes (IES), High frequency oscillations (HFOs),.....

Model Architecture and Neuron Types The model focuses on the CA1 subfield of the hippocampus, a region frequently implicated in temporal lobe epilepsy (TLE) due to its well-characterized anatomy and significant role in epileptic dynamics.

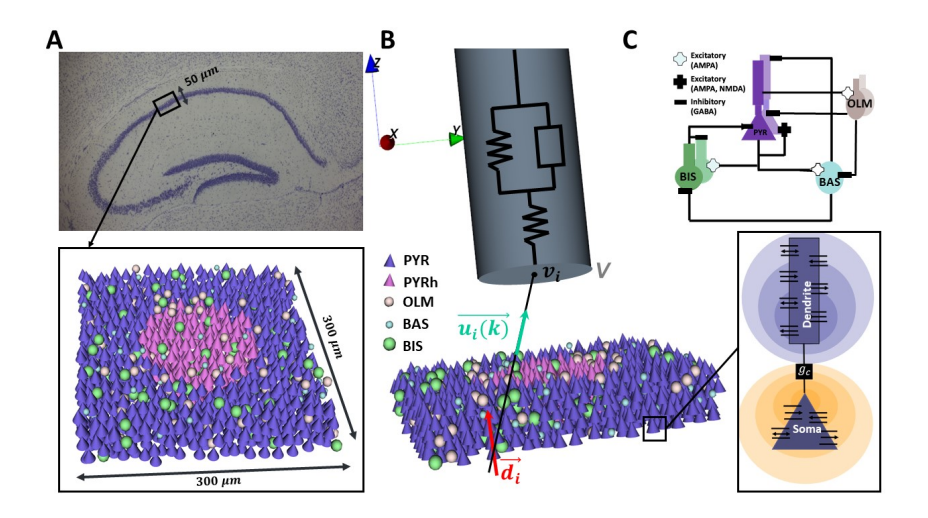


Figure 1.12: Neural Network Model Structure. (A) The simulated 3D volume is designed with the essential elements needed to reproduce the behavior of CA1 subfield (hippocampus). It includes in addition to pyramidal cells (PYR), oriens-lacunosum moleculare (OLM), Basket (BAS), and Bistratified (BIS) interneurons. The PYR cells in pink are the hyperexcitable PYR cluster. (B) The extracellular field potential (V) observed by the electrode is obtained by solving the forward problem using the dipole theory and then integrating the result over the active electrode surface. (C) The synaptic interactions between the different cells in the network and the reduced CA1 pyramidal neuron two compartments model. [53].

1. Network Composition and Connectivity: The network comprises approximately 3,000 interconnected neurons, designed to capture the essential features of the hippocampal CA1 subfield. Of these, 80% are pyramidal cells (excitatory principal neurons), while the remaining 20% are interneurons, equally divided between BAS, OLM and BIS cells. Neuronal interactions are mediated through both glutamatergic synapses (AMPA and NMDA receptors) and GABAergic inhibitory synapses. Connectivity patterns, as well as intercellular distances, are constrained by experimental data from the literature. The probability of connection follows a Gaussian distribution, such that neurons in closer proximity are more likely to form synapses.

2. Cellular Models

• Pyramidal Cells (PCs): These are the main excitatory neurons, represented by a reduced two-compartment model (soma and dendrites) [54]. Each compartment

incorporates various ionic currents crucial in epilepsy, including voltage-dependent sodium (INa), potassium delayed-rectifier (IKDR), calcium (ICaL, ICaT, ICaR), calcium-dependent potassium (IAHP), fast inactivating potassium (IKA), hyperpolarization-activated cationic (Ih), and muscarinic potassium (Im) currents. The membrane voltage of each compartment follows the classical current balance equation of HH formalism.

• Interneurons: The GABAergic interneurons (BAS, BIS and OLM cells) are represented by simpler single-compartment models.

External Stimulation and LFP Reconstruction The network is stimulated with an afferent volley of quasi-synchronous APs with adjustable delay (jitter) and spatial distribution. This input mimics the crucial drive from the CA3 area to the CA1 network via Schaffer collaterals, a known initiator of interictal activity. Simulated LFPs usually observed in iEEG, are obtained by solving the forward problem using dipole theory. PCs are considered the primary contributors to the LFP due to their "palisade" spatial arrangement, and each is treated as a point source (current dipole). The potential at the electrode is then obtained by summing the contributions from all PCs. the corresponding mathematical formulation can be found in [6].

Model Validation and Key Findings Model validation was conducted in two stages: first, the reduced pyramidal neuron model was tested against intracellular recordings from rat hippocampal slices, and second, simulated LFPs were compared to actual human depth-EEG signals from epileptic patients. The model successfully reproduced events closely resembling actual epileptic spikes. It also provided key insights into the mechanisms underlying the generation of different epileptic events.

Graphical User Interface (GUI): "Modele Micro 3D" The Hippocampus model is implemented within a software application called "Modele Micro 3D Software" illustrated in Figure 1.13, which provides a user-friendly graphical interface (GUI). This GUI allows researchers to interact with the model without extensive programming, offering a main control panel for configuring tissue and simulation parameters, a 3D environment for visualizing network structure, and dedicated panels for displaying temporal signals like LFP and intracellular activity.

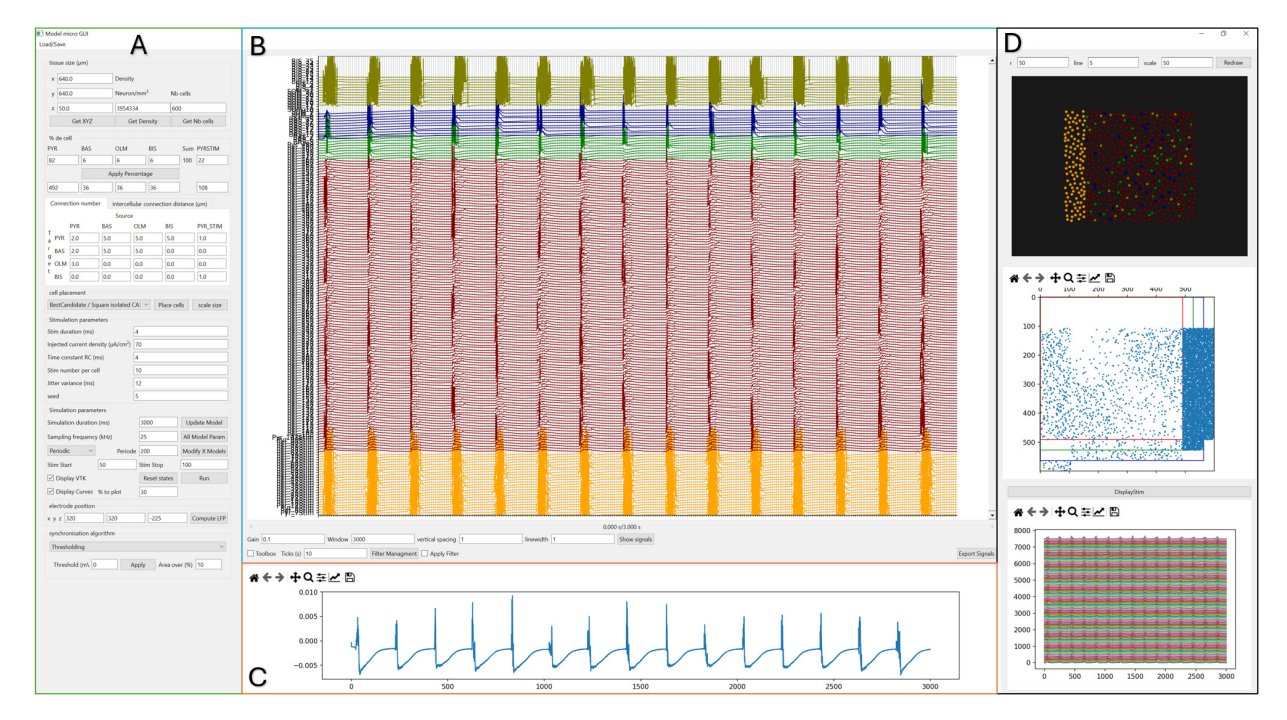


Figure 1.13: The graphical user interface of the Hippocampus model. A: hippocampal network parameter configuration panel. This panel includes tissue dimensions, cell density, cell distribution and placement, external stimulation parameters, simulation duration, sampling rate. B: The intracellular activity representation panel which displays membrane potential traces of individual neurons. C: The local field potential plot. D: The 3D cortical tissue representation with the corresponding connectivity matrix as well as the stimulation signals plot panel.

This modeling framework achieves a compromise between biological realism and computational tractability by using reduced neuron models while maintaining essential physiological characteristics. It successfully links microscopic cell-level dynamics to macroscopic LFP signals, supporting the interpretation of electrophysiological data.

1.4.2.2 Microcircuit model of the Neocortex: NeoCoMM Model

NeoCoMM (Neocortical Computational Microscale Model) [5], is an advanced software platform designed for realistic microscale simulations of neocortical networks at the cellular level. It balances physiological and biophysical accuracy with computational efficiency, offering a user-friendly framework for studying microscopic mechanisms in both healthy and pathological brains, particularly in epilepsy.

Model Architecture and Neuron Types

NeoCoMM simulates a **single neocortical column** across all six layers, with species-specific adaptations for humans, rats, and mice, including layer thickness, column volume, neuronal density, distribution, and morphology [5].

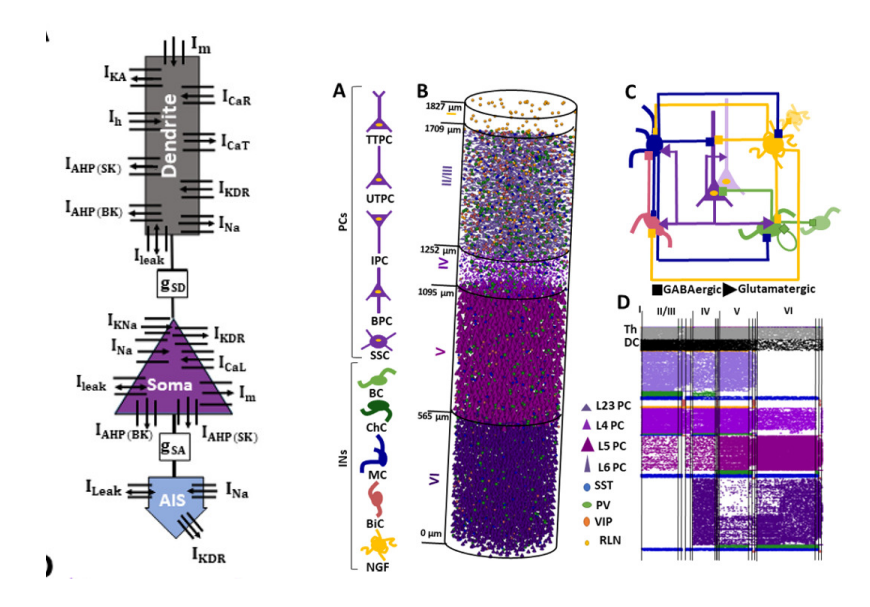


Figure 1.14: Left: Pyramidal neuron computational model with three compartments: Soma, Dendrites, and Axon initial segment (AIS). Right: Anatomy of a cortical patch. (A) The different cell types included in the model. (B) A 3D rendering of the cortical patch with all the cell types for 13760 cells. (C) The synaptic connectivity affinity diagram between the different cell types. (D) an example of the connectivity matrix[5].

1. Neuron Models:

- Pyramidal Cells (PCs): PCs are excitatory neurons represented by a three-compartment model (soma, dendrites, axon initial segment(AIS)) as illustrated in Figure 1.14-left. This design allows rich electrophysiological dynamics across layers II/III/IV and V/VI. Membrane potential of each compartment evolves according to HH-based differential equations, accounting for ionic currents (e.g., I_{Na} , I_{KDR} , I_{CaL}) and inter-compartmental coupling (g_{SD} , g_{SA}). PC subtypes include Tufted (TTPCs), Untufted (UTPCs), Inverted (IPCs), Bipolar (BPCs), and Spiny Stellate cells (SSs).
- Interneurons (INs): Single-compartment cells modeling a diverse set of inhibitory neurons, including PV+, SST+, VIP+, and RLN+ types, further categorized into Basket (BC), Chandelier (ChC), Martinotti (MC), Bipolar (BiC), and Neurogliaform cells (NGF).
- 2. Network Structure and Connectivity: The neocortical patch comprising approximately 13,760 interconnected neurons, is modeled as a cylindrical volume, with species-dependent dimensions (e.g., 2622 μm height for humans). Neurons are spatially distributed using an optimized packing algorithm, with PCs comprising 70–80% of the population. Synaptic connectivity is determined by neurite overlap (Peter's rule) and literature-based afference matrices. Glutamatergic (AMPA/NMDA) and GABAergic synapses follow bio-

logically constrained rules, e.g., PV+ cells inhibit within their layer, and VIP+ interneurons target SST+ cells, illustrated in Figure 1.14right.

External Stimulation and LFP Reconstruction

External Stimulation: NeoCoMM incorporates thalamic and distant cortical inputs, adjustable in intensity, duration, and jitter, with optional noise. Distal cortical pyramidal neurons in layers II/III and V/VI contribute $\sim 7\%$ of PCs to evoke network activity. Conductance and firing profiles are adapted from experimental data [5].

Local Field Potential (LFP) Reconstruction: LFPs are computed using volume conductor theory, considering PCs as the primary transmembrane current sources. A realistic Electrode-Tissue Interface (ETI) model incorporates electrode characteristics (shape, position, diameter, orientation, material). The extracellular potential at each electrode contact is obtained by summing contributions from all transmembrane currents, and the total LFP is calculated accordingly. The detailed mathematical formulation can be found in [5].

Model Validation and Key Findings

NeoCoMM reproduces a variety of interictal epileptiform events (IEEs), including interictal epileptic spikes (IESs), spike-and-waves (SWs), double spikes-and-waves (DSWs), and high-frequency oscillations (HFOs, ripples, and fast ripples). It can be rendered epileptic through synchronous external input combined with hyperexcitable network of cells obtained through adjustment of cellular and network parameters. This model allows simultaneous intracellular and extracellular representations, which facilitate mechanistic understanding of epileptic activity

Graphical User Interface (GUI)

NeoCoMM features a user-friendly GUI represented in Figure 1.15, enabling researchers to configure and analyze simulations without programming expertise.

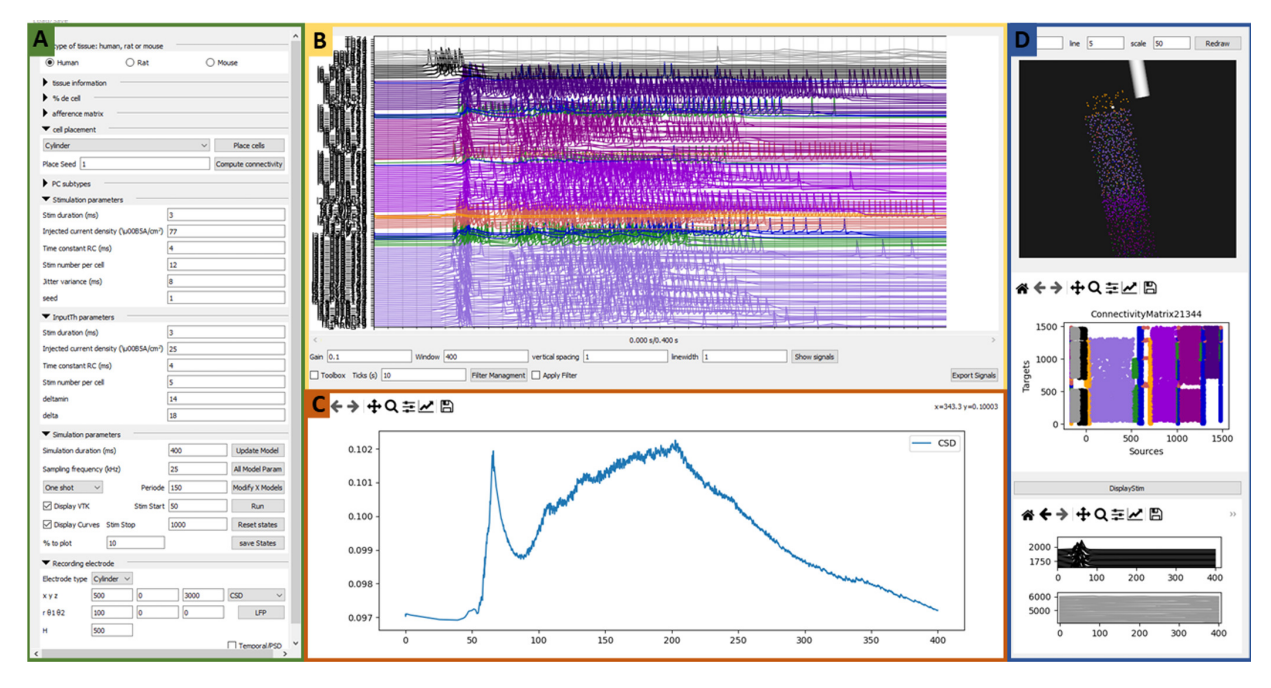


Figure 1.15: The graphical user interface of NeoCoMM. A: The cortical column parameter configuration panel. This panel includes the type of tissue, tissue information, cell distribution percentage, connectivity afference matrix, cell placement type, PC subtypes distribution, external input stimulation parameters, simulation parameters, and the recording electrode characteristics parameters. B: The intracellular activity representation panel which displays membrane potential traces of individual neurons. C: The local field potential plot. D: The 3D cortical tissue representation with the corresponding connectivity matrix as well as the stimulation signals plot panel.

NeoCoMM is a powerful tool for studying neocortical microcircuits, understanding epileptic phenomena, and testing neuromodulation strategies. Integration of neuroplasticity mechanisms, described in later chapters, further enhances its utility for exploring epileptogenic activity and interventions like tDCS.

1.4.3 Computational Modeling of Neural Plasticity

Neural plasticity, "the brain's capacity to modify its structure and function in response to experience", has long inspired computational models aimed at understanding learning and adaptation. [55]

Early models centered on Hebbian learning [48], where synaptic strength increases with coincident activity. To prevent instability from unbounded weight growth, homeostatic mechanisms such as synaptic scaling and meta-plasticity (the modulation of synaptic plasticity by previous activity of the same neuron/cell or cellular network [56]) were introduced [57]. Self-organizing networks demonstrated how activity-dependent synaptic changes could generate feature-selective responses and topographic maps [58, 59], while anti-Hebbian learning, Oja's rule, and BCM theory provided mathematically regulated

frameworks for competitive and stable synaptic modifications [60].

Modern Models integrate precise spike timing and biological mechanisms:

- STDP adjusts synaptic weights based on the relative timing of pre- and post-synaptic spikes, with extensions including bi-phasic, tri-phasic, and reward-modulated STDP.
- Voltage-Dependent Plasticity [61] updates synapses based on membrane potential rather than spikes alone.
- Calcium-Controlled Plasticity [8, 9] links synaptic changes to calcium dynamics at the synapse, providing a more biologically grounded framework compatible with STDP observations.

This thesis specifically implements calcium-based synaptic plasticity models proposed by Shouval [8] and Brunel [9], which provide a biologically grounded framework linking synaptic weight changes to the dynamics of intracellular calcium concentration, which is essential for exploring how plasticity alters epileptogenic dynamics and modulates the efficacy of interventions like tDCS.

1.4.3.1 Shouval Model of Calcium-Dependent Plasticity

The model proposed by Shouval, Bear, and Cooper [8], "A unified model of NMDA receptor-dependent bidirectional synaptic plasticity," provides a theoretical framework for describing LTP, LTD, and STDP under a single mechanistic principle.

Core Hypotheses The Shouval model is based on two main assumptions:

- Different calcium concentrations lead to distinct forms of synaptic plasticity: moderate levels induce LTD, while higher levels produce LTP.
- NMDA receptors (NMDARs) are the primary source of postsynaptic calcium influx.

The Calcium Control Hypothesis At the heart of the model lies the calcium control hypothesis, which states that the direction and magnitude of synaptic weight change are determined by postsynaptic calcium concentration. Moderate increases in calcium drive LTD, whereas large increases drive LTP. This hypothesis unifies different induction protocols under a common calcium-dependent mechanism.

Mathematical Formulation The evolution of the synaptic weight W_j at synapse j depends on local calcium concentration [Ca]_j according to:

$$\frac{dW_j}{dt} = \eta([Ca]_j) \left(\Omega([Ca]_j) - \lambda W_j\right)$$
(1.2)

where η is the learning rate, Ω encodes the plasticity outcome, and λ is a decay constant $(\lambda = 1)$.

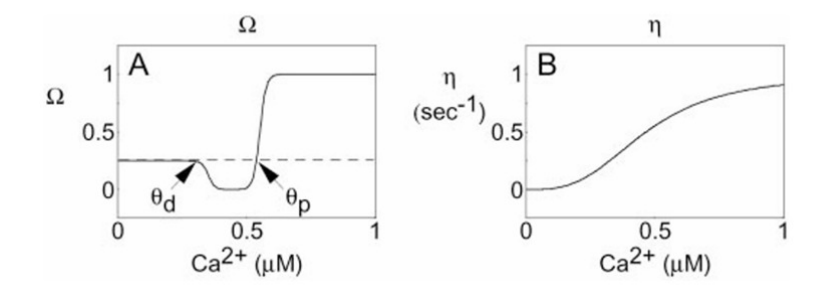


Figure 1.16: The calcium control hypothesis: (A) The Ω function: Synaptic weight change depends on the postsynaptic calcium concentration $[Ca]_i$. Calcium below the depression threshold θ_d yields no modification, intermediate levels induce LTD, and high levels above θ_p produce LTP. (B) The learning rate $\eta([Ca]_i)$ as a function of intracellular calcium[8].

Learning Rate Function η : The calcium-dependent learning rate is inversely related to the learning time constant, the functional form of η and τ is as follows:

$$\eta = \frac{1}{\tau}, \qquad \tau = \frac{P_1}{P_2 + [\text{Ca}]^{P_3}} + P_4.$$
(1.3)

Omega Function Ω : The function Ω is sigmoidal and defines three calcium regimes:

$$\Omega = \Omega_0 + A\operatorname{sig}([\operatorname{Ca}] - \theta_p, \beta_2) - B\operatorname{sig}([\operatorname{Ca}] - \theta_d, \beta_1), \tag{1.4}$$

with

$$\operatorname{sig}(x,\beta) = \frac{e^{\beta x}}{1 + e^{\beta x}}.$$
(1.5)

Where $\theta_p > \theta_d$ represent depression and potentiation thresholds, respectively, such that:

- [Ca] $< \theta_d$: no synaptic modification,
- $\theta_d < [Ca] < \theta_p$: LTD,
- [Ca] $> \theta_n$: LTP.

Here, A > B are the potentiation and depression rates, and $\beta_{1,2}$ are the slopes at the potentiation and depression thresholds (Figure 1.16 left).

Calcium Dynamics: The intracellular calcium concentration evolves as:

$$\frac{d[\mathrm{Ca}](t)}{dt} = I_{\mathrm{NMDA}}(t) - \frac{[\mathrm{Ca}](t)}{\tau_{\mathrm{Ca}}},\tag{1.6}$$

where τ_{Ca} is the calcium decay constant and I_{NMDA} is the calcium current through NM-DARs.

NMDA Current: The NMDAR calcium current is modeled as:

$$I_{\text{NMDA}} = P_0 G_{\text{NMDA}} \left[I_f \, \theta(t_i) e^{-t/\tau_f} + I_s \, \theta(t_i) e^{-t/\tau_s} \right] H(V), \tag{1.7}$$

where P_0 is the fraction of NMDARs that move from closed to open state after each presynaptic action potential, G_{NMDA} the NMDA receptor conductance, I_f and I_s the relative contributions of fast and slow components of the NMDA receptor current, τ_f and τ_s their time constants, and H(V) a voltage-dependent function capturing relief of magnesium block.

1.4.3.2 Brunel Model of Spike-Timing Dependent Plasticity (STDP)

The calcium-based plasticity model introduced by Graupner and Brunel [9] is a biophysically inspired framework of synaptic plasticity that explains how changes in synaptic strength, namely LTP and LTD, arise from the dynamics of postsynaptic calcium concentration. The motivation behind this model stems from the observation that both the **timing** and **frequency** of spikes between pre- and postsynaptic neurons significantly influence synaptic efficacy, and that calcium entry into the postsynaptic spine, primarily through NMDA receptors and voltage-dependent calcium channels (VDCCs), plays a central role in triggering the biochemical pathways responsible for synaptic plasticity.

Synaptic Efficacy Dynamics In this model, the state of a synapse is represented by a synaptic efficacy variable, $\rho(t)$. This variable's temporal evolution is described by a first-order differential equation, which evolves over time based on the calcium transients elicited by pre- and postsynaptic action potentials (APs). The dynamics of the synaptic efficacy ρ follows a stochastic differential equation that includes a bistable term (allowing for stable UP and DOWN states), plasticity induction terms based on the calcium thresholds, and a noise term representing biological variability:

$$\tau \frac{d\rho}{dt} = -\rho(1-\rho)(\rho^* - \rho) + \gamma_p(1-\rho)\Theta[c(t) - \theta_p] - \gamma_d\rho\Theta[\theta_d - c(t)] + \text{Noise}(t)$$
 (1.8)

where τ is the time constant for synaptic efficacy changes, $\rho^* = 0.5$ is the unstable fixed point separating the UP and DOWN basins of attraction, γ_p and γ_d are the potentiation and depression rates, respectively, and $\Theta[x]$ is the Heaviside step function:

$$\Theta[x] = \begin{cases} 0, & x < 0 \\ 1, & x \ge 0 \end{cases} \tag{1.9}$$

The first term, $-\rho(1-\rho)(\rho^*-\rho)$, introduces bistability into the system, ensuring that the synapse tends to remain in either the UP or DOWN state in the absence of stimulation. The second and third terms model synaptic changes due to calcium crossing the potentiation or depression thresholds, respectively. The final term, Noise(t), represents activity-dependent stochastic fluctuations arising from biological variability, such as probabilistic neurotransmitter release or channel dynamics.

Thresholds and Plasticity Induction The model posits two calcium thresholds: a lower threshold θ_d for LTD and a higher threshold θ_p for LTP. If calcium remains between these values, the synaptic strength is stable; crossing either threshold triggers depression or potentiation, respectively. The rate and duration of calcium crossing the thresholds, modulated by spike timing, firing rate, and the temporal overlap of calcium transients, determine the net direction of plasticity.

Model Predictions The model successfully reproduces a wide range of experimentally observed synaptic plasticity phenomena, including at least ten distinct forms of spike-timing-dependent plasticity (STDP) curves. Furthermore, the model captures the frequency dependence of plasticity, predicting little or no change at low frequencies, LTD at intermediate frequencies, and LTP at high frequencies due to cumulative calcium dynamics. These predictions align with experimental findings.

1.5 Problem Statement and Objectives

1.5.1 Research Gap and Motivation

Despite significant advancements in noninvasive neuromodulation techniques, there is still a lack of understanding of the effects of both tDCS and tACS on network dynamics at the cellular level in general and in epilepsy in particular. This is critical especially in the case of patient-specific stimulation protocols. This is where computational models offer the advantage allowing systematic exploration of underlying mechanisms and individualized

optimization of stimulation strategies.

The realistic biophysically detailed microcircuit models of the hippocampus and neocortex that are considered in the Galvani project suffer from a major limitation: the absence of dynamic synaptic plasticity mechanisms. This gap is profound, as neuroplasticity plays a pivotal, dual role in both the pathological development of hyperexcitable networks and their potential therapeutic modulation[7]. To bridge this critical knowledge deficit and enhance the utility of computational modeling for informing precision neuromodulation strategies, this thesis systematically integrates, calcium-dependent synaptic plasticity models, including the Shouval[8] and Brunel[9] frameworks, along with a novel Hybrid model, into these foundational neural circuit simulations. This work thus lays the essential groundwork for mechanistically exploring how plasticity alters epileptogenic dynamics and, how it modulates the impact of tES (tACS and tDCS) on epileptic network activity and events.

1.5.2 Specific Thesis Objectives

1. Develop Activity-Dependent Synaptic Plasticity Models

- Integrate and implement biologically realistic calcium-dependent plasticity models (Shouval and Hybrid) into detailed models of CA1 and neocortical pyramidal neurons.
- Qualitatively validate all plasticity models in small-scale networks (2–3 cells), ensuring accurate LTP/LTD induction and physiologically plausible STDP curves.

2. Investigate the Influence of Plasticity on Epileptogenic Dynamics in the Hippocampal Network

- Integrate validated neuroplasticity models into a large-scale computational model of the hippocampal CA1 subfield.
- Induce epileptiform activity via systematic modulation of biophysical and synaptic parameters (e.g., GABA reversal potential, glutamatergic conductances) to mimic excitation-inhibition imbalances.
- Assess how plasticity mechanisms affect emergent epileptiform activity, including LFP characteristics, firing rates, and action potential amplitudes across PCs and INs populations.

3. Explore Plasticity's Role in Neocortical Epileptogenesis and tDCS Modulation

- Integrate validated neuroplasticity models into the NeoCoMM neocortical microcircuit, adapted for human cortical column dimensions and cell type distributions.
- Analyze how plasticity-driven dynamics influence the generation and propagation of epileptiform activities in the neocortex.
- Investigate how tES modulate these plasticity-driven dynamics.

Through this work, we aim to provide a more physiologically realistic and comprehensive computational framework to inform the development of personalized neuromodulation strategies for drug-resistant epilepsy, aligning with the objectives of the GALVANI project.

Chapter 2

Modeling neuroplasticity in multicompartment neuron models

2.1 Introduction

This chapter details the methodological approaches and materials employed to model and integrate neuroplasticity mechanisms into existing computational models of single neurons. We will describe the modifications made to a biologically inspired PC model and present the implementation of the well-established neuroplasticity model by Shouval, alongside a novel Hybrid model developed in this work that combines key features of both the Shouval and Brunel frameworks. Furthermore, this chapter outlines the systematic testing framework used to validate these integrated plasticity models in different network settings and under epileptic conditions.

2.2 PC Model

The computational models in this thesis are built upon a foundation of biophysically detailed single-neuron models developed within the GALVANI project by the Cynetics team, representing hippocampal CA1[6] and neocortical[5] PCs. As mentioned in section 1.4.2.1 and section 1.4.2.1, for the hippocampal model, pyramidal neurons are described using a **two-compartment structure**, consisting of a soma and a dendritic compartment (Figure 2.1A). In contrast, the neocortical model extends this approach to a **three-compartment structure** by including an additional axon initial segment (AIS) compartment alongside the soma and dendrite (Figure 2.1B). These compartments are coupled via an axial conductance, allowing current exchange and enabling interactions between dendritic integration and somatic spike initiation.

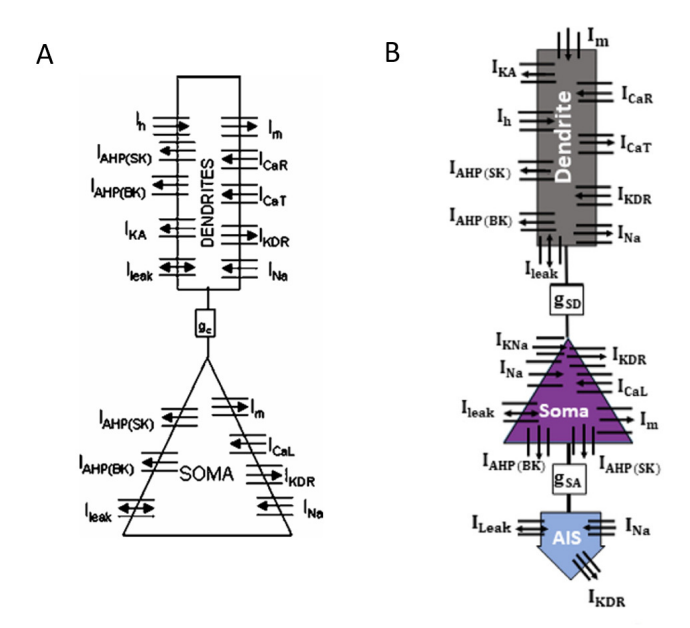


Figure 2.1: A: the two-compartment hippocampal CA1 Pc model, B: the three-compartment neocortical Pc model

Each compartment had a different set of channels. The key active ionic currents chosen for the soma and dendrites accounted for seven and ten different voltage-gated channels respectively (Figure 2.1A), [6]. The AIS compartment had only two voltage-gated channels (Figure 2.1B), the sodium I_{Na} and the potassium delayed rectifier I_{KDR} , [5]. All compartments had a leak current that portrayed the resting membrane potential variation with a Gaussian noise. The CA1 PCs membrane potential variation (V) for each compartment was computed following the electric charge conservation equation described in the following differential equations:

$$-C_m \frac{dV_s}{dt} = I_{Na}(V_s) + I_{KDR}(V_s) + I_{CaL}(V_s) + I_{AHP}(V_s) + I_m(V_s) + g_{SD} p_{SD}(V_s - V_d) + g_{SA} p_{SA}(V_s - V_a) + I_{leak}(V_s) + I_{syn} + I_{stim}$$
(2.1)

$$-C_{\text{md}} \frac{dV_d}{dt} = I_{Na}(V_d) + I_{KDR}(V_d) + I_{CaT}(V_d) + I_{CaR}(V_d) + I_{AHP}(V_d) + I_m(V_s) + I_h(V_s) + I_{SD}(1 - p_{SD})(V_d - V_s) + I_{\text{leak}}(V_d) + I_{\text{syn}} + I_{\text{stim}}$$
(2.2)

For the neocortical three-compartment PC, the membrane potential of the AIS compartment V_a is governed by:

$$-C_m \frac{dV_a}{dt} = I_{Na}(V_d) + I_{KDR}(V_d) + g_{SA}(1 - p_{SA})(V_a - V_s) + I_{leak}(V_a) + I_{syn} + I_{stim}$$
 (2.3)

where V_s , V_d and V_a are the membrane potentials of the three compartments (soma, dendrites and AIS), C_m is the membrane capacitance of the Soma and AIs and $C_{\rm md}$ is that of the dendrite, g_{SD} and g_{SA} are the conductances between soma/dendrites and soma/AIS respectively, p_{SD} and p_{SA} are the proportions of the soma area to the sum of soma/dendrites and soma/AIS respectively, $I_{\rm stim}$ is the external stimulation and $I_{\rm syn}$ is the sum of the synaptic currents.

All ionic currents (I_{ion}) follow the general Hodgkin-Huxley formulation:

$$I_{ion} = g_{ion} m^x h^y (V - E_{ion}) (2.4)$$

Here, g_{ion} denotes the maximum conductance for the specific ion, while m and h are the gating variables representing channel activation and inactivation, respectively. The term E_{ion} corresponds to the reversal potential for that ion.

This model has been validated against experimental data, successfully reproducing key neuronal behaviors and pharmacological effects. All parameter values, including all channel conductances and reversal potentials for the hippocampal two-compartment PC model were taken from [6], and those for the neocortical three-compartment PC model from [5].

2.2.1 Calcium Dynamics

Intracellular Ca is modeled explicitly due to its key role in regulating dendritic excitability and activating Ca-dependent potassium channels. The dynamics of Ca are described by the following equation according to [6] in the base model:

$$\frac{dCa}{dt} = dc - \frac{0.0001 - Ca_{in}}{\tau_{Ca}}$$
 (2.5)

dc represents the contribution of Ca influx and removal through pumps, expressed as:

$$dc = \frac{-10\sum I_{Ca}}{0.2F} \tag{2.6}$$

where F is Faraday's constant, I_{Ca} is the total current through voltage-gated Ca channels, and τ_{Ca} is the Ca decay constant, here defined as $\tau_{Ca} = 100 \, ms$.

2.2.2 Synaptic Dynamics and NMDA Current

Synaptic inputs are modeled through AMPA, NMDA, and GABA receptors, with NMDARs playing a particularly important role due to their voltage-dependent and Ca-permeable properties. I_{NMDA} is the current specifically through NMDARs, which are a major source

of postsynaptic Ca influx. The original I_{NMDA} expression was:

$$I_{NMDA} = G_{NMDA}RB(V - E_{NMDA}) (2.7)$$

Where R is the fraction of NMDARs transitioning from closed to open after neurotransmitter release, B represents the voltage-dependent magnesium block of the channel, G_{NMDA} is the maximum NMDA conductance, and E_{NMDA} is the NMDA reversal potential. All the parameter values were directly adopted from [6].

2.2.3 Numerical Integration and Extensions

The complete set of coupled nonlinear differential equations describing membrane voltage, gating variables, ion concentrations, and synaptic currents is solved numerically using a fourth-order Runge–Kutta method. This base PC model provides a physiologically realistic foundation, which was systematically extended in the present work to incorporate dynamic mechanisms of synaptic plasticity. While the original formulation allowed for NMDA-dependent Ca entry, synaptic efficacy itself was static and did not change with activity. In order to study how synaptic strength evolves under different conditions, a new dynamic state variable was introduced to represent the synaptic weight (W). This variable modulates the strength of excitatory synaptic currents, particularly NMDA conductance, and is updated according to Ca-dependent plasticity rules. The modifications introduced in later sections extend this model by allowing dynamic changes in synaptic efficacy, enabling the study of LTP and LTD in healthy and epileptic conditions. These NMDA currents modification are explicitly described in the following sections.

2.3 Implemented Neuroplasticity Models: Modifications to the PC Model

This section presents the implementation of two neuroplasticity models used in this study: the Shouval model and a novel Hybrid model that integrates features from the two plasticity models described in Section 1.4.3.

To incorporate synaptic plasticity, several modifications were introduced to the two and three compartments PC models. The most important changes involved (i) the integration of a synaptic efficacy variable (W), (ii) an extended formulation of Ca dynamics, and (iii) the modification of the NMDA receptor current to include synaptic efficacy. These modifications are common across implemented plasticity frameworks (Shouval and Hybrid models).

2.3.1 Main modification to the PC models

2.3.1.1 Modified Ca Dynamics

In the extended model, the I_{NMDA} was explicitly included as an additional source of Ca influx. The Ca-concentration now evolves according to:

$$\frac{dCa}{dt} = dc - \frac{Ca}{\tau_{Ca}} + \frac{0.0001}{\tau_{Ca}} + \frac{I_{NMDA}}{2F}$$
 (2.8)

Here, F is Faraday's constant (C/mol), ensuring unit consistency to express intracellular Ca-concentration in mM. Since I_{NMDA} is expressed in μ A/cm², the additional term provides the correct scaling to convert ionic current into concentration changes. This modification fundamentally links synaptic activity, specifically through NMDARs, to the intracellular Ca transients that drive plasticity.

2.3.1.2 Modified NMDA Current

The I_{NMDA} was also adapted to incorporate the dynamically evolving synaptic weight (W). The new formulation is:

$$I_{\text{NMDA_new}} = W \cdot I_{NMDA} \tag{2.9}$$

This modification thus establishes a direct mechanistic link: stronger synapses (higher W) produce larger NMDA-mediated Ca transients, which in turn influence the likelihood of subsequent potentiation or depression according to the selected plasticity rule.

2.3.1.3 Synaptic Efficacy Variable (W)

The synaptic efficacy, W, was introduced as a new dynamic state variable absent in the base model. Its temporal evolution is governed by equations directly adopted from established plasticity models. In the Shouval model, W evolves as a Ca-threshold dependent process, while in the Hybrid formulation, W exhibits bistability. In both cases, W is constrained between biologically plausible limits (0 and W_{max}), preventing runaway potentiation or depression. Overall, these common modifications establish the foundation upon which specific plasticity rules are implemented. By embedding W into both Ca dynamics and NMDA currents, the model ensures a closed feedback loop between synaptic activity, Ca signaling, and long-term changes in synaptic strength.

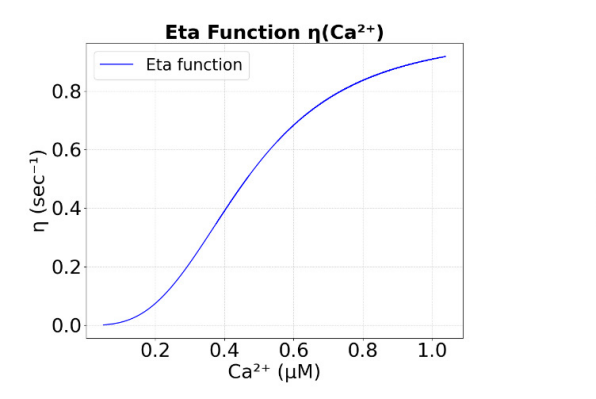
2.3.2 Shouval Neuroplasticity Model

Implementation of η and Ω -functions

The Shouval model, as introduced in Section 1.4.3.1, employs two central intermediate functions: the learning rate η -function (equation 1.3) and the calcium-dependent Ω -function (equation 1.4). Figure 2.2 represents the implemented Ω and η functions in this internship. The parameters were adapted directly from the Shouval model [8]:

Ω-function parameters: $Ω_0 = 0.25$, A = 1, B = 0.25, $\theta_d = 0.3$, $\theta_p = 0.55$, $\beta_1 = 80$, $\beta_2 = 80$.

η-function parameters: $P_1 = 0.1 \text{ s}, P_2 = P_1/10 - 4, P_3 = 3, P_4 = 1 \text{ s}.$



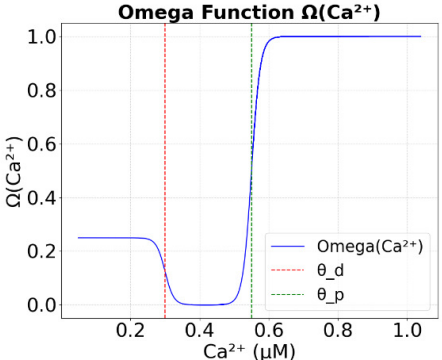


Figure 2.2: The implemented Eta $\eta(Ca^{2+})$ and $\Omega(Ca^{2+})$ functions in this thesis

Shouval Synaptic Efficacy Dynamics

The synaptic weight (W_j) for synapse j evolves over time according to the equation 1.2, which reflects the interplay between Ca-concentration and the Ω and η functions:

$$\frac{dW_j}{dt} = \eta([Ca]_j) \left(\Omega([Ca]_j) - \lambda W_j \right)$$

where $[Ca]_j$ is the Ca-concentration at synapse j and $\lambda = 1$ is a decay constant. This formula directly governs how the synaptic efficiency changes based on the local Ca levels.

2.3.3 Hybrid Neuroplasticity Model

In this work, we propose a new hybrid model of plasticity that combines the bistable synaptic efficacy of the Brunel model with the sigmoidal Ca dependence derived from the Shouval model's Ω -function. While similar concepts have been explored in neural mass models [62], our work applies this principle at the cellular level to capture neuron-specific plasticity processes.

Hybrid Model Synaptic Efficacy Dynamics

The synaptic efficacy dynamics in the Hybrid model was adapted from Brunel's formulation according to equation 1.8. However, instead of the original Heaviside functions for potentiation and depression, Shouval's continuous Ω -function is used:

$$\tau_w \frac{dW}{dt} = -W(1 - W)(W^* - W) + (1 - W)\Omega_p([Ca]) - W\Omega_d([Ca]) + \text{Noise}(t)$$
 (2.10)

where the potentiation (Ω_p) and depression (Ω_d) components are given by:

$$\Omega_p([Ca]) = A \cdot \operatorname{sig}([Ca] - \theta_p, \beta_2), \qquad \Omega_d([Ca]) = B \cdot \operatorname{sig}([Ca] - \theta_d, \beta_1), \tag{2.11}$$

The model parameters are the ones introduced in the original Brunel and Shouval models: $W^* = 0.5$, τ the time constant of synaptic efficacy changes happening on the order of seconds to minutes, A = 1 the potentiation rate, B = 0.25 the depression rate, $\theta_d = 0.3$ the lower threshold, $\theta_p = 0.55$ the upper threshold, and $\beta_1 = \beta_2 = 80$. This formulation allows for the characteristic bistable behavior of Brunel's model, while the continuous output of the Ω -function provides a smoother plasticity dynamic.

To enable a comparison between the implemented plasticity models (Shouval and Hybrid) and for compatibility reasons, the Ca and I_{NMDA} dynamics were implemented consistently with the Shouval model (according to Sections 2.3.1.1 and 2.3.1.2).

2.3.4 Epileptogenic Plasticity Parameterization

We introduced a pathological form of synaptic plasticity to represent epileptogenic conditions, hypothesizing that LTP becomes enhanced while LTD is diminished, reflecting the LTP/LTD imbalance reported in epilepsy [63]. The Ω -function used in both the Shouval and Hybrid models provides a direct means to simulate this pathological form of synaptic plasticity, where potentiation dominates over depression. To investigate both physiological and pathological forms of synaptic plasticity, the parameters of the Ω -function were systematically modified to represent conditions characteristic of epileptic networks.

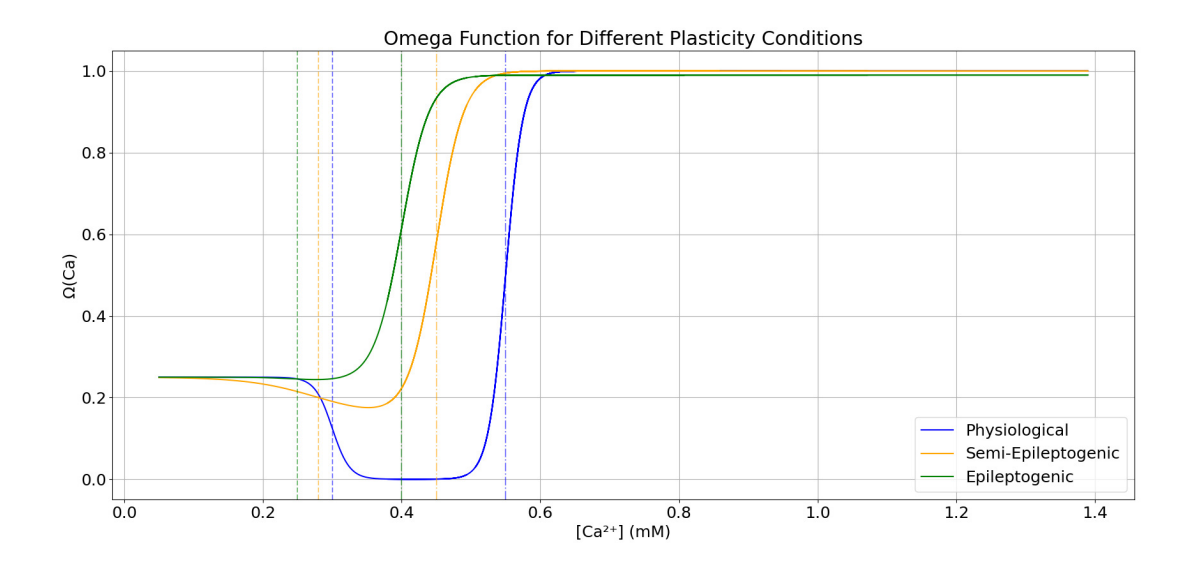


Figure 2.3: Ω-function for physiological (blue), semi-epileptogenic (yellow), and epileptogenic (green) conditions. The depression threshold was fixed at $\theta_d = 0.3$ for all three cases. The parameters were set as follows: physiological: $\theta_p = 0.55$, $\beta_1 = \beta_2 = 80$; semi-epileptogenic: $\theta_p = 0.45$, $\beta_1 = 20$, $\beta_2 = 50$; epileptogenic: $\theta_p = 0.4$, $\theta_1 = 40$, $\theta_2 = 50$.

By adjusting its parameters, it was possible to reproduce a pathological form of the Ω curve in which potentiation dominates and depression is suppressed. Specifically, altering
the slope parameters β_1 and β_2 around the thresholds allowed us to prevent the function
from dropping below baseline, thereby eliminating LTD induction. At the same time,
reducing the potentiation threshold θ_p enabled the generation of LTP even at relatively
low calcium concentrations. As illustrated in Figure 2.3, the epileptogenic condition was
obtained by decreasing both θ_p and the slope parameters β_1 and β_2 . This modification
increases the sensitivity of the system to calcium influx, facilitating LTP at lower calcium
levels. Consequently, LTD is strongly suppressed, and the model exhibits a bias toward
synaptic strengthening, reflecting the E/I imbalance and hyperexcitability observed in
epileptic networks.

2.4 Testing Framework

To validate and analyze the behavior of the implemented plasticity models, a standardized testing framework was employed. This involved simulations in small, controlled neural networks.

2.4.1 Network of Three Cells

A miniature neural network consisting of three PCs was constructed to test the fundamental Ca-dependent plasticity mechanisms. In this setup, one neuron (Cell 1) serves as the presynaptic source for the other two. A sufficiently high-intensity current $I_1(t)$ was injected into the soma of this source cell to generate an AP, which was then transmitted to the two postsynaptic neurons.

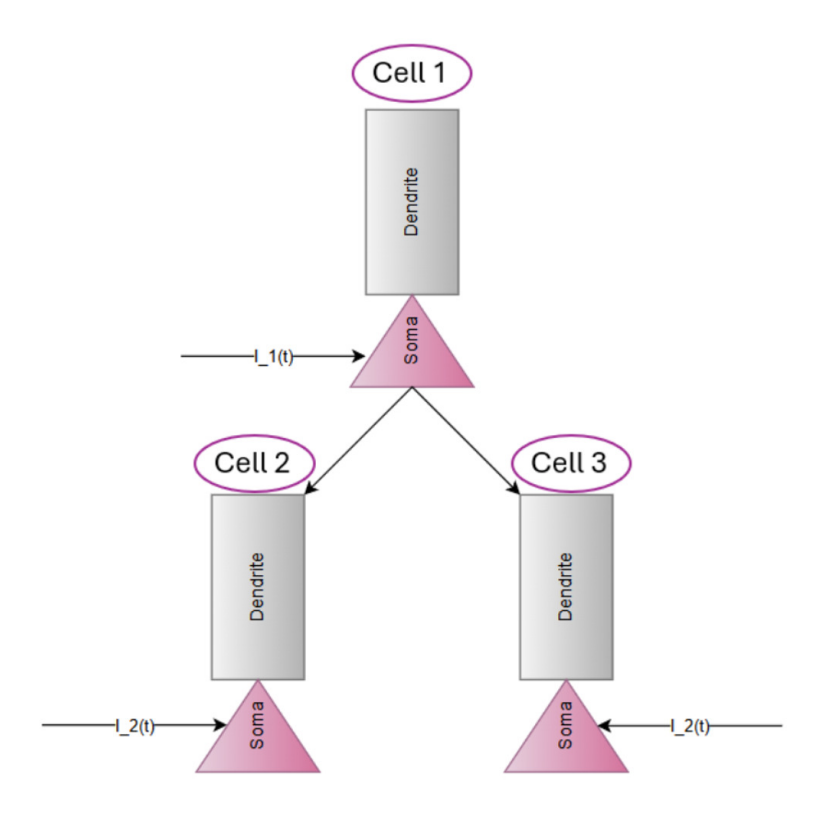


Figure 2.4: Overview of the simulated system to establish potential differences between the base and new model.

The postsynaptic Cell 2 simulated the "base" model (without plasticity), and Cell 3 simulated the "new" model (with the integrated Shouval or Hybrid plasticity). To ensure the postsynaptic cells were sufficiently depolarized to respond to synaptic input and enable plasticity induction studies, current $I_2(t)$ was also injected into their somas. Figure 2.4 illustrates the scheme adopted for our simulations, with the injected currents. Periodic stimulations were used, with a stimulation period (P) of 100 ms, and the Ca time constant (τ_{Ca}) was set to 100 ms. The synaptic weight was initialized at a baseline value of $W_0 = 0.25$, for the Shouval model, and $W_0 = 0.5$, for the Hybrid model with a maximum of 1. The depression and potentiation thresholds were set at $\theta_d = 0.3 \,\mu\text{M}$ and $\theta_p = 0.55 \,\mu\text{M}$, following Shouval's parameters for both the Shouval and Hybrid plasticity models.

2.4.2 Results

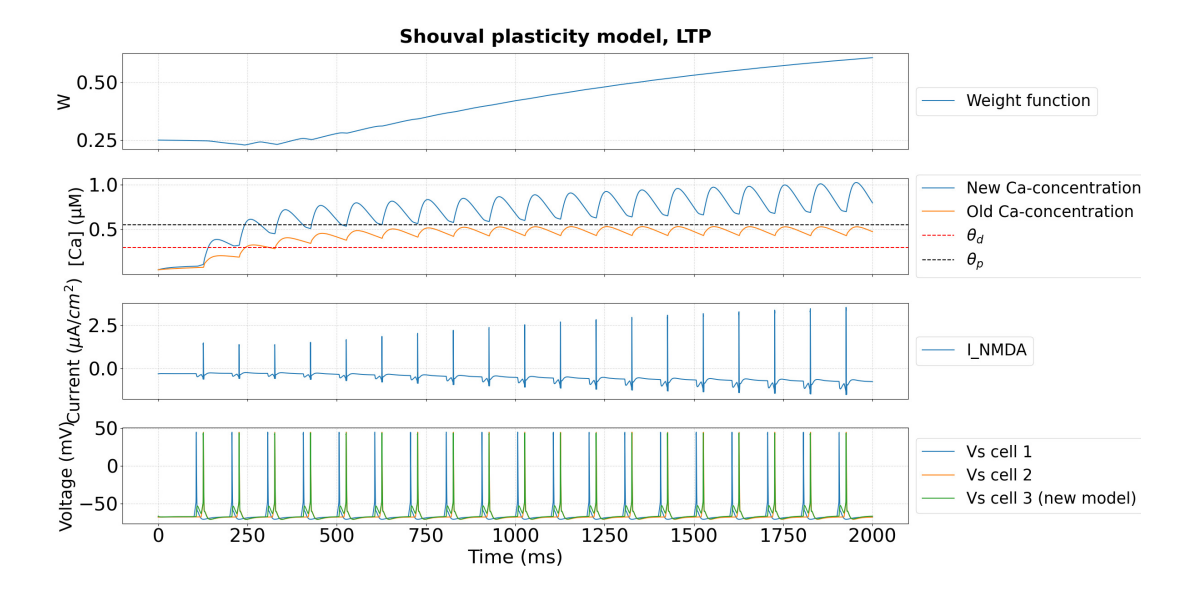
In this section, we present the results of stimulations across different plasticity models.

2.4.2.1 Simulating LTD and LTP: Shouval Model

As previously mentioned, according to the Shouval model: **No plastic changes:** occur if the Ca-concentration remains below the depression threshold (θ_d) , i.e., the synaptic efficacy and the output of the Ω -function would remain unchanged. **LTD Induction:** Induced when there is a moderate increase the Ca-concentration, while remaining within the depression and potentiation thresholds $(\theta_d \text{ and } \theta_p)$. This results in a decrease of synaptic efficacy, driven by a decrease in the output of the Ω -function. **LTP Induction:** If the Ca-concentration exceeded the upper threshold (θ_p) , particularly due to accumulation from high-frequency stimulation (where new APs arrived before Ca levels dropped), the Ω -function increased, leading to LTP induction and an increase in synaptic efficacy towards its maximum value of 1.

LTP and LTD were generally induced using higher or lower stimulation frequencies, respectively. The **stimulation parameters** were set as follows: for LTP induction, the stimulation period was P = 100 ms (f = 10 Hz), while for LTD induction, it was P = 200 ms (f = 5 Hz). The amplitude of the injected current was I = 40 mA, with an inter-stimulus interval of $\Delta t = 20$ ms between injections into cell 2 and cell 3. The calcium decay time constant was $\tau_{\text{Ca}} = 100$ ms.

As shown in Figure 2.5, our implementation of the Shouval model successfully reproduced intracellular Ca-dependent plasticity, accurately inducing both LTP and LTD induction. In the plots, the **Shouval plasticity model** is represented by variations in synaptic weight, intracellular Ca concentration (blue), and the membrane potential of cell 3 (green).



(a) LTP-Induction

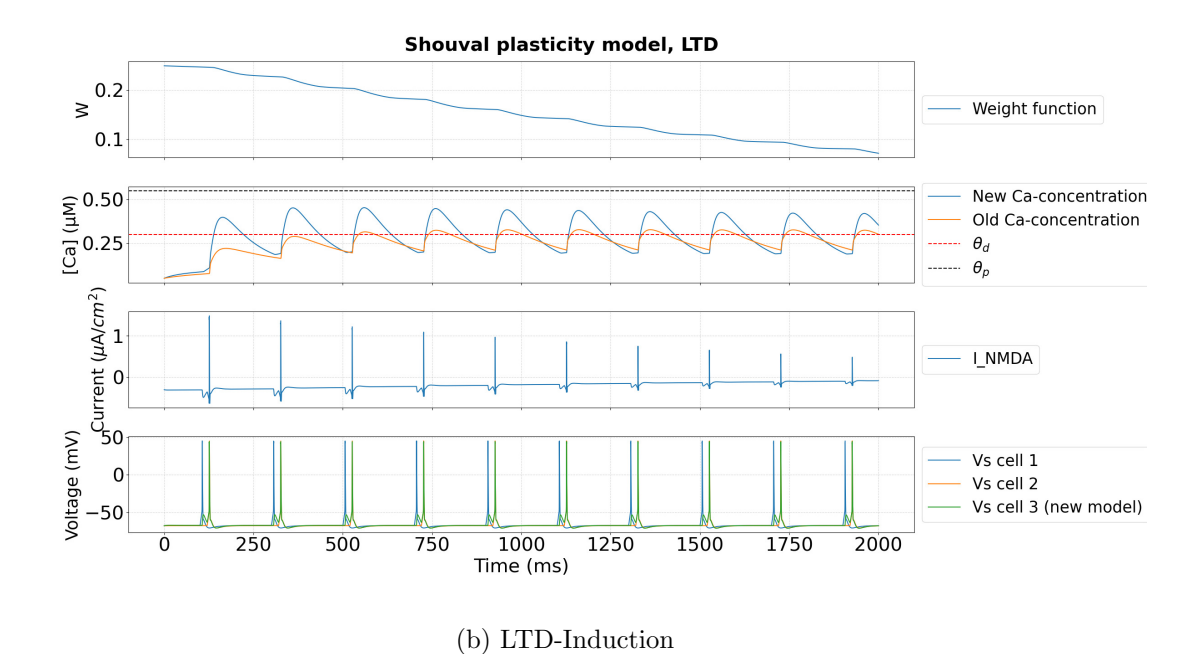


Figure 2.5: This figure illustrates a graphical display with four boxes, which allows better visualization of the direct link between the variables. The top box represents the variation in synaptic weight associated with the new model. The second box shows the intracellular Ca-concentration related to cell 2: base model (blue) and cell 3: Shouval plasticity model (orange). The third box shows the $I_{\rm NMDA}$ current in cell 3, and the fourth shows membrane potentials of all three cells, with APs of the base model in orange, and the Shouval plasticity model in green. (a): LTP-Induction, (b): LTD-Induction.

The two figures above compare the behavior of the base model (Cell 2), and the Shouvalplasticity model (Cell 3). Initially, since the system was at rest, there was no stimulation and the Ca-concentration remained below the depression and potentiation thresholds. In accordance with the properties described by [8], the synaptic weight W remained constant because the Ω -function is also constant.

Synaptic efficacy began to rise when the Ca-concentration exceeds the depression threshold $\theta_d = 0.3 \ \mu\text{M}$. The first postsynaptic AP in cells 2 and 3 occured around t = 150 ms, leading to a Ca-concentration increase between 0.3 and 0.55 μM . Within this range, the function Ω decreased, corresponding to a reduction in synaptic weight. As long as Ca remains between these thresholds, the synapse undergoes long-term depression (LTD).

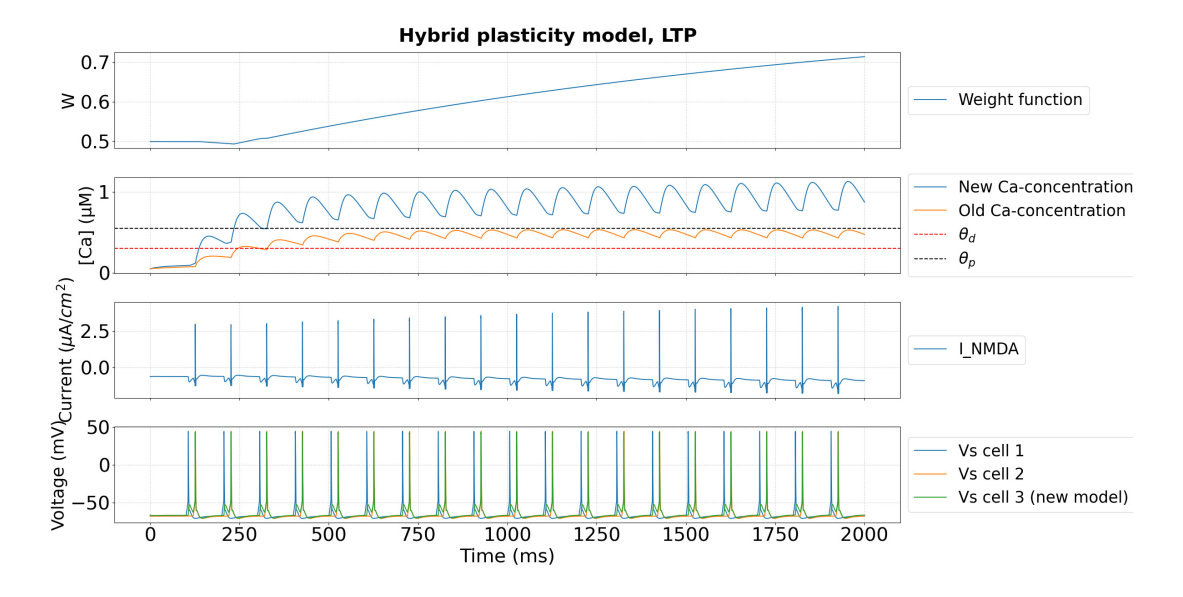
In the LTP protocol (Figure 2.5-a), the stimulation frequency is higher (f = 10 Hz). Here, Ca does not have time to return to its pre-stimulation baseline between spikes, leading to progressive accumulation. Eventually, the Ca-concentration crosses the potentiation threshold, causing Ω to rapidly approach its maximum, and synaptic weight to converge toward its upper bound ($W_{\text{max}} = 1$), I_{NMDA} starts to increase as well.

In contrast, in the LTD protocol (Figure 2.5-b), the stimulation frequency is lower (f = 5 Hz), allowing Ca levels to decay towards baseline before the next AP. This explains why Ca level stays within the threshold range and never exceeds the potentiation threshold, there is insufficient Ca accumulation. As a result we have a decrease in Synaptic efficacy W and consequently I_{NMDA} decrease.

2.4.2.2 Simulating LTP and LTD: Hybrid Model

The implemented Hybrid model was also validated in the three-cell network, successfully producing both LTP and LTD based on Ca levels relative to its thresholds. Its mechanism, relying on the bistable equation (2.10) and the Ω -function equation (2.11), ensures that synaptic efficacy transitions between discrete states (UP or DOWN), once the Ca signal crosses the specific potentiation (θ_p) or depression (θ_d) thresholds. When Ca levels are sustained above θ_p , potentiation terms dominate, pushing the synapse towards the UP state. Conversely, when Ca levels are predominantly between θ_d and θ_p , depression terms lead to the DOWN state. Below θ_d , the influence of the plasticity terms diminishes, and the bistable term guides the synapse towards its stable fixed points.

In the following simulations, the **stimulation parameters** are as follows: for the LTP induction, the stimulation period is $P=100~\mathrm{ms}$ ($f=10~\mathrm{Hz}$), whereas for the LTD induction, it is $P=200~\mathrm{ms}$ ($f=5~\mathrm{Hz}$). The amplitude of the injected current is $I=60~\mathrm{mA}$, with an inter-stimulus interval of $\Delta t=20~\mathrm{ms}$. The Ca decay time constant is set to $\tau_{\mathrm{Ca}}=100~\mathrm{ms}$.



(a) LTP-Induction

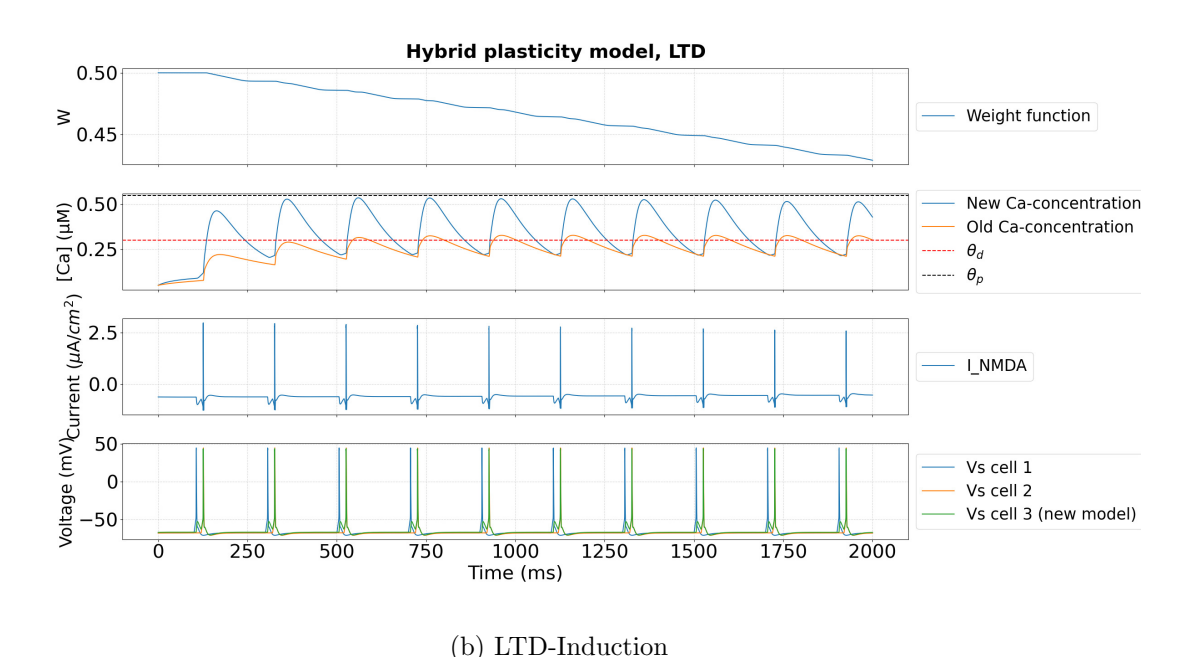


Figure 2.6: Visualization of LTP and LTD Induction in the Hybrid plasticity model, using the same four-box plot as Figure 2.5 to depict synaptic weight, intracellular calcium concentration, NMDA current, and membrane potentials. (a): LTP-Induction, (b): LTD-Induction.

As illustrated in Figures 2.6, the Hybrid model exhibits Ca-dependent synaptic plasticity consistent with theoretical predictions. Initially, in the absence of APs, the system remains at rest, and the intracellular Ca-concentration stays below both the depression and potentiation thresholds. Consequently, there is no change in synaptic efficacy or in the NMDA-mediated current, $I_{\rm NMDA}$. Upon the arrival of the first AP at approximately 150 ms, the Ca-concentration begins to rise. During the LTP protocol (Figures 2.6-a),

the high-frequency stimulation ($f = 10 \,\text{Hz}$) leads to a cumulative increase in intracellular Ca, surpassing the potentiation threshold and resulting in an increase of synaptic efficacy. Conversely, during the LTD protocol (Figures 2.6-b), the lower-frequency stimulation ($f = 5 \,\text{Hz}$) allows Ca to decay between successive APs, keeping its concentration primarily within the depression range and inducing a decrease in synaptic strength.

These results demonstrate that the novel Hybrid model effectively captures Ca-dependent synaptic plasticity, reproducing both LTD and LTP induction in a frequency-dependent manner, in agreement with the theoretical framework of both Brunel and Shouval plasticity models.

2.4.3 STDP Testing in Two-Cell Networks

As discussed in Section 1.3.2.2, STDP is a fundamental form of synaptic plasticity where the precise temporal interval and order between presynaptic and postsynaptic APs dictate the sign and magnitude of long-term synaptic change. To investigate STDP, a simplified two-neuron setup was employed: one presynaptic and one postsynaptic cell. Controlled stimulations, denoted as $I_1(t)$ for the presynaptic neuron and $I_2(t)$ for the postsynaptic neuron, were delivered to their somas to elicit single spikes per trial (Figure 2.7). A parameter $\Delta t_{stim} = t_1 - t_0$ defined the timing difference between stimulation injections.

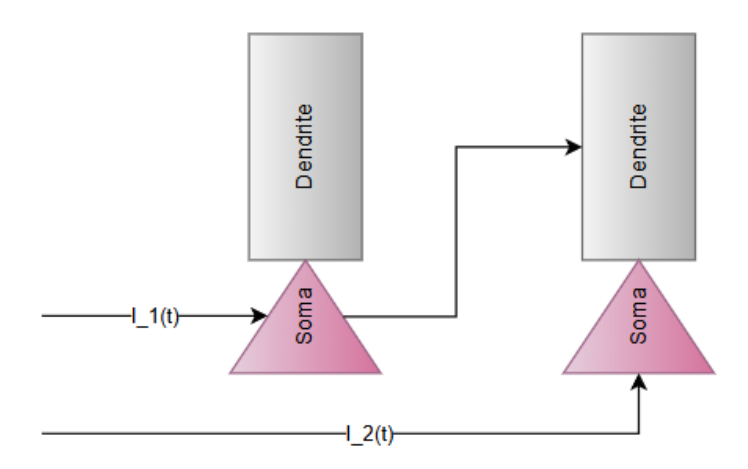


Figure 2.7: Configuration used for STDP verification.

A Delta-t spike detection function was used to calculate the exact time difference $(\Delta t_{\rm spike} = t_{\rm post} - t_{\rm pre})$ between the actual presynaptic and postsynaptic APs, allowing for precise measurement of synaptic weight changes. The initial synaptic weight was set to 0.25 in the case of Shouval and 0.5 in the case of Hybrid model.

2.4.3.1 Shouval Model

The Shouval model successfully reproduced a physiological STDP curve characterized by distinct phases. At a stimulation frequency of 3 Hz (Figure 2.8, Orange curve), the curve exhibited three distinct regions across the interval $\Delta t_{\rm spike} \in [-50, 50]$. Initial Depression: For negative spike-timing differences $(-50 \le \Delta t_{\rm spike} \le -7 \text{ ms})$ where the postsynaptic action potential preceded the presynaptic action potential, the model produced LTD. Potentiation Phase: This was followed by a potentiation phase for spike-timing differences close to zero (about $-7 \le \Delta t_{\rm spike} \le +7 \text{ ms}$), corresponding to LTP. Late Depression Phase: Finally, for positive spike-timing differences (about $+7 \le \Delta t_{\rm spike} \le +50 \text{ ms}$), a second depression phase was observed. As demonstrated, the larger the absolute value of $\Delta t_{\rm spike}$, the smaller the amplitude of depression, with the synaptic weight tending towards its baseline or initial value. This pattern reflects the principle that neurons firing with closely aligned spike times undergo potentiation, while neurons with firing times that are further apart, undergo synaptic depression.

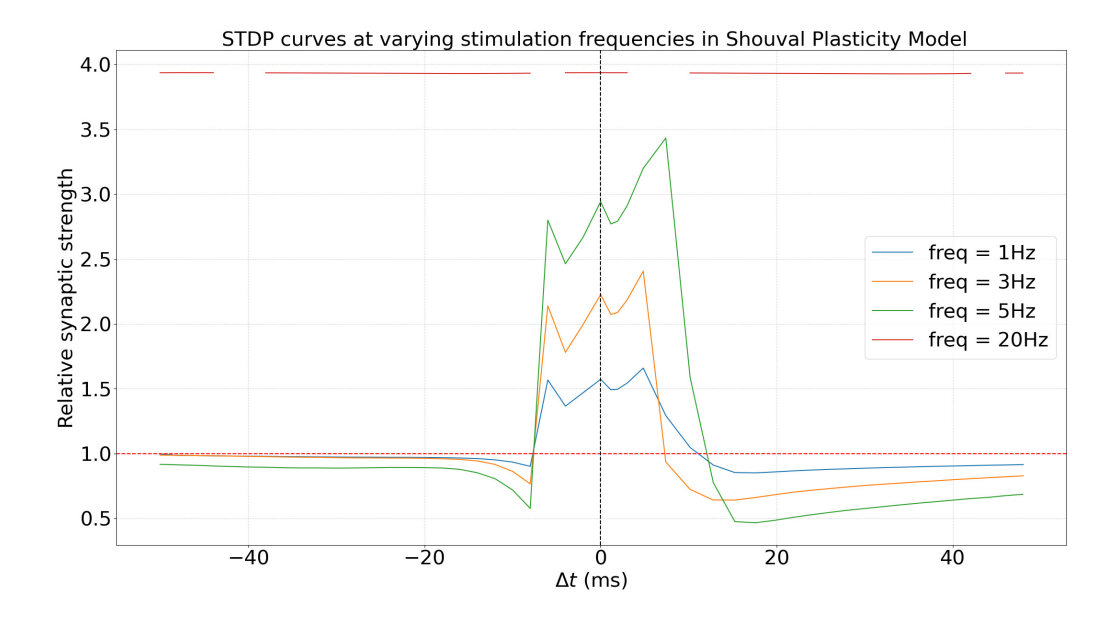


Figure 2.8: This figure illustrate the triphasic profile of STDP under shouval plasticity. The impact of frequency on Shouval-based STDP is also demonstrated under 1,3 and 5 HZ

The impact of stimulation frequency on STDP

The impact of stimulation frequency on STDP was also investigated (e.g., at 1, 3, 5, and 20 Hz). As we can see in Figure 2.8, higher frequencies generally resulted in greater amplitudes of both potentiation and depression phases. For excessively high frequencies, such as 20 Hz (red line in the figure), the STDP curve tended to level off at its maximum synaptic

weight across all Δt_{spike} values, indicating a dominant potentiation.mThese results are in line with [8], suggesting that higher stimulation frequencies intensify synaptic plasticity by enhancing both the potentiation and depression components of STDP.

Epileptogenic Plasticity

As discussed in Section 2.3.4, pathological plasticity is modeled by adjusting the Ω -function parameters, including a decrease in the potentiation threshold θ_p and modifications to the slope parameters β_1 and β_2 , while keeping the depression threshold θ_d constant (Figure 2.3). These combined adjustments lower the Ca-level required for LTP induction and effectively suppress LTD induction, thereby enhancing potentiation sensitivity and suppressing LTD expression.

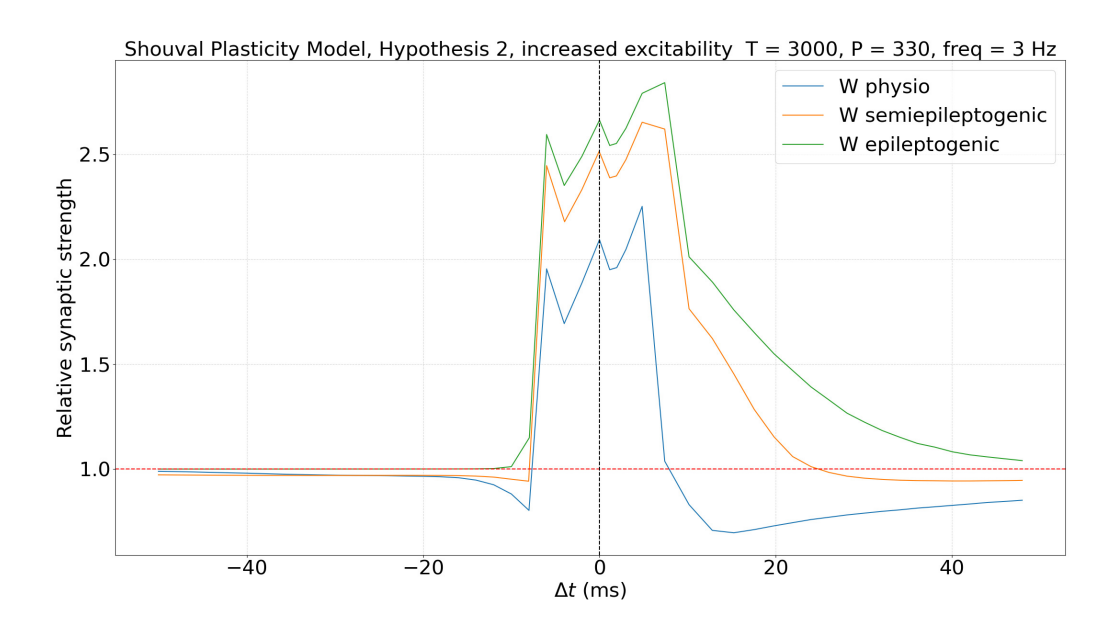


Figure 2.9: Shouval STDP profile across physiologic, semi-epileptogenic, and epileptogenic plasticity conditions.

As illustrated in Figure 2.9, under physiological condition ($\theta_p = 0.55$), the STDP curve exhibits a clear triphasic profile: an initial depression phase for negative spike-timing differences(Δt), followed by a central potentiation peak within a narrower temporal window, and finally a late-phase depression lobe at larger positive Δt . This balance between depression and potentiation is crucial for stabilizing synaptic weights.

In the semi-epileptogenic case ($\theta_p = 0.45$), the reduction of θ_p broadens the central LTP window, allowing potentiation to occur at lower Ca levels and over a wider range of spike-timing differences. Consequently, the first depression lobe is weakened, and the late-phase depression is shifted, resulting in an overall bias toward potentiation.

In the epileptogenic case ($\theta_p = 0.4$), the effect is even more pronounced: both depression lobes are strongly diminished, and the potentiation component dominates a large part of Δt domain. Thus, instead of the triphasic depression-potentiation-depression(DPD) profile observed physiologically, the epileptogenic plasticity curve collapses into a predominantly potentiation-driven shape. In practice, this means that even for large spike-timing differences, where physiological plasticity would normally induce LTD, the epileptogenic profile still produces LTP.

This transformation of the triphasic STDP curve into a predominantly LTP regime reflects a pathological destabilization of synaptic dynamics.

2.4.3.2 Hybrid Model

The Hybrid model also reproduced triphasic STDP curves in the two-cell setup (Figure 2.10). Importantly, its results closely matched those of Shouval model, confirming that the Hybrid formulation is capable of expressing the same canonical STDP features.

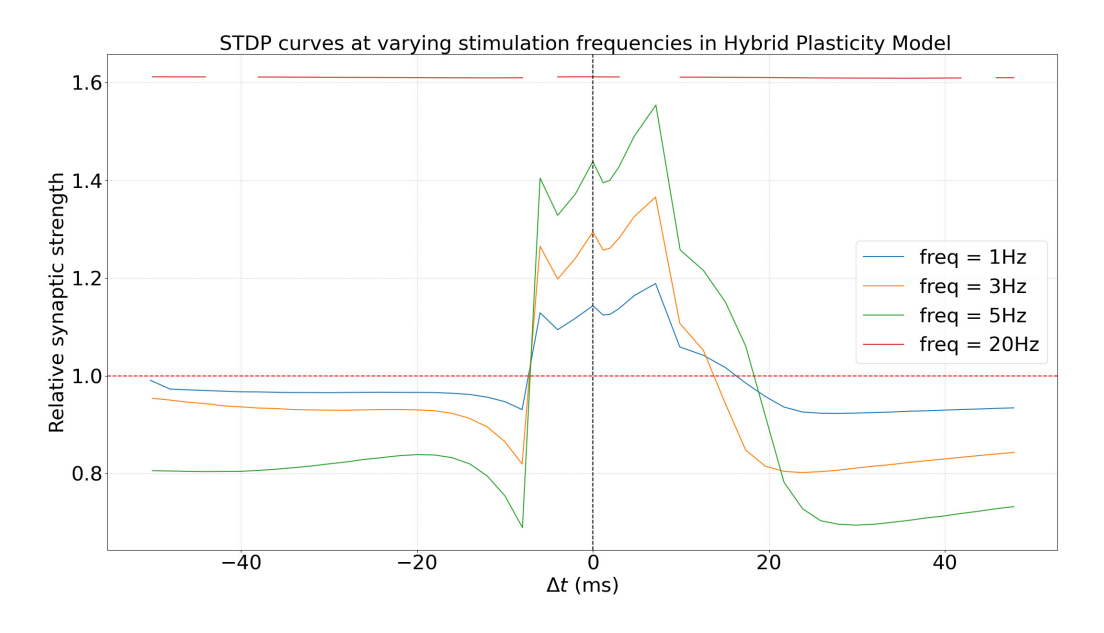


Figure 2.10: STDP curve generated by the Hybrid plasticity model.

The impact of stimulation frequency on STDP

The frequency dependence of STDP was systematically investigated in the Hybrid model at stimulation frequencies of 1, 3, 5, and 20 Hz. As demonstrated in Figure 2.10 Similar to the Shouval plasticity model, higher frequencies generally resulted in greater amplitudes of both potentiation and depression phases. The results demonstrate a clear modulation of the STDP profile by frequency. At low frequencies (e.g., 1–3 Hz), the Ca-concentration has

sufficient time to decay between spikes, leading to weaker potentiation. At intermediate frequencies (5 Hz), potentiation becomes more pronounced due to temporal summation of Ca transients. At excessively high frequencies (20 Hz), the Ca-concentration accumulates and remains consistently above the potentiation threshold. As a result, the STDP curve saturates at its maximal potentiation value across the full range of spike-timing differences $\Delta t_{\rm spike}$, effectively suppressing depression. This frequency dependence highlights how the Hybrid model captures key physiological features of Ca-dependent plasticity.

Epileptogenic Plasticity

Beyond frequency modulation, the Hybrid model was also evaluated under physiological and epileptogenic conditions by adjusting the parameters of the Ω -function, as described in Section 2.3.4. Specifically, the potentiation threshold θ_p was decreased and the slope parameters β_1 and β_2 were modified to suppress LTD, while the depression threshold θ_d remained constant. These adjustments increased the model's sensitivity to calcium transients, allowing LTP to be induced at lower calcium levels while effectively suppressing LTD.

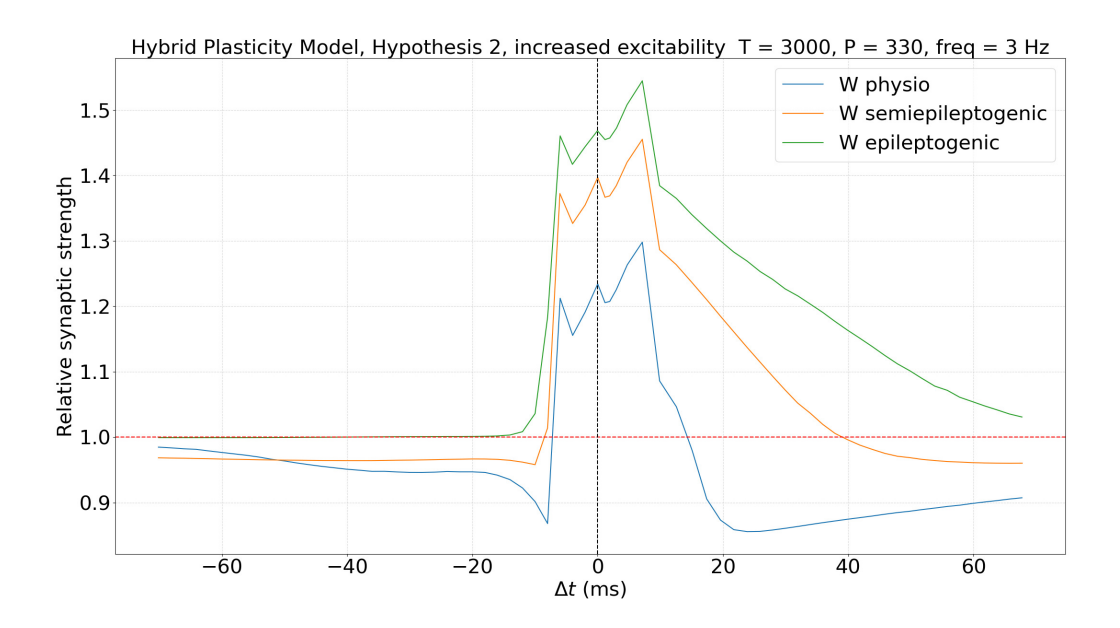


Figure 2.11: Hybrid STDP curve across physiological, semi-epileptogenic, and epileptogenic plasticity conditions.

As shown in Figure 2.11, only the physiological case exhibited a clear DPD profile. In contrast, for the semi-epileptogenic and epileptogenic conditions, the potentiation window broadened substantially, extending to larger spike-timing differences $\Delta t_{\rm spike}$. This behavior demonstrates how epileptogenic plasticity diminishes LTD expression and biases synaptic

modifications toward potentiation, consistent with the enhanced excitability observed in epileptic networks.

Overall, these results confirm that the Hybrid model not only captures physiological Ca-dependent STDP but also successfully reproduces epileptogenic alterations in synaptic plasticity by parameter shifts in the Ω -function. The loss of LTD and the expansion of the LTP domain provide a mechanistic explanation for how epileptogenic synaptic plasticity may contribute to hyperexcitability in epileptic circuits.

2.5 Discussion

In this chapter, we detailed the foundational methodological steps employed to integrate activity-dependent neuroplasticity into a two-compartment CA1 PC computational model. This process involved systematically modifying the biophysical framework of the PC model, including the integration of a new dynamic synaptic efficacy variable (W) and the extension of calcium dynamics to explicitly account for calcium influx through the NMDA receptor current (I_{NMDA}) . This setup established a closed feedback loop: synaptic activity generates I_{NMDA} , which modulates dendritic calcium signaling, and this calcium signal, in turn, governs the dynamic adaptation of the synaptic efficacy W.

A novelty introduced in this work was the development of a new neuroplasticity model, which was called **Hybrid plasticity model**. This model integrates features of two established frameworks introduced in this thesis. Specifically, it combines the continuous, graded calcium dependence of the Shouval model's Ω -function with the bistable synaptic dynamics derived from the Brunel framework. The inclusion of bistability is critical for maintaining long-term stability of synaptic states, preventing unbounded potentiation (runaway LTP) or excessive depression (runaway LTD), and thereby offering a potentially more physiologically plausible mechanism for sustained synaptic weight changes relevant to epilepsy modeling.

Initial validation confirmed the basic functionality and physiological relevance of both implemented models in small-scale networks. Both the Shouval and Hybrid models successfully reproduced canonical calcium-dependent plasticity features, including the induction of LTP and LTD in a frequency-dependent manner. Importantly, both frameworks captured the triphasic STDP profile observed physiologically. Additionally, by adjusting plasticity parameters through the modifications to the Ω -function, it was possible to simulate and characterize pathological plasticity. For instance, decreasing β_1 , β_2 (reducing depression) or decreasing θ_p (enhancing potentiation) shifted the STDP curve excessively toward LTP and suppressed LTD, providing a mechanistic explanation for the hyperexcitability observed in

epileptic circuits.

Based on the performed validation and the theoretical advantages of the Hybrid formulation, both the Shouval and Hybrid models were selected for large-scale computational studies. Extending from single-cell and small-network analyses to full-scale circuit simulations represents a critical next step. By incorporating these plasticity mechanisms into large-scale computational networks of the hippocampus and neocortex, this work aims to investigate how neuroplasticity shapes emergent epileptogenic activity and eventually how it influences the effectiveness of therapeutic interventions, such as tCS in epilepsy, in line with the objectives of the **GALVANI project**.

Chapter 3

Investigating the Impact of Calcium-Dependent Plasticity Models on Epileptiform Dynamics in the Hippocampal Network

3.1 Introduction

The hippocampus is one of the most critical brain regions implicated in the generation and propagation of epileptic seizures [64]. Computational models of hippocampal networks are a useful tool to systematically investigate the mechanisms underlying hyperexcitability and epileptiform activity. In this chapter, we extend previously developed plasticity models to a biologically inspired model of hippocampal CA1 network described in Section 1.4.2.1, with the dual objectives of:

- Inducing epileptiform dynamics by parameter modification, and
- Studying the influence of different neuroplasticity models for pathological states.

To achieve this, we first modify key synaptic and cellular parameters to simulate an epileptogenic hippocampal network. These modifications represent the altered excitation—inhibition imbalance and hyperexcitability that is characteristic of epileptic tissue. Once the epileptic network was established, we incorporated the two calcium-based synaptic plasticity models (Shouval- and Hybrid-model), one-at-a-time, into the network. The comparison of these models outcomes allows us to evaluate the influence of the plasticity model in simulating epileptiform discharges within the hippocampus.

3.2 Network Construction and Parameter Modulation Toward Epileptic States

The simulated hippocampal network consisted of 600 neurons, including 492 PCs and 108 interneurons, which were further divided into 36 basket (BAS), 36 bistratified (BIS), and

36 somatostatin-expressing (SST) interneurons. The cell placement and their connectivity patterns were directly adopted from [6]

3.2.1 Methods to Induce Epileptic Activity: Establishing Excitation/Inhibition Imbalance

The hippocampal network model used here reproduces the main physiological features of the CA1 subfield, comprising excitatory PCs and inhibitory interneurons (INs). To introduce epileptic activity capable of generating interictal epileptiform spikes (IESs), we followed the approach described in [6] by altering specific biophysical and synaptic parameters associated with both excitatory and inhibitory populations as well as external inputs. These modifications were implemented through the model's GUI, which allows systematic tuning of single-cell and synaptic properties. The general strategy was to increase pyramidal cell excitability while reducing inhibitory control from INs, thereby creating a hyperexcitable network state capable of generating interictal epileptiform events (IEEs) driven by a highly or quasi-synchronous external input. This shift mimics the E/I imbalance that is well established as a hallmark of epileptic networks. The impact of these modifications was evaluated by analyzing the firing rate (FR) of PCs and INs, and the morphological features of local field potentials (LFPs) and epileptic spikes.

3.2.1.1 Modification of Cellular and Synaptic Parameters

Pyramidal Cells: Based on [54, 5], the synaptic parameters of PCs were adjusted as follow:

- Increased Glutamatergic Excitability. Excitatory conductances g_{AMPA} were increased from 8 to 13 mS/cm²) and g_{NMDA} from 0.15 to 0.65.
- Reduced GABAergic Efficacy. E_{GABA} was shifted from its baseline value of -75 mV to -60 mV and the conductance of GABAergic synapses g_{GABA} was decreased from 25 mS/cm^2 to 20 mS/cm^2 .

Interneurons: the INs excitability was reduced by decreasing their AMPA conductance from 6 mS/cm² to 2 mS/cm². This modification weakens excitatory drive onto interneurons, thereby reducing their inhibitory output to PCs.

The combination of these parameter changes constitutes a systematic approach to modeling the transition from physiological to epileptogenic states within a biologically inspired hippocampal CA1 network.

3.2.1.2 External Stimulation Protocol

As mentioned earlier, a second requirement for simulating an epileptic network is providing a highly synchronous or quasi-synchronous input from the CA3.

- Stimulation Input: The model allows control over both the stimulation intensity and the number of stimulations delivered to each cell of the CA3 PCs. In this study, we used an injection intensity of $70 \,\mu\text{A/cm}^2$ with 10 stimulations per cell.
- **Jitter:** In the model's GUI (Figure 1.13-panel A), the jitter parameter controls the temporal variability in the arrival times of external input spikes, effectively determining the level of synchrony in the stimulation. A jitter value of 8 was chosen to deliver stimulations nearly simultaneously to all cells. Literature reports that lower jitter values (< 4 ms) yield higher synchrony and spike amplitude [5]; however, when combined with the modified parameters of the PCs and INs introduced in this work, such low values would produce unrealistically sharp epileptic spikes. To avoid this, a higher jitter value was selected, resulting in more physiologically realistic epileptiform discharges.
- Addition of Noise: To add variability to the stimulation pattern, a noise parameter with a fixed seed ensured reproducibility and physiological realism. The percent parameter in the GUI was set to 1 to introduce controlled noise across stimulations.

3.2.1.3 Inclusion of Neuroplasticity Parameters

For this work, the plasticity parameters were added directly to the parameter panel in the GUI, as shown in supplementary Figure 5.1, including:

- Type of plasticity. (0: No plasticity, 1: Shouval plasticity, 2: Hybrid plasticity)
- Initial value of synaptic efficacy. (W₀-Hybrid=0.5, W₀-Shouval=0.25, W₀-Noplasticity=0.5)
- Ω -function parameters. $(\theta_d, \theta_p, A, B, \beta_1, \beta_2, \Omega_0)$
- Synaptic efficacy time constant. (τ_W)

This implementation provides users with direct access to plasticity parameters, enabling real-time testing of different scenarios and facilitating systematic exploration of how various plasticity rules influence epileptic dynamics. The combination of a hyperexcitable neuronal network with high-intensity, quasi-synchronous external stimulation allows for the generation of realistic epileptic discharges as observed in the LFP.

3.2.2 Simulation Protocols

In our stimulations, each pyramidal cell received 10 current injections of 4 ms duration with an amplitude of 70 μ A/cm². A random seed of 5 ensured reproducibility of stimulation patterns across trials. The temporal jitter was set to 8 ms. Simulations lasted 5 s with a stimulation period of 100 ms and a sampling frequency of 25 kHz. All conditions, No plasticity, Shouval plasticity, and Hybrid plasticity were simulated using the same stimulation protocol. This ensured that observed differences in network activity could be attributed exclusively to plasticity rules rather than differences in external input.

3.3 Results

In this section, we present the impact of Plasticity Models on Neuronal and Network Dynamics.

3.3.1 Network Firing Patterns

The following figures present the overlapping firing traces of all 492 PCs under three conditions: No plasticity (Figure 3.1) served as a baseline, showing synchronous firing in a hyperexcitable network. Shouval plasticity (Figure 3.2) produced distinct changes in spike timing and synchrony, increasing pyramidal cells activity, and Hybrid plasticity (Figure 3.3) showed intermediate effects, with firing patterns more physiologically regulated than under Shouval plasticity. This qualitative comparison illustrates how plasticity mechanisms can amplify or regulate epileptiform dynamics.

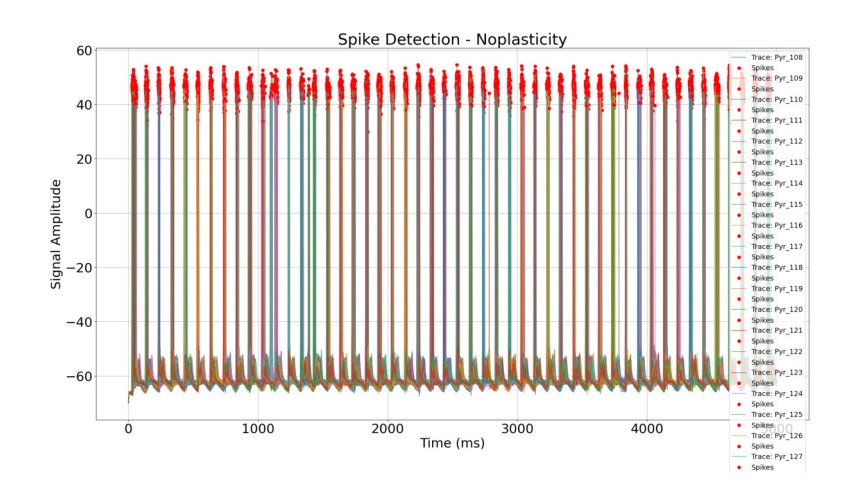


Figure 3.1: PCs AP spike detection _ No plasticity: This plot serves as a baseline to observe the firing patterns of PCs without dynamic synaptic weight changes, showing their synchronous firing activity in the induced hyperexcitable state.

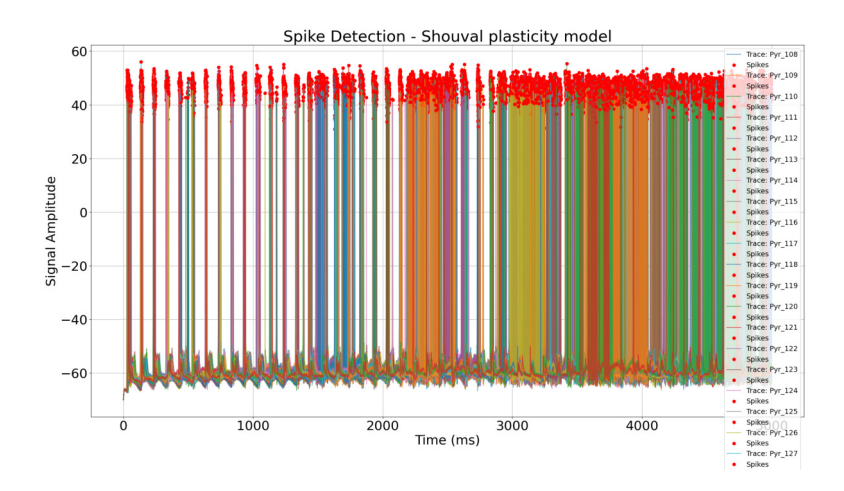


Figure 3.2: PCs AP spike detection _ Shouval plasticity: This figure presents a spike detection plot for PCs under the Shouval plasticity condition. As observed, Shouval plasticity results in excessively elevated firing activity of PCs, leading to reduced synchrony but increased overall spiking activity.

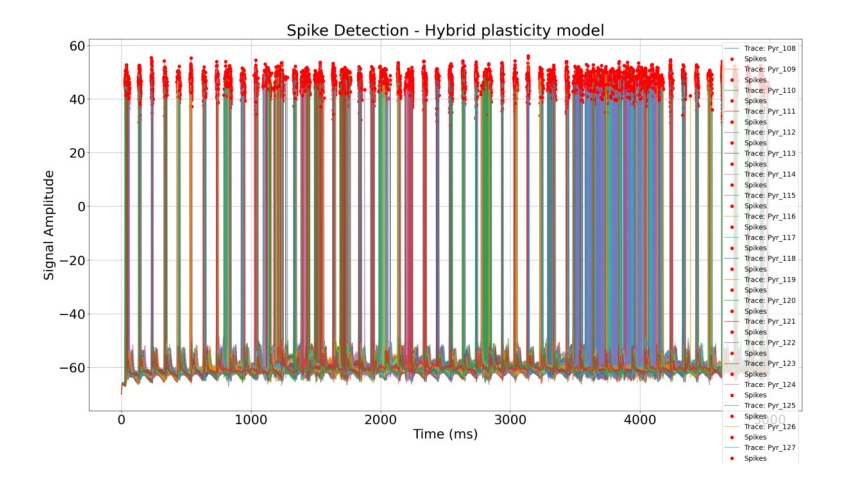


Figure 3.3: PC AP Spike Detection _ Hybrid Plasticity: This figure shows the spike detection results for PCs under Hybrid plasticity model. An increase in PCs firing is observed, but to a lesser extent than under the Shouval model, resulting in more realistic and physiologically plausible activity patterns.

By comparing these figures, one can observe how the implementation of Shouval and Hybrid plasticity models influences the firing pattern, synchrony, and overall activity of the PCs, particularly in the context of epileptic activity within the hippocampal network.

3.3.2 Analysis of Cellular and Population Activity

To complement visual inspection of spike rasters and firing patterns, we performed a quantitative analysis of network activity across different plasticity conditions. Specifically, we examined (i) FRs and spike amplitudes of PCs and INs, and (ii) LFP signals as a measure of population-level dynamics.

3.3.2.1 Pyramidal Cell Activity

The activity of PCs was first illustrated at the single-cell level. As shown in Figure 3.4, the representative trace from a single PC highlights the membrane potential fluctuations

and the detected APs. This provides a view of the firing dynamics of epileptic PCs and validates the spike detection method applied throughout the analysis.

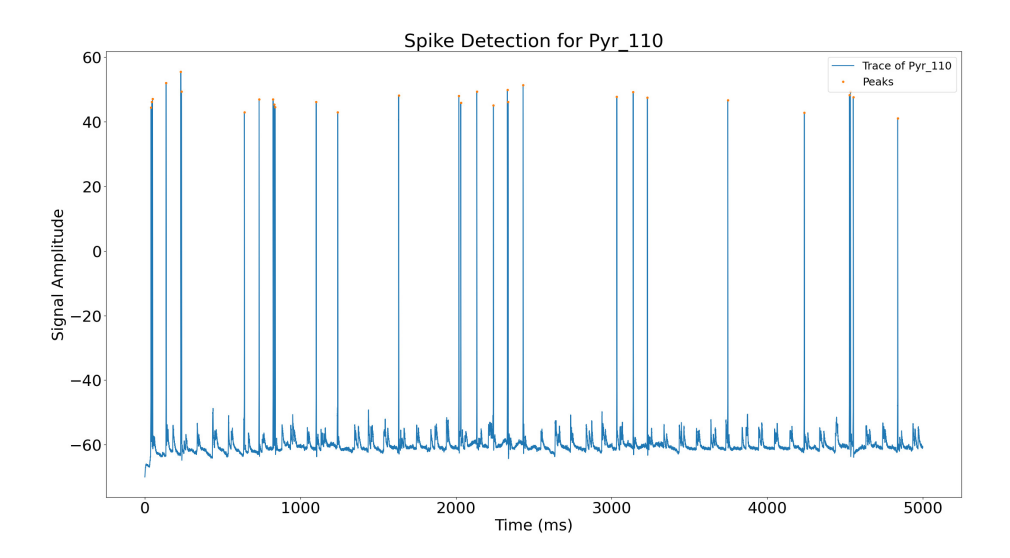


Figure 3.4: This figure displays the membrane potential of a single PC (Pyr_110) over time, with clear indications of detected individual spikes.

Firing Rate Analysis To quantitatively assess how plasticity influences neuronal activity, the FRs of PCs were compared across the three conditions (No plasticity, Shouval plasticity, and Hybrid plasticity). As summarized in Figure 3.5, the FR distributions show notable differences between groups.

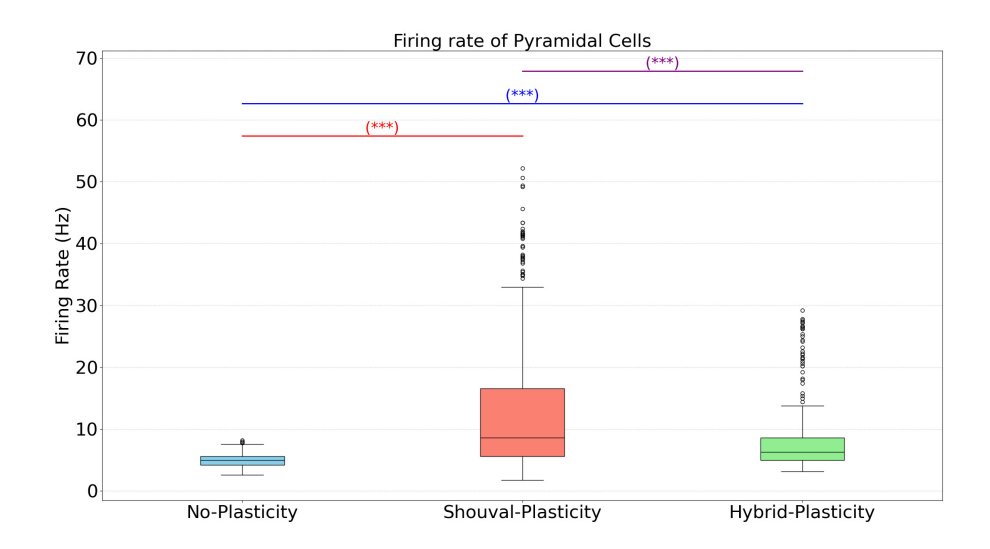


Figure 3.5: Comparison of PC firing rates across three plasticity conditions: "No plasticity," "Shouval plasticity," and "Hybrid plasticity," showing a very highly significant difference between the groups (***) Asterisks indicate statistically significant differences between conditions: * for p < 0.05, ** for p < 0.01, and * * * for p < 0.001.

The baseline mean FR of PCs (4.95 Hz) shows a pronounced increase under Shouval plasticity (13.40 Hz) and a more moderate elevation with the hybrid model (8.10 Hz). The higher spiking frequency observed with Shouval plasticity suggests that this rule strongly enhances excitability, but the effect appears exaggerated. In contrast, the hybrid plasticity condition produces a moderate increase in FR, reflecting a more balanced adjustment of activity. There were notable and statistically significant differences between the groups, as confirmed by the Mann–Whitney U test and indicated by the high significance levels (***), confirming that the underlying plasticity mechanisms can directly modulate spiking frequency in an epileptic context.

Amplitude Analysis In addition to the FR analysis, the amplitudes of PCs' APs were examined (refer to Figure 5.3 in supplementary). Analysis revealed that the mean amplitudes remained almost unchanged (No plasticity: 95.95 mV; Shouval plasticity: 95.67 mV; Hybrid plasticity: 96.23 mV). This indicates that while the implemented plasticity models strongly affect firing frequency, their impact on the amplitude of APs is negligible. Thus, the primary influence of plasticity in these simulations lies in modulating the firing rate rather than altering the intrinsic magnitude of neuronal responses.

3.3.2.2 Interneuron Activity

Since INs play a critical role in regulating network excitability and maintaining the balance between excitation and inhibition, examining their firing patterns under the different plasticity conditions provides important complementary insight into the overall dynamics of the epileptic network. In the simulated hippocampal network, the plasticity is integrated only into PCs, and the excitatory connections exist from PCs to BAS and SOM INs, while BIS cells are not directly connected to PCs. This structural difference plays a key role in shaping how plasticity influences IN firing. As BAS and SOM INs are directly driven by PC activity, their firing patterns are expected to closely reflect changes in PC excitability. In contrast, BIS INs receive identical inputs (External Stimulation (CA3)) across conditions, and therefore display a more stable firing dynamics regardless of the plasticity mechanism.

BAS interneurons

Similar to PCs, the activity of BAS cells as a representative of INs was first assessed at the neuron level (Supplementary Figure 5.4), showing a spike trace for a single BAS neuron, highlighting its individual firing pattern and validating spike detection in this inhibitory population.

Firing rate analysis: As shown in Figure 3.6, BAS FRs increase most under Shouval plasticity, reflecting the strong excitatory drive from PCs, which are themselves hyperactive in this condition. The hybrid plasticity rule leads to a moderate and more regulated increase. This demonstrates that interneuron excitability in the model is largely a downstream effect of pyramidal cell firing patterns. For comparison, the mean FRs of BIS cells across conditions are as follows: No plasticity: 8.99 Hz; Shouval plasticity: 21.84 Hz; Hybrid plasticity: 13.23 Hz.

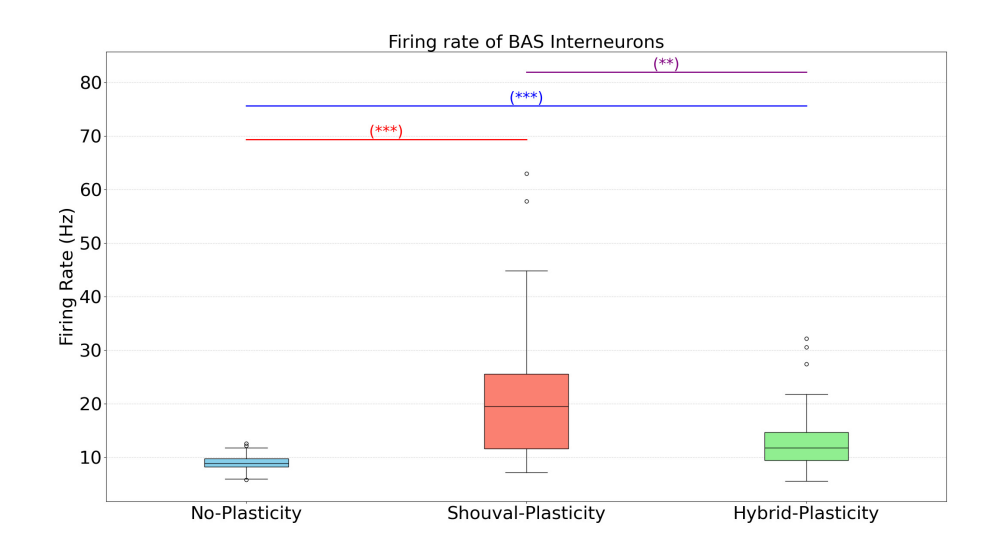


Figure 3.6: Firing rate distribution of BAS interneurons across conditions. BAS cells show the highest firing rate under Shouval plasticity, due to higher excitatory drive from PCs, whereas the hybrid model preserves a more physiological activity level.

SOM interneurons

Similar to BAS cells, SOM interneurons receive excitatory input from PCs.

Firing rate analysis: Figure 3.7 shows that SOM interneurons fire significantly more under Shouval plasticity. This is a direct consequence of PC hyperexcitability. The hybrid model also produced significantly higher FRs than baseline but lower than in the case of Shouval palsticity. This demonstrates that the effect of plasticity on SOM activity is indirect, mediated by changes in PC output. BIS cells' mean FRs for each condition are as follows: No plasticity: 16.56 Hz; Shouval plasticity: 28.44 Hz; Hybrid plasticity: 22.43 Hz.

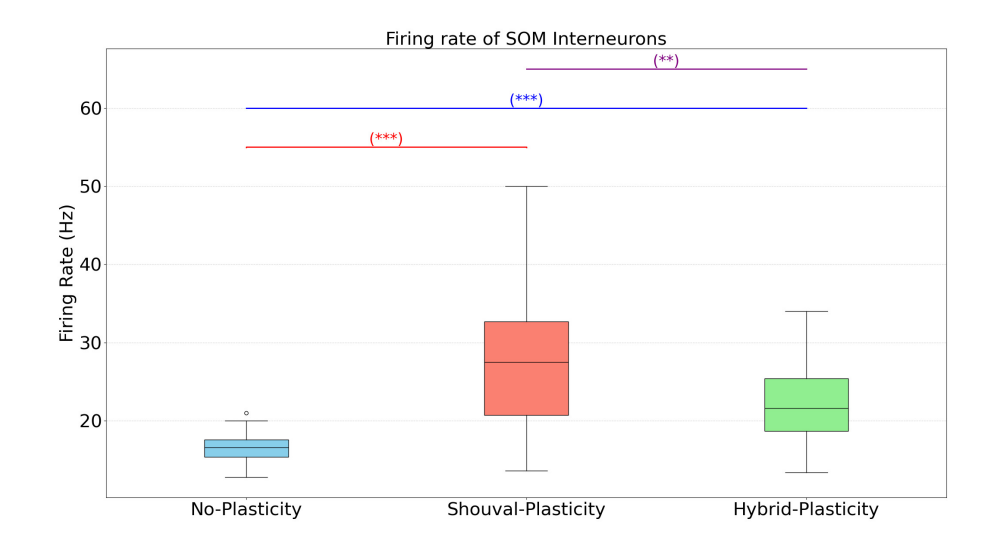


Figure 3.7: Boxplot of SOM firing rates under the three plasticity conditions. Shouval plasticity drives the highest increase, reflecting the excitatory influence of hyperactive PCs, while hybrid plasticity maintains a more balanced firing pattern.

BIS interneurons

As mentioned earlier, BIS interneurons do not receive excitatory input from PCs in CA1, but instead are driven directly by CA3. Because plasticity mechanisms were implemented only at excitatory PC synapses, BIS firing remains largely unaffected by changes in PC excitability. In contrast to BAS and SOM interneurons, which indirectly reflect plasticity through their excitatory drive from PCs, BIS activity is stable across all conditions. This is evident in Figure 3.8: the firing rate distribution (Figure 3.8) shows nearly identical values across all three plasticity conditions. This stability reflects the network connectivity of BIS interneurons and their independence from plasticity-induced changes in pyramidal cell activity.

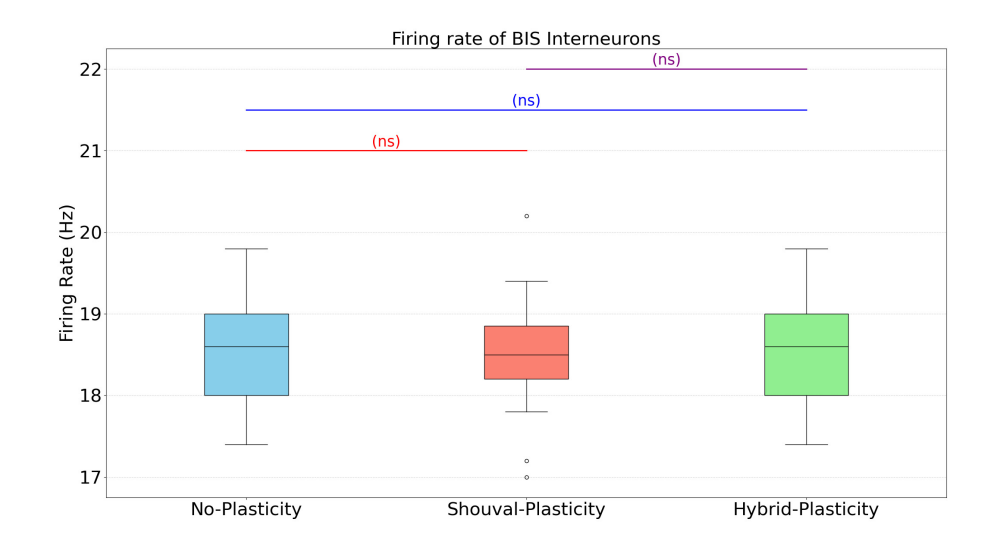


Figure 3.8: Firing rate distribution of BIS interneurons. No significant differences are observed, consistent with their lack of pyramidal cell input and the absence of plasticity in their model.

Summary of interneuron activity: Overall, the interneuron analysis highlights the role of network connectivity in shaping the impact of plasticity. BAS and SOM interneurons, which receive excitatory input from PCs, closely mirror PC dynamics and their FRs are significantly higher in the case of plasticity, reflecting PC hyperactivity. By contrast, BIS interneurons, which do not receive direct PC input, show nearly identical firing rates and amplitudes across all conditions. This confirms that plasticity exerts its primary influence on inhibitory populations indirectly, through its modulation of PC excitability. Statistical analysis further supports these observations. For BAS and SOM INs, changes in FRs across plasticity conditions are generally more pronounced and statistically significant. BIS interneurons show no significant differences in their FR across conditions, consistent with their stable input and the absence of plasticity in their synaptic model. Together, these results highlight that plasticity indirectly exerts a stronger influence on interneuron firing dynamics than on spike amplitude, and that this effect depends on the connectivity of each interneuron type within the network.

3.3.2.3 Local Field Potential (LFP) Analysis

LFP Traces LFP represents the summed transmembrane and synaptic currents within a neuronal population and serves as a mesoscopic indicator of collective network dynamics. It is widely used in both experimental and computational neuroscience to assess neural synchronisation and detect pathological activity, including epileptiform discharges.

In our experimental conditions, the network was configured to exhibit epileptiform activity capable of generating interictal epileptic spikes (IESs). This was achieved by making the network hyperexcitable and providing a strong and quasi-synchronous external input, which promoted the emergence of IESs. In our simulated hippocampal network, the LFP traces revealed clear differences across plasticity conditions (Figure 3.9). In the **baseline** (no plasticity), the network exhibited clear, high-amplitude IESs in the simulated LFP, reflecting strong synchrony among PCs and enhanced excitatory activity consistent with epileptiform dynamics. Over a stimulation duration of 5 seconds, a total of 38 IESs were detected

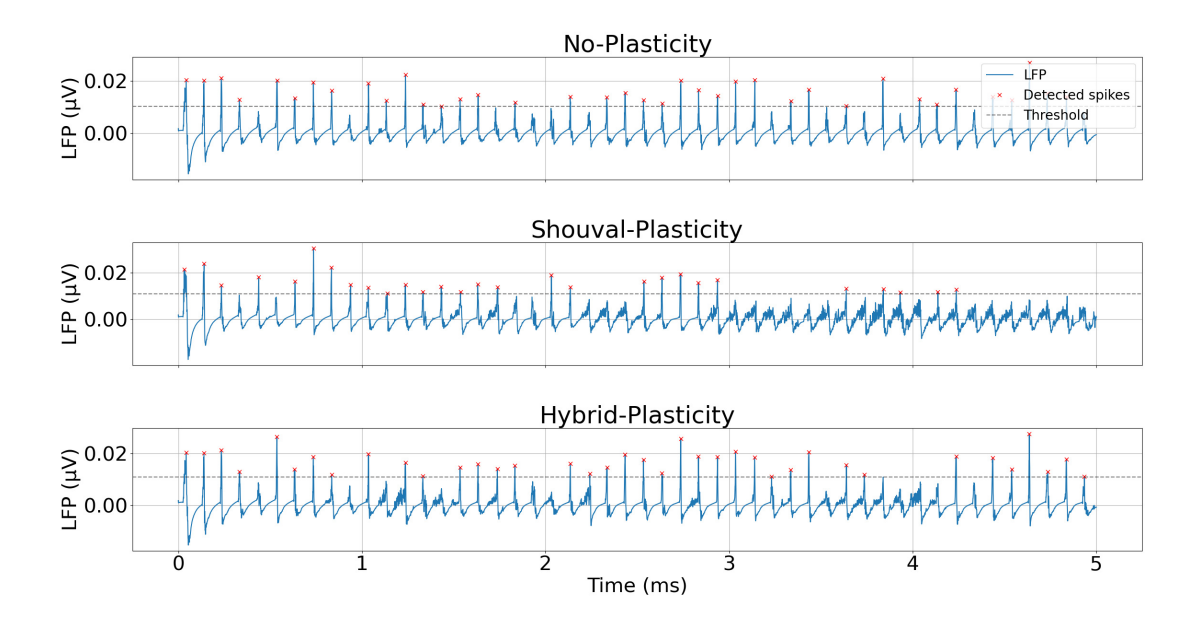


Figure 3.9: LFP recordings from the simulated epileptic hippocampal network under three different conditions: "No plasticity," "Shouval plasticity," and "Hybrid plasticity." Interictal-like spikes (IESs) and voltage fluctuations are shown over time, enabling a qualitative comparison of spike morphology, frequency, and network synchrony across the plasticity models.

However, upon introducing **Shouval plasticity**, the network dynamics changed markedly over time. During the initial seconds, the discharges resembled the baseline pattern, but as synaptic potentiation accumulated, the network became progressively more excitable (particularly evident in the final seconds of the simulation). This led to more frequent but fragmented discharges, marked by enhanced high-frequency activity. In this regime, the firing rate of pyramidal cells increased, yet global synchrony decreased—the neurons were so active that they tended to fire independently, no longer waiting for external input to trigger collective discharges. Consequently, the LFP spikes became smaller and less distinct, reflecting a desynchronized yet hyperexcitable network state. The number of IESs decreased to 28 under Shouval plasticity model. In contrast, the **Hybrid plasticity** model produced an intermediate dynamic profile. While overall excitability and firing rates increased compared to the baseline, the network continued to generate dis-

tinct, high-amplitude interictal-like spikes, indicating that population synchrony among PCs was largely preserved. Occasional bursts of higher-frequency activity reflected the elevated excitability of individual neurons, yet this did not disrupt the global synchrony required for collective discharges. These results suggest that the hybrid rule moderated the excessive synaptic potentiation seen with Shouval plasticity, maintaining a balanced regime that preserves both network stability and physiologically realistic spike generation. Hybrid plasticity preserved the same number of IESs as observed in the baseline condition.

Total LFP Energy: To quantify these effects, we computed the total LFP energy as the integral of the squared signal amplitude over time, representing the total power of the activity within the signal. Higher LFP energy values indicate more widespread or sustained population activity, which is often associated with pathological states. As shown in Figure 3.10, both Shouval and Hybrid plasticity led to increased LFP energy compared to the no-plasticity condition. Importantly, Shouval plasticity produced the highest energy values, consistent with the qualitative observation of increased PC and high-frequency activities. The Hybrid model also enhanced LFP energy relative to baseline but to a lesser extent, suggesting that while plasticity promotes pathological sate, its effect depends strongly on the underlying plasticity rule.

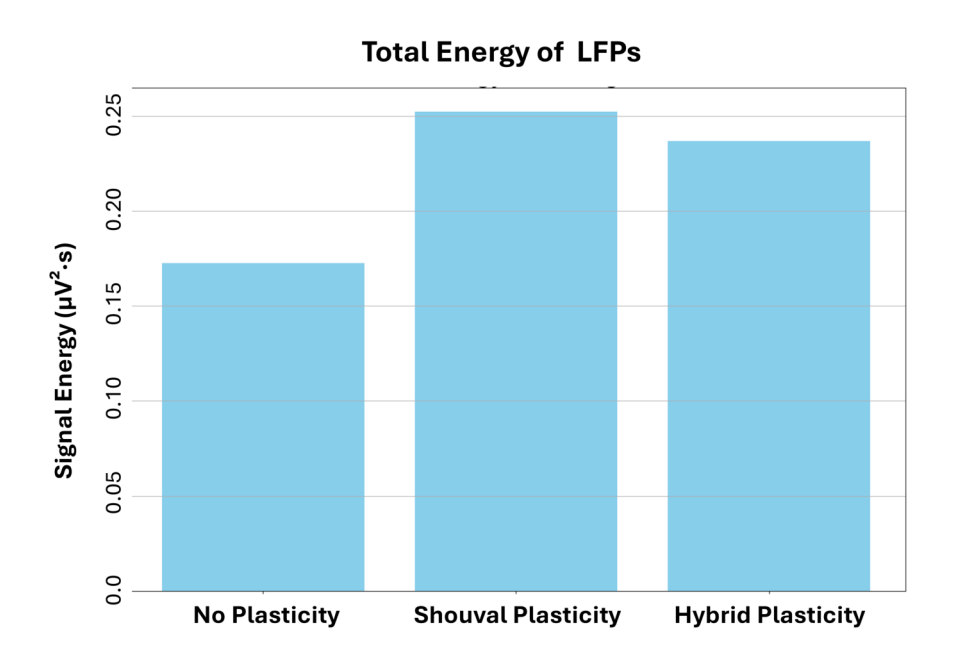


Figure 3.10: Total energy contained within the LFP signal across plasticity conditions. LFP energy provides a global measure of the magnitude and persistence of synchronized population activity.

Taken together, these results show that the inclusion of synaptic plasticity substantially reshapes network dynamics. While Shouval plasticity induces excessive hyperex-

citability and loss of coordinated synchrony, the Hybrid model preserves a more organised and physiologically realistic pattern of activity, representing a more balanced—though still pathological—network state.

3.4 Discussion

This chapter explored how two calcium-based plasticity models, Shouval and Hybrid, influence the dynamics of a hippocampal CA1 network in an epileptiform state. By enhancing PCs' excitability, reducing inhibitory drive, and applying strong external stimulation, the network was shifted into a hyperexcitable regime that produced biologically relevant epileptiform discharges. The resulting activity provided a suitable framework for assessing how plasticity rules alter cellular behaviour and network-level synchronisation.

At the level of PCs, both plasticity models increased excitability relative to the baseline, but in different ways. Shouval plasticity strongly amplified FRs, which were accompanied by more asynchronous spiking and reduced LFP amplitudes. In contrast, the Hybrid model produced a moderate increase in FRs while maintaining amplitudes closer to baseline, suggesting a more coherent adjustment of activity.

The effects on interneurons followed the same logic, as their firing depended on excitatory input from PCs. BAS and SOM cells mirrored pyramidal dynamics: they showed the highest FRs under Shouval plasticity and more moderate increases under the Hybrid model, with spike amplitudes declining most in the Shouval condition. BIS interneurons, which do not receive direct pyramidal input in the model, remained stable across all conditions. This pattern confirmed that the observed changes in inhibition were secondary to the modulation of pyramidal output.

LFP showed that plasticity markedly reshaped network dynamics. Without plasticity, the network produced sharp, periodic epileptiform spikes, whereas Shouval plasticity gradually led to premature discharges, reduced synchrony, and a noisier signal with fewer large-amplitude events. The Hybrid model showed reduced synchrony but preserved spike features that are closer to physiological patterns. This suggests that the Hybrid rule partially constrained the excessive potentiation observed with Shouval plasticity, producing a more realistic regime that balances excitability and stability. Energy analysis confirmed that both rules enhanced global network activity compared to baseline, with Shouval driving the strongest, and the Hybrid model supporting a more balanced amplification.

Together, these results demonstrate that the form of plasticity embedded in the network strongly determines how hyperexcitability evolves. These insights validate the Hybrid model as a more physiologically consistent framework for studying synaptic plasticity in epileptic networks. Building on this foundation, the next chapter applies these plasticity mechanisms to neocortical circuits, enabling broader exploration of how plasticity influences epileptiform activity and how it may interact with interventions such as transcranial direct current stimulation (tDCS) within the GALVANI project.

Chapter 4

Modeling of Neuroplasticity in the Neocortical Network

4.1 Introduction

Building upon the analysis of plasticity's impact within the hippocampal CA1 network, this chapter shifts focus to the neocortical microcircuit, utilizing the NeoCoMM platform. We do the same procedure as in Hippocampus with the primary objective of integrating the validated Hybrid plasticity model into the neocortical microcircuit. The new version of NeoCOMM will be used to investigate how plasticity influences epileptogenic dynamics in cortical column models adapted from human, rat, or mouse data. Moreover, this work directly addresses the GALVANI project's aim to explore how tACS and tDCS modulate these plasticity-driven dynamics, with the goal of predicting and optimizing their suppressive effects on pathological activity.

4.2 Network Model and Epileptic State Induction

4.2.1 Network Model

As outlined in Section 1.4.2.2, the NeoCoMM platform provides a framework for realistic microscale simulations of neocortical networks at the cellular level. In this study, it is adapted to match human cortical column dimensions and cell type distributions. The model represents a single neocortical column spanning all six layers, including 1,895 cells in total, comprising 1,454 pyramidal cells and 441 interneurons, with cell distributions across layers and synaptic connectivity implemented as described in [5].

4.2.2 Epileptic State Induction

Similar to the methodology employed in the hippocampal network in Chapter 3, epileptiform activity in the neocortical network is generated through a combination of network parameter modulation and synchronous external stimulation. To induce a hyperexcitable state, characteristic of an epileptogenic tissue, an imbalance between excitation and inhibition needs to be present. Here, we focused exclusively on parameter adjustment of the PCs, which was sufficient, given that their structure and connectivity differ substantially from the hippocampal network. An epileptic tissue, characterised by a pathophysiological hyperexcitable network, and a synchronous input of afferent volleys of APs from the distant cortex (DC) are required for the simulation of IEEs. This was achieved through systematic adjustment of parameters according to [5], as described below.

Modifications to the PCs

- Synaptic Conductances: Increasing glutamatergic conductances (AMPA/NMDA). In this work, g_{AMPA} was increased from $8.0 \,\text{mS/cm}^2$ to $13.0 \,\text{mS/cm}^2$ and g_{NMDA} from $0.15 \,\text{mS/cm}^2$ to $0.35 \,\text{mS/cm}^2$.
- Inhibition Modulation: Altering the GABA reversal potential (E_{GABA}) to reduce the hyperpolarizing drive. Specifically, E_{GABA} was shifted from $-75\,\text{mV}$ to $-70\,\text{mV}$, making GABAergic inhibition less effective and thereby increasing the excitability of the PCs.

External stimulation In order to generate epileptic spikes, both the intensity and the synchrony of the external input to the cortical column were increased. In our simulations, each cell received 10 stimulations at an intensity of $60\mu\text{A/cm}^2$. To further enforce synchrony, a jitter of 4, ms was applied to the external stimulation. By minimizing temporal variability between inputs, this approach more effectively coordinates network activity, facilitating the generation of IESs.

4.2.2.1 Inclusion of Hybrid plasticity model's Parameters

The same set of parameters introduced in Section 3.2.1.3 is used here, with the only difference being that Shouval plasticity and its related parameters are not included. Moreover, the PCs in NeoCoMM are represented by a three-compartment model instead of two (Section 1.4.2.2). This setup provides users with direct access to the plasticity parameters, allowing real-time testing of different scenarios and enabling systematic exploration of how various plasticity rules influence epileptic dynamics. In the remainder of this chapter we will refer to the "hybrid plasticity model" as plasticity to avoid repetition.

4.3 Analysis of Network Dynamics and Plasticity Influence

Using the previously described stimulation protocol, a random seed of 4 ensured reproducibility. Simulations ran for 1 s, with a stimulation period of 100 ms and a sampling frequency of 25 kHz. Stimulation protocol remained identical across plasticity and no-plasticity simulations to ensure that observed differences in network activity could be attributed exclusively to plasticity rules rather than differences in external input.

4.3.1 Cellular and Population Activity Analysis:

4.3.1.1 Synaptic efficacy evolution

Figure 4.1 illustrates the evolution of synaptic efficacy (W) in the excitatory connections within the network over a stimulation period of 1 sec. For these simulations, the time constant τ_W was set to a relatively low value of 300 ms, enabling W to respond rapidly over the short stimulation period. As expected, the figure shows a gradual increase in synaptic efficacy over time.

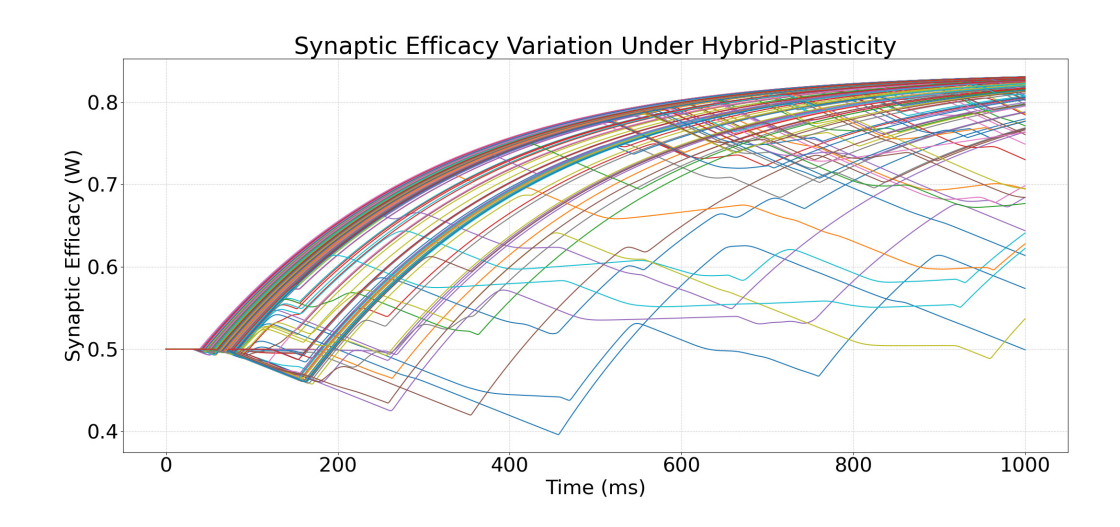


Figure 4.1: This figure illustrates the Evolution of the Synaptic efficacy variable under the hybrid plasticity condition within the network.

Within the bistable dynamics of the hybrid model as introduced in Section 2.3.3, $W^* = 0.5$ represents the unstable equilibrium point: depending on the postsynaptic calcium concentration, synaptic efficacy either decreases toward depression (LTD) or increases

toward potentiation (LTP). In the epileptic, hyperexcitable network considered here, most synaptic connections evolve toward the UP state, reflecting potentiation, while only a subset undergo LTD (falling below W^*). This predominance of potentiation is a hallmark of hyperexcitable networks. An additional observation is that some connections initially exhibit depression but later transition toward potentiation. This suggests that, at the beginning of the simulation, these synapses receive insufficient input from the distant cortex or other pyramidal cells; however, as the network activity strengthens and recurrent inputs accumulate, they gradually cross the threshold required for LTP.

4.3.1.2 Cellular Activity Analysis:

The firing patterns of both principal cells (PCs) and inhibitory interneurons (INs) are quantitatively analyzed:

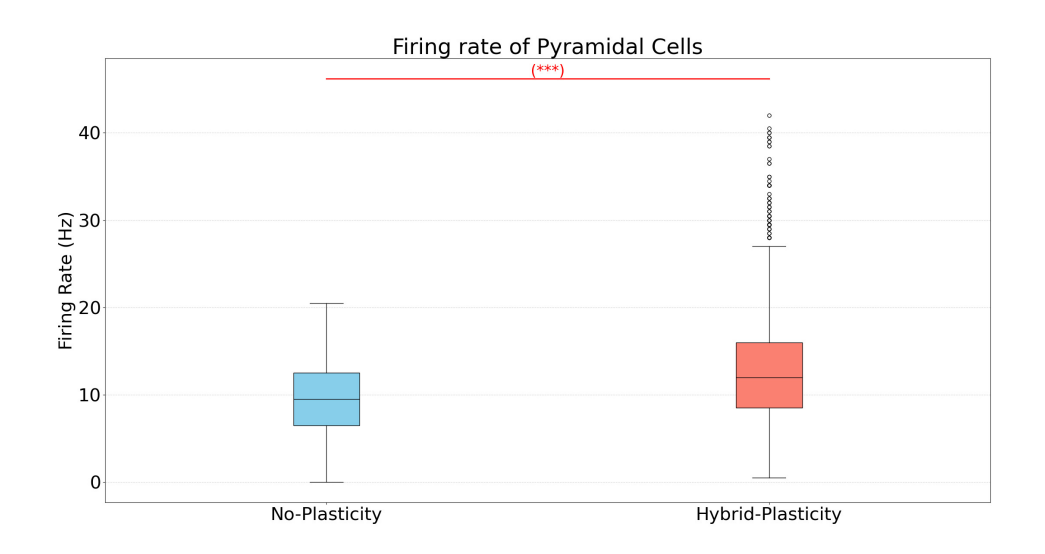


Figure 4.2: Firing rates of PCs under plasticity and no-plasticity conditions. The difference between the two groups is statistically significant, with stars indicating the p-value levels (* p < 0.05, ** p < 0.01, *** p < 0.001), demonstrating that the inclusion of plasticity substantially increases PC activity.

Pyramidal Cell (PC) Activity As illustrated in Figure 4.2, the FR of PCs is higher in the case of plasticity. Quantitative analysis confirms this effect: the maximum FR of PCs without plasticity was 20.50 Hz, with a mean FR of 9.40 Hz. Following the inclusion of plasticity, the maximum firing rate rose to 42 Hz, and the mean FR increased to about 12.92 Hz. This significant increase demonstrates that incorporating plasticity strongly enhances PC activity, highlighting its impact on network dynamics.

Figure 4.3 provides a more detailed view by separating PCs according to cortical layers within the model. Specifically, layer 2/3 contains 667 PCs, layer 3 contains 348 PCs, layer 4 contains 298 PCs, and layer 6 contains 205 PCs. The top row shows the FRs of PCs

in each layer without plasticity, while the second row displays the FRs with plasticity. As demonstrated, the FR of PCs is significantly higher across all layers when plasticity is included. This layer-specific representation allows a direct visual comparison of PC activity before and after plasticity, highlighting both the overall increase in firing and the differences in activity range within individual layers.

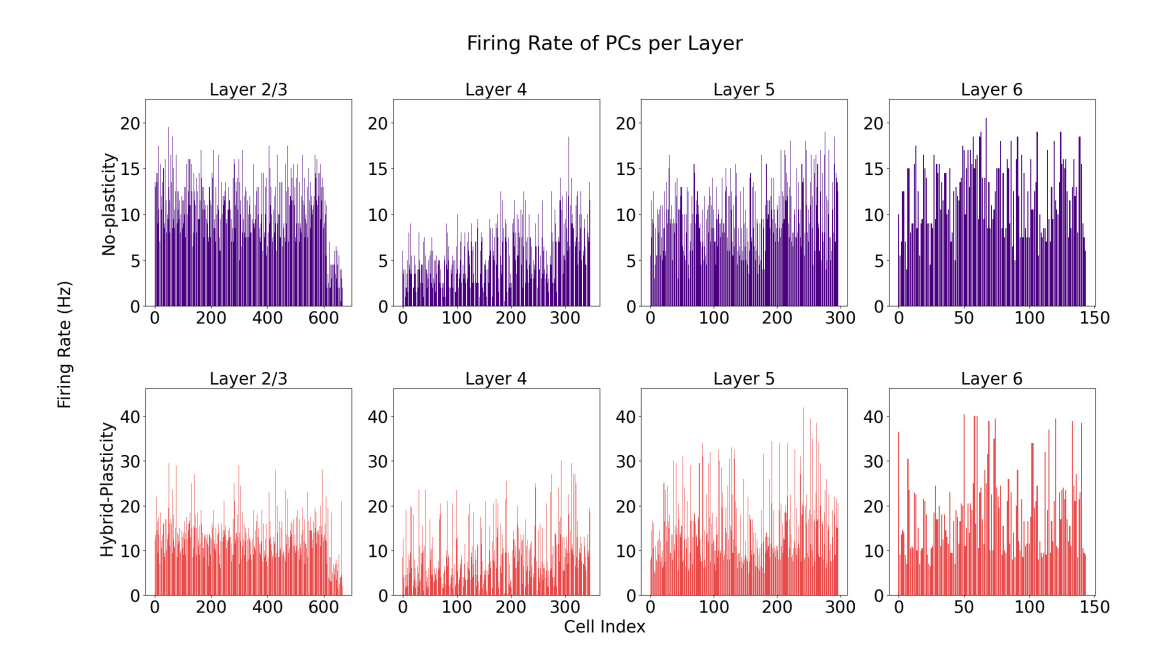


Figure 4.3: Barplot showing the firing rates of PCs across different cortical layers under plasticity and no-plasticity conditions. The layer-specific comparison highlights the increase in PC activity due to the inclusion of plasticity.

Interneurons Activity

PV interneurons The FR of PV INs is shown in Figure 4.4. The FR of PV+ expressing INs is higher with plasticity, primarily due to the excitatory drive from PCs connected to these interneurons. Under the no-plasticity condition, PV INs exhibited a mean firing rate of 41.87 Hz and a maximum of 64.50 Hz. After introducing hybrid plasticity, the mean firing rate increased to 52.56 Hz, with a maximum reaching 86 Hz. This increase highlights the effect of strengthened excitatory input from PCs on PV interneuron activity.

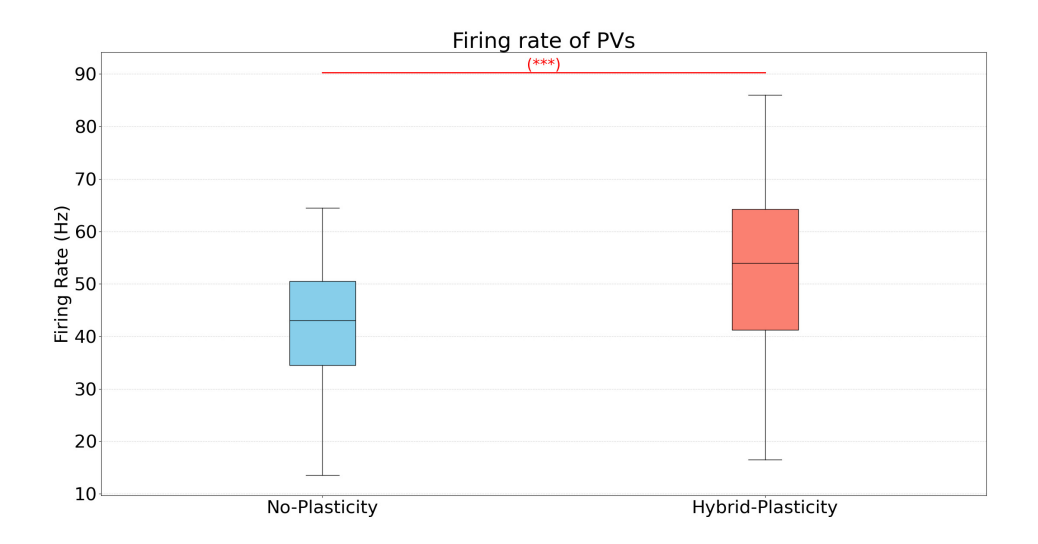


Figure 4.4: Boxplot of PV interneuron firing rates under plasticity and no-plasticity conditions, showing a highly significant increase in activity with plasticity.

Similar to PCs, the layer-specific activity of PV interneurons is illustrated in Figure 4.5. This representation allows a clear comparison of PV firing rates across different cortical layers before and after the inclusion of plasticity, highlighting the impact of increased excitatory drive on PV interneuron activity across layers.

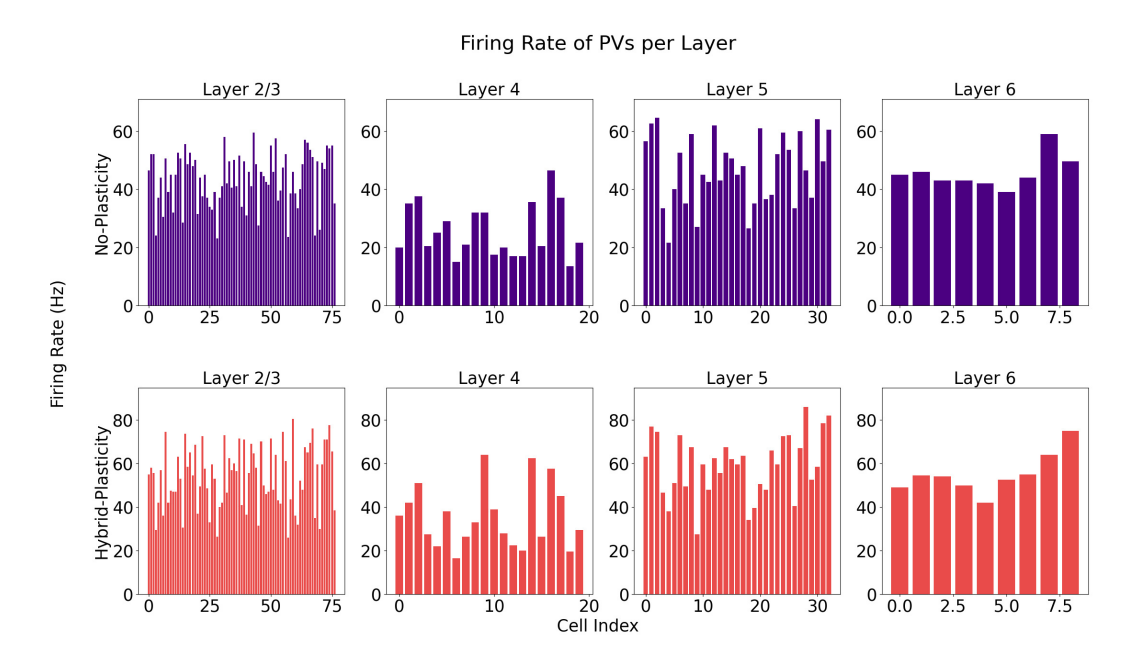


Figure 4.5: Layer-specific firing rates of PV interneurons under plasticity and no-plasticity conditions.

SST and **VIP** interneurons The following figure illustrates the FRs of SST and VIP interneurons. Consistent with expectations, the activity of both interneuron types increases in case of plasticity, reflecting the enhanced excitatory drive received from the network.

Specifically, the mean FR of SST+ expressing INs rises from 28.49 Hz to 35.34 Hz with plasticity, while VIP interneurons exhibit an increase from 47.40 Hz to 60.07 Hz. These results confirm that the inclusion of plasticity substantially amplifies interneuron activity, highlighting the network-wide effect of strengthened excitatory input.

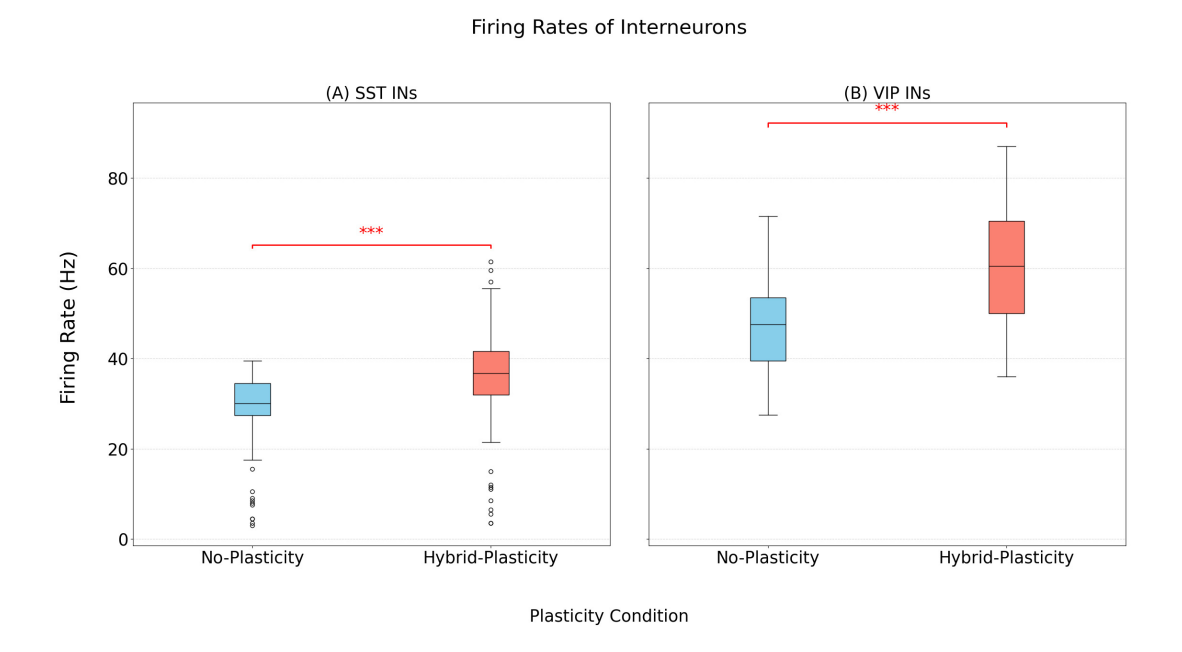


Figure 4.6: Boxplots of interneuron firing rates under no-plasticity and Hybrid plasticity conditions. (A) Firing activity of SST interneurons. (B) Firing activity of VIP interneurons. The asterisks indicate a statistically significant increase in firing rates following the inclusion of plasticity, demonstrating enhanced excitatory input to these interneurons.

4.3.1.3 Local Field Potential Analysis

In Figure 4.7, the LFP of the network is shown under two different conditions. The network was first configured to be epileptic, capable of generating interictal epileptic spikes (IESs) through a combination of hyperexcitability and high-intensity, synchronous input (as introduced in Section 4.2.2). This epileptic baseline serves as the reference state for assessing how synaptic plasticity influences ongoing epileptiform dynamics. The figure highlights a subtle increase in high-frequency components of the LFP, most evident around the fifth spike (approximately 500 ms). At the same time, the mean amplitude of the IESs shows a slight reduction, decreasing from 0.295 V to 0.275 V. This reduction can be attributed to the enhanced firing activity of PCs accompanied by reduced synchrony in their discharges. The combination of higher firing rates with lower temporal synchrony results in an increase in high-frequency activity but smaller LFP spike amplitudes.

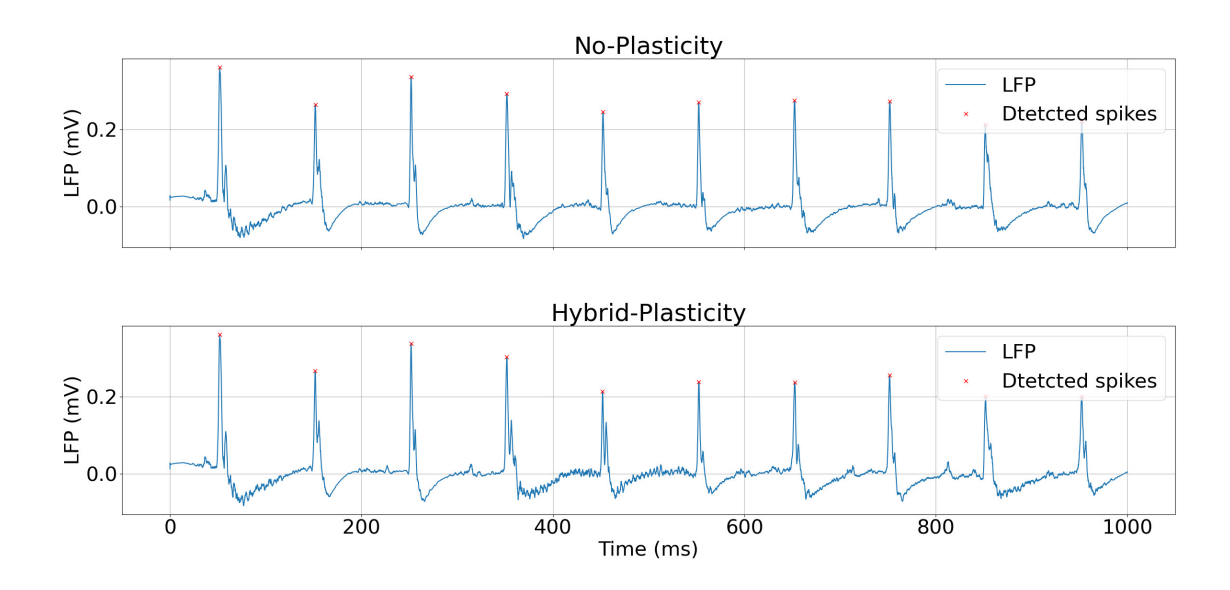


Figure 4.7: LFP of the network under plasticity and no-plasticity conditions.

4.4 Modeling of tES in the NeoCoMM Framework

The last part of this chapter was the investigation of transcranial electrical stimulation (tES) impact on healthy and epileptic activity. The NeoCoMM framework allows for the simulation of electrical stimulation effects, predicting the impact of weak electric fields produced by current flow through the mathematical finite-element modeling of individual brain anatomy. The contribution of tES was modeled based on a recent single-cell study [65] using detailed single-cell models within the NEURON environment [66]. The analysis focuses on analysing the entrainment impact of tACS on healthy alpha rhythms and the effect of tDCS on epileptic activity.

4.4.1 Computation of Single-Cell Polarization Lengths

In this section, we used the detailed NEURON models [66] to simulate extracellular stimulation via transcranial alternating current stimulation (tACS). The simulation was implemented using the extracellular mechanism provided by the NEURON simulator [67]. The quasi-uniform approximation [68] was used to model electric field stimulation, assuming a uniform electric field aligned along the y-axis for all neuronal populations, including inhibitory neurons. This alignment corresponded to the somato-dendritic axis of pyramidal (PYR) cells. The extracellular potential at compartment i was then calculated using Equation 4.1

$$E_i^{\text{extra}}(t) = E_0 \cdot A(t) \cdot y_i \tag{4.1}$$

where Where $E_i^{extra}(t)$ is the extracellular potential at the i^{th} compartment at time t, y_i its coordinate, E_0 the unit electric field vector, and A(t) the stimulation waveform at time t. The stimulation waveform was defined by $A(t) = a \sin(2\pi f t)$, with a the electric field amplitude and f its frequency.

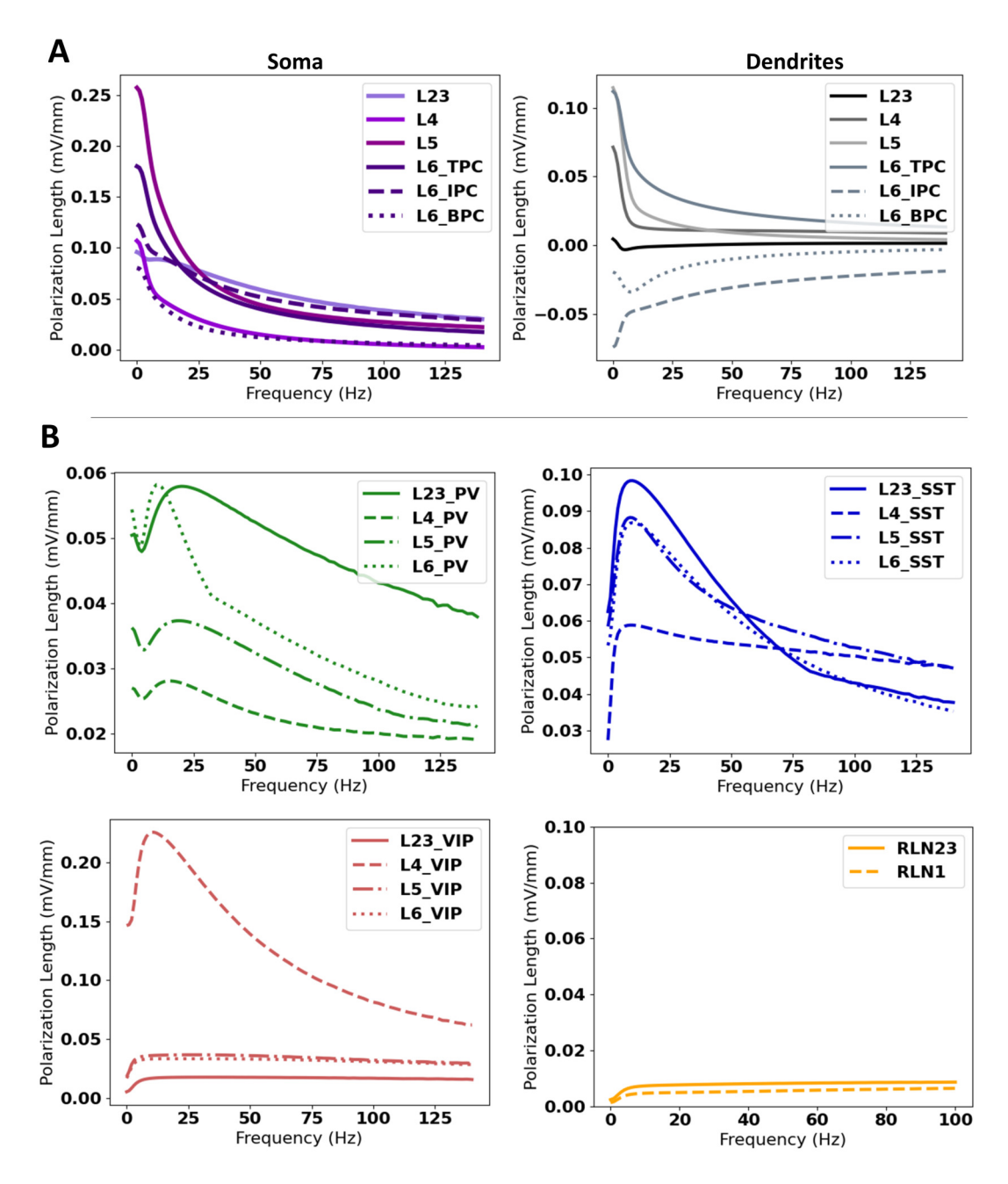


Figure 4.8: Frequency dependence of polarization length for all cell types. (A) Variation of the polarization length with tACS frequency for the soma (left panel) and the dendrites (right panel) of Principal Cells (PCs) of Layers L23, L4, L5, and L6. For L6 we investigated three subtypes of pyramidal cells: Tufted (TPC), Inverted (IPC), and Bipolar (BPC). (B) Variation of the polarization length with tACS frequency for the interneurons of the model (PV+, SST+, VIP+, and RLN+) at each layer (L23, L4, L5, and L6).

After initialization at the steady state without external inputs, simulations (2–4s) were run for stimulation frequencies ranging from 0 to 140 Hz (0.25 Hz step). The polarization length λ for each stimulation profile was defined as half the difference between the last maximum and minimum membrane potentials. These frequency-dependent values are illustrated in Figure 4.8.

4.4.2 Implementation of tES in NeoCoMM

In the NeoCoMM model, the "lambda-E" formalism was used [69], which proposes that under weak and uniform electric fields, the membrane polarization across all compartments varies linearly with stimulation current amplitude. Consequently, the membrane polarization induced by the electric field at each compartment is represented as the dot product of the electric field vector and a length vector (polarization length) that characterizes the coupling constant, as shown in Eq 4.2. In the remainder of the manuscript, we will be referring to polarization length as λ .

$$\delta v(x) = \lambda(x, f) \cdot E \tag{4.2}$$

For each cell type and layer, the corresponding polarization value was incorporated into the membrane potential, expressed as $V'(x) = V(x) + \delta V(x)$ with x the compartment type and cell layer.

4.4.3 Entrainment Analysis

Neural entrainment was quantified using the phase-locking value (PLV) [70], which quantifies the synchronization of spike timing relative to an ongoing signal. PLV is determined using Eq 4.3:

$$PLV = \left| \frac{1}{N} \sum_{k=1}^{N} e^{j\theta_k} \right| \tag{4.3}$$

Here, N represents the total number of APs and θ_k denotes the phase of the tACS waveform at which the k-th spike occurs. Under the tACS condition, the PLV was computed relative to the tACS waveform. A PLV of 0 indicates a uniform distribution of spike timings across all phases (0 to 2π), while a value of 1 signifies complete synchronization to a specific phase of the tACS.

The Rayleigh test [71] was chosen to evaluate deviations from a circular uniform distribution. Polar plots were used to visually represent these quantitative values, as a preferred phase direction corresponds to higher bin counts in a specific angular direction.

To ensure that the tACS impact portrayed by the PLV was significant compared to baseline, especially in the case of alpha rhythm where the network is already entrained to the 10 Hz frequency, We conducted a permutation test. Spike phases from stimulation and baseline were pooled and randomly reassigned into surrogate groups for 10,000 permutations to generate a null distribution of PLV difference between stimulation and baseline. PLV variation was considered as statistically significant for p ; 0.05.

4.4.4 Integration with the Plasticity-Enabled NeoCoMM

By incorporating the plasticity model into the NeoCoMM framework already including tES effects, we can now examine how externally applied electric fields interact with a network in which synaptic plasticity is active. This setup enables the investigation of tES-induced modulation in epileptic network dynamics, providing a more physiologically realistic model of the cortical column that combines acute electrical stimulation with activity-dependent synaptic adaptation, providing a framework to explore how tES may reshape the E/I balance and contribute to seizure suppression through synaptic plasticity modification.

4.4.5 Results

The computational analysis of tES was performed using the NeoCoMM framework, which was configured to simulate a physiological alpha rhythm and epileptic activity by inducing a hyperexcitable state. The λ -E formalism was included for tES modeling integrated with the Hybrid plasticity model in the PCs.

4.4.5.1 tACS Impact on Physiological Cortical Oscillations

We first quantified neural entrainment of PCs and interneurons (INs) to tACS across stimulation frequencies (5 to 120 Hz), and electric field intensities (0.3 to 3 mV/mm). For PCs, we grouped together those with similar electrophysiological properties: specifically, layer 2/3 and layer 4 PCs (PC23 and PC4), as well as layer 5 and layer 6 tufted PCs (PC5 and TPC6). For clarity, we present results for only one representative from each group. However, for layer 6, we additionally report results for inverted (IPC) and bipolar (BPC) pyramidal cells, as their morphologies differ in directionality from the other PC types.

Figure 4.9-A shows the variation of the PLV across stimulation frequencies and intensities for PCs. Even in the absence of stimulation (baseline), the network simulating a 10 Hz alpha rhythm exhibited a strong endogenous PLV at 10 Hz, even without stimulation. Under tACS, entrainment of LFP was consistent at 10 Hz, starting at the lowest tested

intensity of 0.3 mV/mm. Weaker entrainment was also observed at 20 Hz and 30 Hz, consistently across all PC layers.

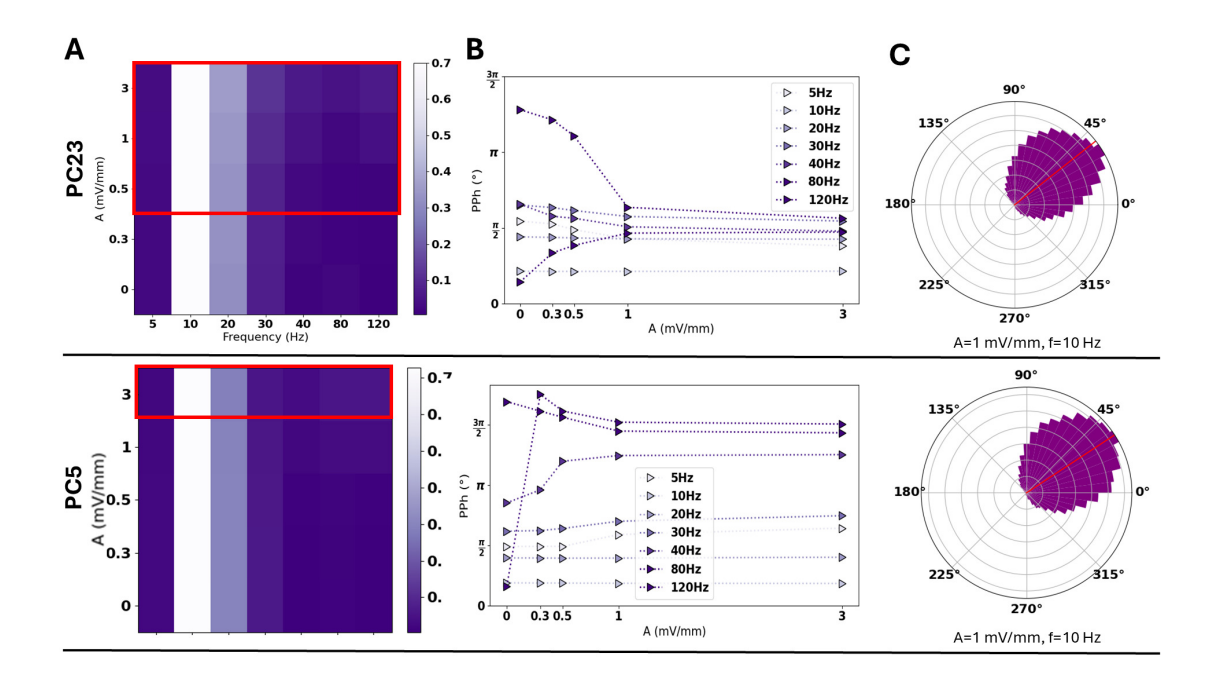


Figure 4.9: This figure illustrates the impact of transcranial alternating current stimulation (tACS) on the network activity of PCs in layer 2/3 (PC23) and layer 5 (PC5), during the 10 Hz alpha rhythm. (A) Entrainment maps of PCs to tACS with varying intensity and frequency. Red rectangles indicate conditions in which the phase-locking value (PLV) during tACS was significantly greater than baseline (permutation test, p < 0.05). (B) Preferred Phase (PPh) variation with tACS parameters. (C) Example of PC action potential entrainment under 1 mV/mm, 10 Hz tACS.

A key finding concerning the plasticity-enabled network was the layer-specific sensitivity to tACS: Permutation testing demonstrated that PCs in Layers 2/3 exhibited significant PLV increases relative to baseline, even at low intensity of 0.4 mV/mm across all stimulation frequencies tested, whereas PCs in Layers 5 only showed significantly elevated PLV values relative to baseline when the applied tACS amplitude exceeded 1 mV/mm. The corresponding preferred phase (PPh) distributions are shown in Figure 4.9. B. In L2/3 Pcs, PPh values varied but tended to converge toward a consistent phase with increasing stimulation intensity, indicating phase alignment driven by tACS in these populations. For L5 Pcs, this happened only when the stimulation frequencies were above 40 Hz. Polar plots in Figure 4.9.C further illustrate strong neural entrainment at 10 Hz under 1 mV/mm stimulation.

4.4.5.2 tDCS Impact on Epileptic Events

We next analyzed the effects of tDCS on epileptic network activity, considering both cathodal (ctDCS) and anodal (atDCS) stimulation. In our plasticity-enabled network, the ob-

served effects of stimulation polarity were reversed, driven by changes in synaptic efficacy (W). As shown in Figures 4.10, cathodal stimulation increased mean synaptic efficacy (W) in PCs as the stimulation intensity increased, while anodal stimulation led to a gradual synaptic depression.

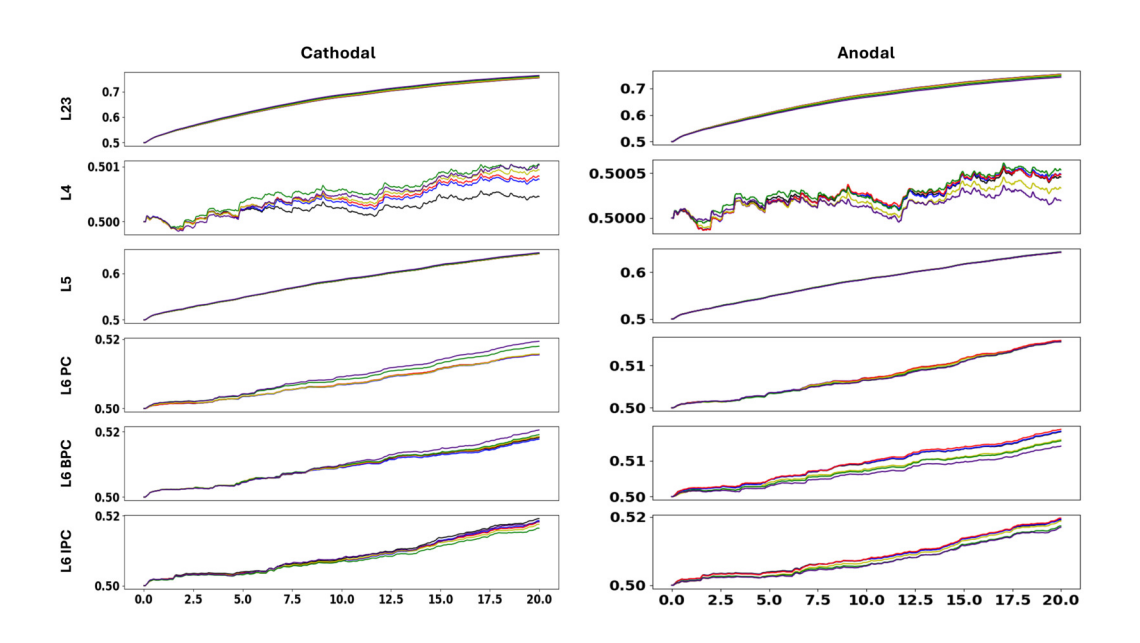


Figure 4.10: Temporal evolution of the mean synaptic weight of PCs across different cortical layers under varying intensities of cathodal and anodal tDCS.

This relationship is illustrated in more detail in Figure 4.11, where the synaptic efficacy increases proportionally with ctDCS intensity. In the figure, the baseline (blue trace) represents the mean synaptic efficacy of the network without stimulation. As the cathodal stimulation intensity increases from -0.3 mV/mm to -5 mV/mm, the corresponding synaptic efficacy traces (orange and brown, respectively) show a clear upward trend, with stronger stimulation producing greater synaptic potentiation. Intermediate intensities of -0.5 mV/mm (green), -1 mV/mm (red), and -3 mV/mm (purple) exhibit a consistent increase in synaptic efficacy, confirming a direct relationship between stimulation intensity and synaptic strengthening under cathodal tDCS.

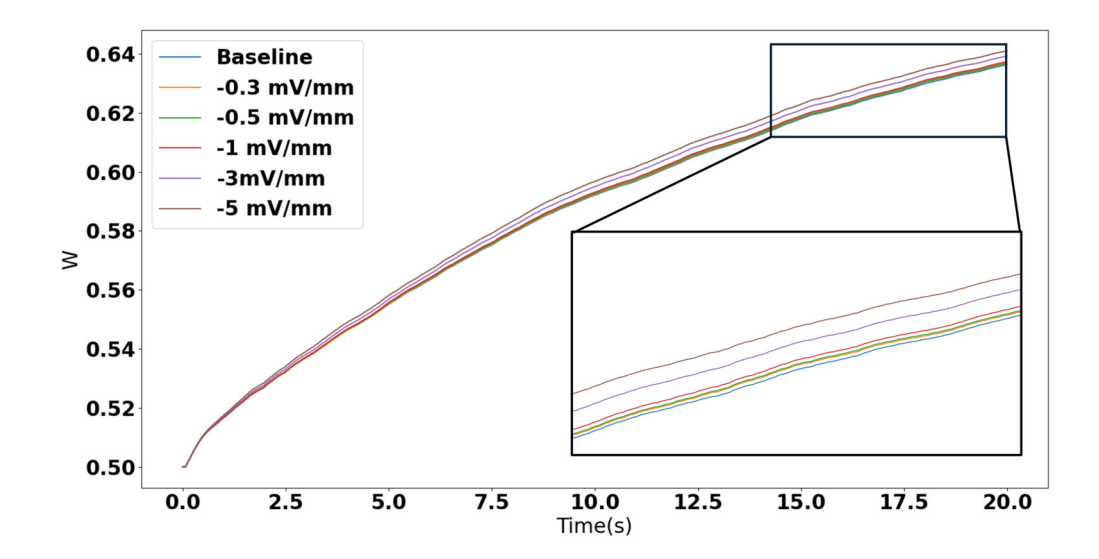


Figure 4.11: Magnified view illustrating the effect of ctDCS on the temporal variation of mean synaptic efficacy in PCs under different stimulation intensities.

These results demonstrated divergence from some works in which Cathodal tDCS (ct-DCS) is commonly reported to exert anti-epileptic effects, typically reducing hyperexcitable activity, whereas anodal tDCS (atDCS) is thought to increase excitability [72, 4]. Other publications such as kronberg et al. [73] showed that ctDCs increases LTP and overall synaptic strength. Functionally, these changes translated into modest shifts in epileptiform activity that were qualitatively observed: ctDCS slightly reduced the amplitude of IESs, whereas atDCS increased them (Figure 4.12).

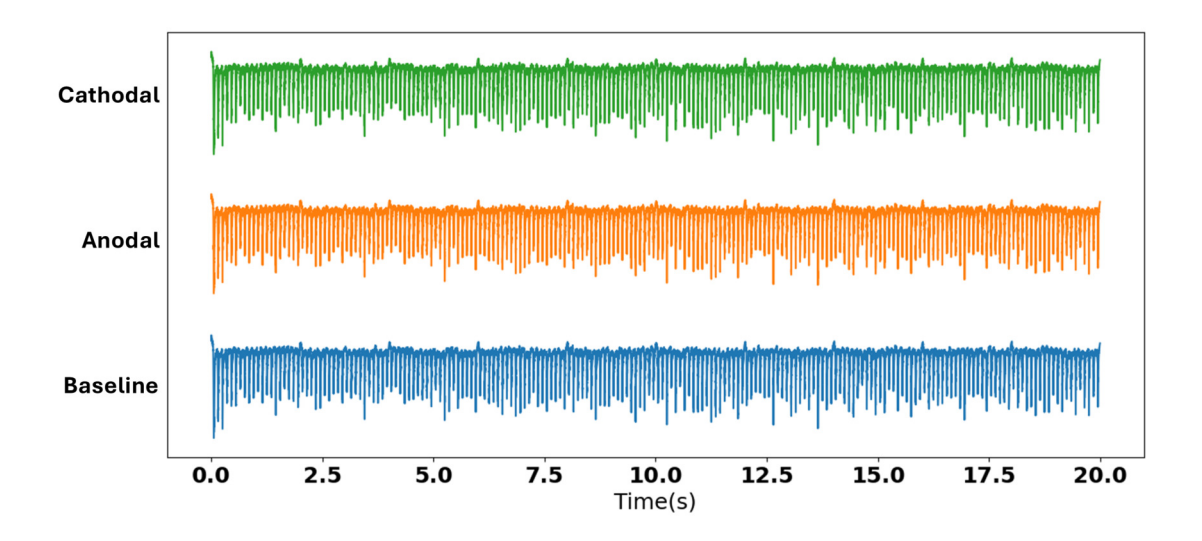


Figure 4.12: Variation of the amplitude of IESs under cathodal, anodal, and baseline conditions.

These preliminary simulations suggest that the inclusion of plasticity in PCs may alter

the commonly reported polarity-based effects of tDCS on synaptic weight. In our network, cathodal stimulation tended to increase mean synaptic efficacy and slightly reduce interictal spike amplitude, whereas anodal stimulation produced the opposite trend. While these results indicate that synaptic plasticity can modulate the network response to tDCS, the effects observed here are modest and layer-specific. Further simulations and detailed analysis will be required to systematically characterize how plasticity shapes tDCS-induced modulation of epileptiform activity.

4.5 Discussion

This chapter presented a critical extension of the NeoCortical Computational Microscale Model (NeoCoMM) by integrating the Hybrid plasticity model into the PCs. This work aimed to establish a dynamic, physiologically more realistic model of an epileptogenic state within the neocortical column and subsequently investigate how this plastic state modulates the effects of transcranial electrical stimulation (tES). The initial phase successfully characterized the epileptogenic state. By adjusting network parameters, specifically increasing glutamatergic conductances (g_{AMPA} and g_{NMDA}) and reducing GABAergic inhibition by shifting E_{GABA} , a hyperexcitable network capable of generating IESs was generated. The inclusion of the Hybrid plasticity model in the PCs confirmed the hypothesis that the chronic environment strongly biases synaptic dynamics toward LTP. This synaptic strengthening drove a significant amplification of activity across the entire network, raising the mean PC firing rate from 9.40 Hz to 12.92 Hz. This highlights that chronic plasticity is responsible for sustaining and amplifying the pathological activity through synaptic adaptation. The latter part of the chapter investigated neuromodulation, implementing tES via the λ -E formalism, which incorporates polarization lengths derived from detailed single-cell models. While tACS analysis showed interesting layer-specific sensitivities (e.g., L2/3 PCs being more sensitive to low intensity than L5 PCs), the most surprising results came from tDCS. Normally, cathodal tDCS is expected to reduce activity, but in our plastic network. it actually increased synaptic strength. On the other hand, anodal tDCS decreased synaptic strength. This suggests that the chronic, highly potentiated synaptic state created by plasticity can change the usual response to tDCS. These findings are still preliminary, and further work is needed to fully understand how plasticity shapes the network response to tDCS. For example, plasticity was only included in PCs here, so including inhibitory interneurons, testing different stimulation intensities, and looking at long-term dynamics could reveal more about how tDCS affects epileptiform activity in chronic networks.

Chapter 5

Discussion and Conclusion

5.1 Discussion

The focus of this thesis was to analyze how neuroplasticity influences neuronal and network excitability, particularly in the context of epileptic activity. Within the GALVANI project, the Cinetyks team at LTSI developed neuroinspired computational models of the hippocampus and the neocortex. However, these models lacked a fundamental property of the brain: neuroplasticity. This work addressed that limitation by implementing calcium-dependent plasticity mechanisms in a detailed multi-compartment pyramidal cell model and integrating them into large-scale network simulations. The implemented mechanisms, derived from the Shouval and Brunel frameworks, allowed the exploration of synaptic plasticity based on postsynaptic calcium dynamics and ultimately enhanced the physiological realism of the models for future studies on epilepsy and personalized neuromodulation treatments.

A key contribution of this thesis is the introduction of a new Hybrid plasticity model, inspired by the works of the team at the neural mass level [62], here implemented at the cellular scale. The rationale stems from the observation that Shouval's calcium-based synaptic rule, as discussed by the authors [8], can become unstable under sustained or high activity, leading to unbounded potentiation. To overcome this, the Hybrid model incorporated the bistable synaptic efficacy term from Brunel's model $-W(1-W)(W^*-W)$, introducing two stable synaptic states (low and high efficacy). This bistability acts as a self-regulating mechanism that prevents runaway potentiation or depression and constrains the system within physiological limits. Consequently, the Hybrid model provides a more stable and realistic representation of long-term synaptic dynamics, enabling simulations of chronic or pathological conditions such as epilepsy. Evidence of Shouval model instability was reflected in the simulated LFP signals as shown in Figure 3.9. In this case, throughout the simulation and more precisely the second half, high-frequency activity intensified while interictal spikes diminished and transitioned into high-frequency oscillations. For a simulation period of five seconds, the Shouval model produced an unrealistically high level of network excitation, indicating limited stability under conditions of sustained and elevated activity. These results motivated the subsequent choice of the Hybrid model alone

in the neocortical simulations. This further suggests that purely calcium-driven plasticity models, although biologically grounded, require additional stabilizing mechanisms such as bistability to maintain realistic long-term behavior.

During STDP validation, a secondary observation was the occurrence of multiple local maxima in the LTP phase of the STDP curve (Figure 2.8 and Figure 2.10). As detailed in Section 2.4.3, in the configured network Figure 2.7, both neurons were forced to fire through brief current injections, and the relative spike timing (Δt) between pre- and postsynaptic cells was measured. Occasionally, the overlap between externally applied currents and spontaneous depolarization led to double firing of the postsynaptic neuron within a single stimulation cycle. This resulted in two effective Δt intervals per cycle and generated small local peaks in the potentiation region. These fluctuations were artifacts of the stimulation protocol rather than biological irregularities. Overall, the resulting STDP profile closely matched theoretical and experimental expectations, showing three canonical regions: an initial depression phase followed by a potentiation window and a final depression phase for larger positive Δt values. Moreover, increasing stimulation frequency amplified both LTP and LTD amplitudes and broadened their respective windows, consistent with [8].

In our analysis, the focus was on modeling epileptic networks capable of generating interictal epileptic events mainly IES. To achieve this, hippocampal and neocortical networks were constructed following the approaches described in previous studies, where epileptiform activity was reproduced by modifying synaptic parameters such as glutamatergic and GABAergic conductances and the external input parameters. After these modifications, both networks exhibited increased excitability and produced interictal-like discharges. However, in the hippocampal network, despite the enhanced activity of pyramidal cells, their firing remained insufficient to induce the calcium levels required for synaptic efficacy to evolve through plasticity. This was due to the strong inhibitory input from BIS interneurons, which limited pyramidal cell depolarization. To address this, the AMPA conductance of BIS cells was reduced from 6 to 2 mS/cm², decreasing their inhibitory impact and allowing pyramidal neurons to fire more frequently, thereby enabling calcium-dependent plasticity to develop naturally. In contrast, no such modification was necessary in the neocortical network, as its connectivity and dynamics already supported sufficient pyramidal cell activation for plasticity expression.

Another important consideration concerns the choice of synaptic efficacy parameters in the Hybrid model within the NeoCoMM simulations. The NeoCoMM framework represents a realistic cortical microcircuit composed of nearly 1,900 neurons across multiple excitatory and inhibitory layers, introducing substantial computational complexity. After adjusting the model to simulate epileptic activity, synaptic efficacy evolution was examined under the Hybrid plasticity rule. Due to the model's scale, each one-second simulation generated large datasets, making long-duration runs impractical. To observe plasticity within this short simulation window, the synaptic efficacy time constant (τ_W) was reduced to 300 ms. Although this timescale is shorter than physiologically realistic values (typically on the order of seconds to minutes[9]), it allowed detectable weight changes within a manageable runtime. This choice represents a practical compromise between biological realism and computational feasibility.

Finally, it is generally accepted that tDCS produces shifts in cortical excitability, with anodal stimulation increasing excitability and cathodal stimulation decreasing it [74]. This excitability hypothesis is supported by physiological evidence showing that direct current stimulation modulates neuronal membrane potentials, thereby altering firing rates and spike timing [75, 76]. Based on these findings, anodal and cathodal tDCS are often assumed to induce LTP- and LTD-like effects, respectively. However, our preliminary tES simulations revealed a reversal of this expected polarity effect: cathodal stimulation increased synaptic efficacy, whereas anodal stimulation led to depression. This result aligns with the findings of [73], who showed that tDCS facilitates LTP and diminishes LTD in hippocampal slices. They suggested that these effects can be polarity independent, as both anodal and cathodal tDCS can produce similar effects. The outcomes depended on dendritic location and endogenous synaptic activity, demonstrating that tDCS can directly modulate synaptic plasticity by influencing calcium-dependent signaling pathways involved in LTP and LTD. Depending on the network's ongoing activity and baseline excitability, such calcium-driven mechanisms can alter the direction of synaptic modification, explaining why, in hyperexcitable tissue, the typical polarity effects of tDCS may reverse.

Despite these findings, this study faced some limitations that should be acknowledged. The first concerns computational constraints: simulating large-scale, detailed neuroinspired networks such as NeoCoMM (around 1,900 neurons) required substantial processing time, which limited the feasible duration of simulations. Because synaptic plasticity evolves over minutes in biological systems, this constraint prevented us from capturing the slower, cumulative changes that would occur under realistic timescales. For instance, simulating 20 seconds of tES stimulation under realistic conditions, would require several days of computation. Although some synaptic changes began to appear within this time frame, longer simulation durations would be necessary to fully capture and analyze the evolution of synaptic plasticity over biologically relevant timescales. The second limitation relates to the lack of experimental literature describing the precise mechanisms of neuroplasticity in epilepsy. Although plasticity is known to play a key role in both the development and potential recovery of hyperexcitable networks, the exact processes remain insufficiently

characterized. This gap in current knowledge restricted our ability to directly compare or validate the simulated results with experimental data.

5.2 Implications and Future Work

This work successfully modeled calcium-dependent synaptic plasticity within microscale models of the hippocampus and neocortex, moving closer to a physiologically grounded representation of epileptic microcircuits. The new models provide a powerful platform for exploring personalized stimulation strategies in the context of epilepsy. Ultimately, this study advances the GALVANI project's mission by providing a computational tool capable of linking cellular plasticity processes with neuromodulation effects. This can contribute toward the rational design and optimization of personalized therapeutic interventions in drug-resistant epilepsy. Building on this foundation, future research can focus on addressing remaining biological complexities and exploring long-term dynamics. Moreover, in this work, synaptic plasticity was implemented only in the excitatory PCs. A future direction could focus on extending the model to include plasticity in interneurons, allowing a more complete representation of the excitation-inhibition balance that characterizes chronic epilepsy.

In this study, the focus was placed on physiological plasticity within an epileptic network. However, by modifying the Ω -function parameters, we were able to simulate a pathological form of plasticity, which provides a useful framework to explore how biased plasticity might contribute to epileptogenesis. Future work could explore the effect of such pathological plasticity on a physiological network to investigate whether it can drive the transition toward epileptogenesis.

Finally, although some preliminary studies have examined the impact of tES on epileptic networks, our initial findings are only a first step, and more extensive research and longer-duration stimulation are needed to obtain reliable and comprehensive insights. The new version of NeoCoMM, which includes the implementation of transcranial electrical stimulation (tES) and synaptic plasticity, provides a powerful platform for systematic investigations of how tES influences the epileptic brain. In particular, it enables exploration of the bidirectional interactions between stimulation and plasticity mechanisms, helping to reveal how tES can modulate hyperexcitability in pathological conditions. This version will be further used by Dr. Al Harrach and her team within the GALVANI project to investigate tES-epilepsy interactions toward the goal of personalized treatment strategies.

5.3 Conclusion

This thesis has advanced the Physiological realism of hippocampal and neocortical computational models by integrating calcium-dependent neuroplasticity mechanisms into detailed multicompartment neuron frameworks. The simulations demonstrated that synaptic plasticity, while essential for adaptive neural processes, can also contribute to the emergence and worsening of epileptiform activity by reinforcing hyperexcitable network states. The enhanced models now provide a solid and flexible foundation for investigating how long-term synaptic adaptation influences network behavior and its modulation by transcranial electrical stimulation. Overall, this work represents a significant step toward developing computational tools that better reflect real brain behavior and directly contribute to the GALVANI project's objectives of creating mechanistically grounded and personalized neuromodulation strategies for drug-resistant epilepsy.

5.4 Funding Acknowledgement

This project has received funding from the European Research Council (ERC) under the European Union's Horizon 2020 research and innovation program (grant agreement No. 855109).

Supplementary Materials

This supplementary section provides additional figures supporting the main results presented in the thesis. It includes visualizations of the implemented plasticity parameters in the model's GUI, neuronal firing behaviors under different conditions, and the effects of pathological plasticity on network excitability and epileptiform activity.

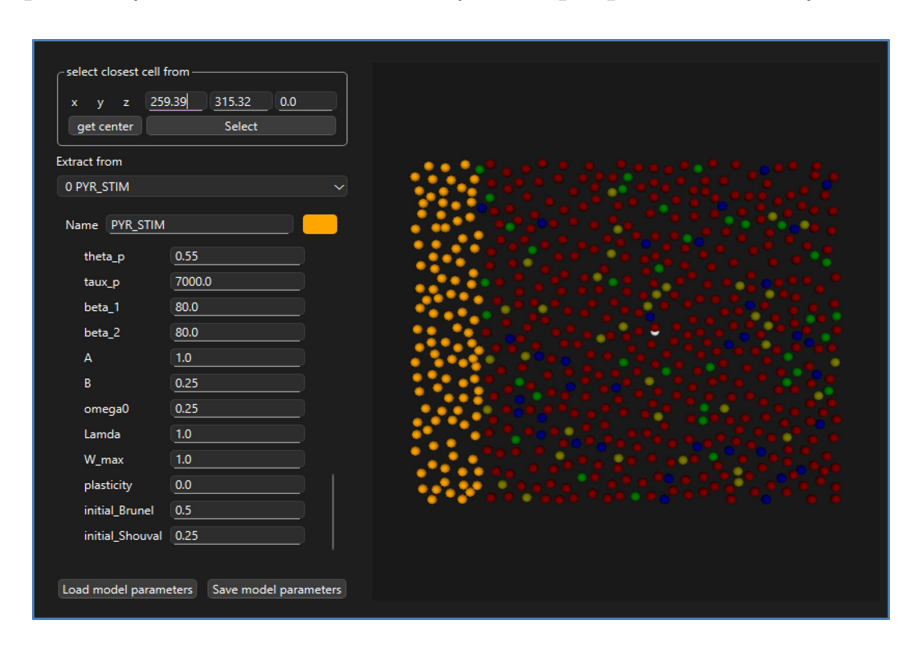


Figure 5.1: Inclusion of plasticity parameters in the simulation GUI. The left panel allows the selection and adjustment of Shouval and Hybrid plasticity parameters.

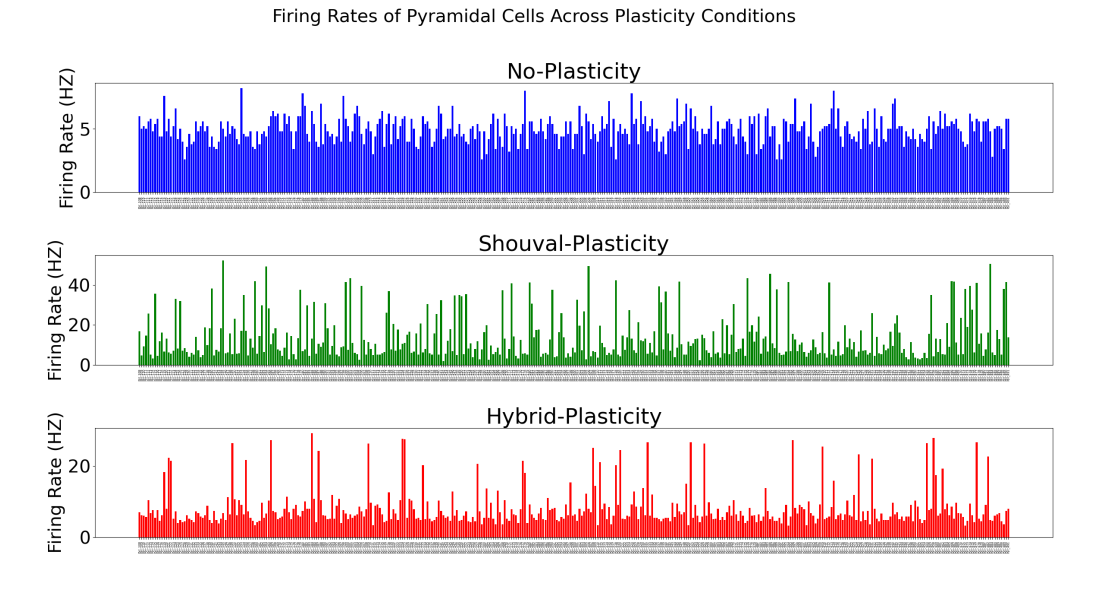


Figure 5.2: Distribution of pyramidal cell (PC) firing patterns under "No plasticity," "Shouval plasticity," and "Hybrid plasticity" conditions.

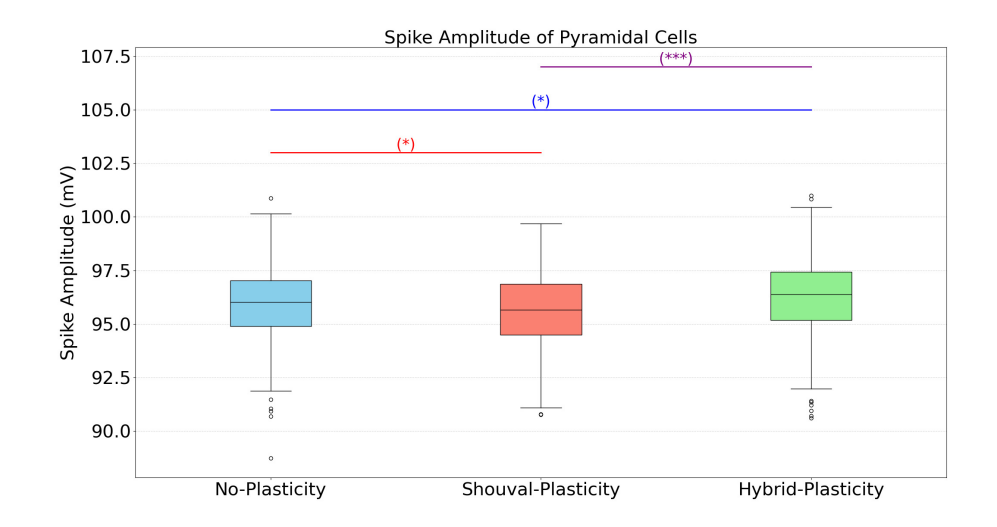


Figure 5.3: Distribution of action potential (AP) amplitudes for PCs across the three plasticity conditions.

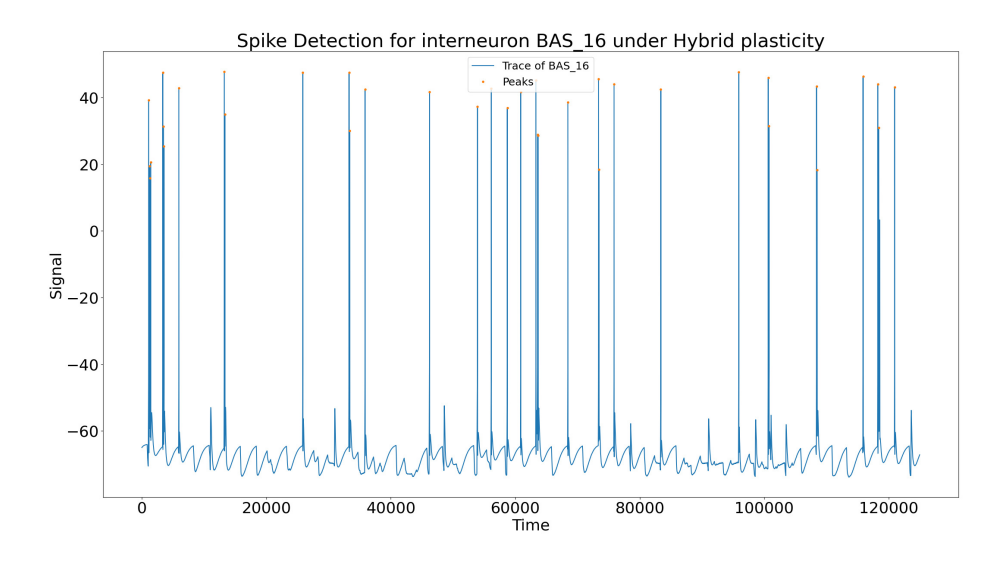


Figure 5.4: Spike activity of a single basket (BAS) interneuron, illustrating the firing dynamics of inhibitory neurons within the network.

Pathological Plasticity and Epileptiform Activity

The following figures present the impact of the pathological Hybrid plasticity model (introduced in Section 2.3.4) on the epileptic network. Pathological plasticity was implemented by modifying Ω -function parameters to exaggerate synaptic potentiation. As shown in the results, this led to a pronounced increase in excitatory synaptic strength, heightened firing activity of pyramidal cells, and an overall escalation of network hyperexcitability. The excessive long-term potentiation resulted in desynchronization of population activity and

increased high-frequency components in the local field potential (LFP), consistent with enhanced epileptogenic behavior.

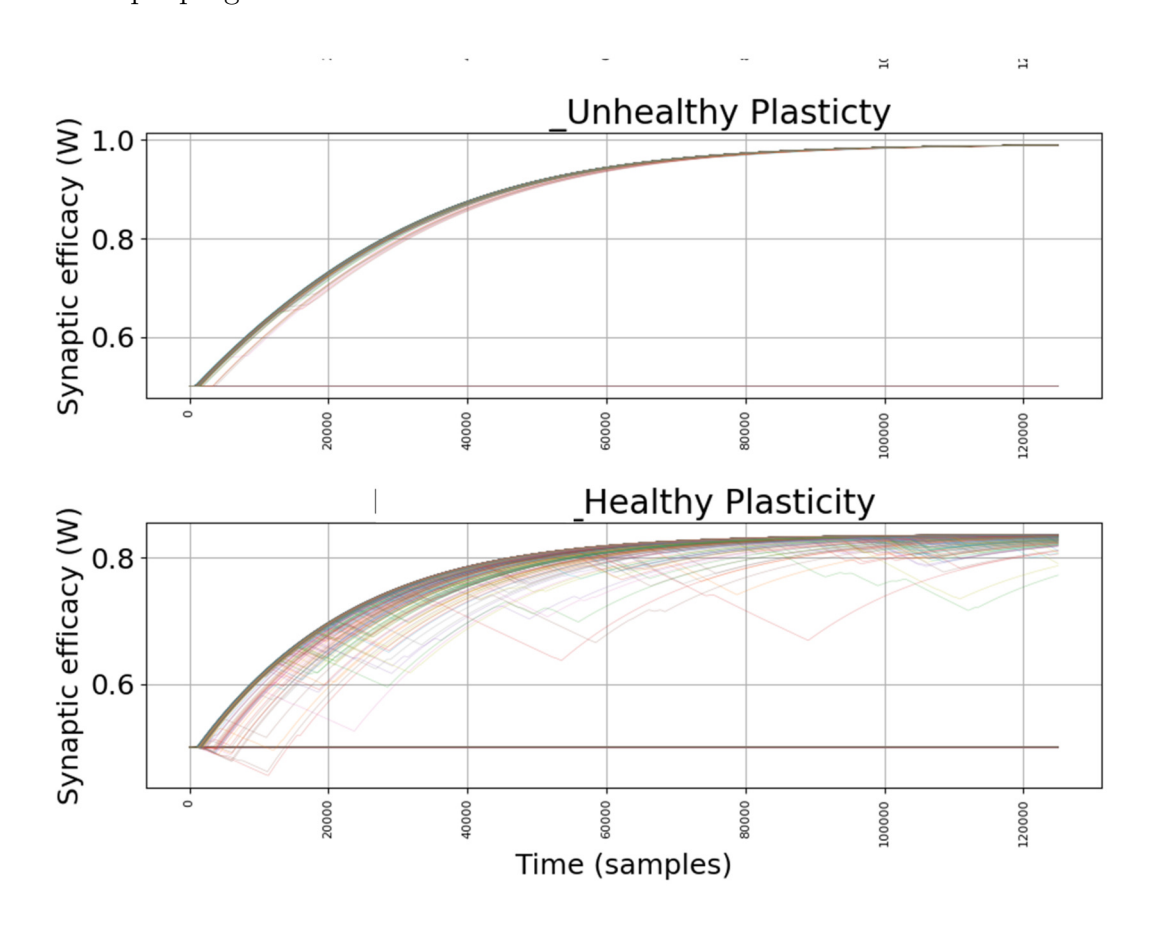


Figure 5.5: Temporal evolution of synaptic strength under physiological (healthy) and pathological Hybrid plasticity conditions. In the pathological case, all synapses exhibit rapid and excessive long-term potentiation (LTP), reaching saturation much faster than in the physiological case, where potentiation develops more gradually.

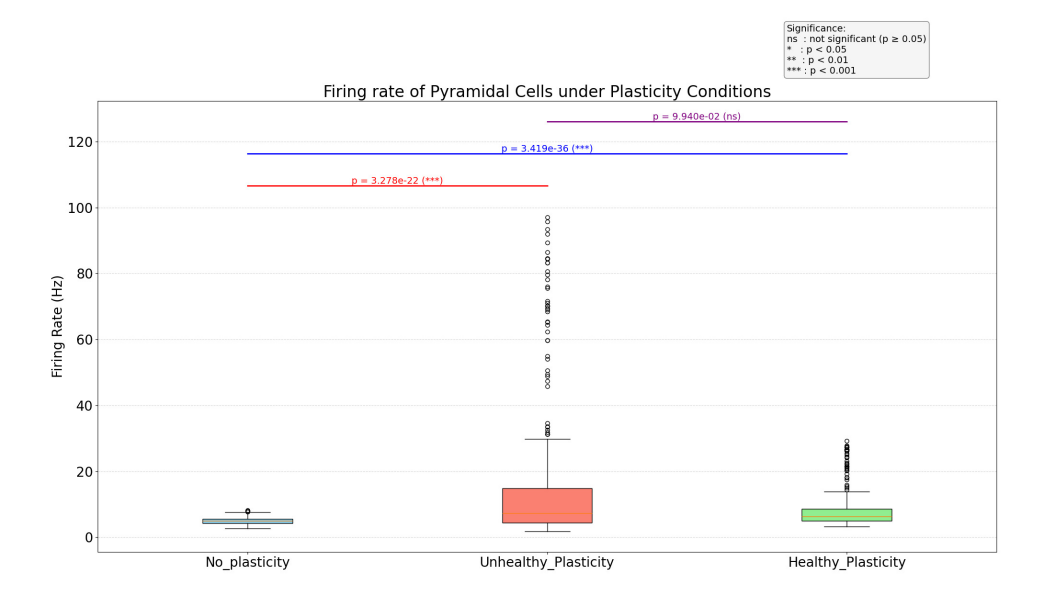


Figure 5.6: Comparison of pyramidal cell firing rates under physiological and pathological Hybrid plasticity models. A substantial increase in firing rate is observed under pathological conditions, indicating elevated network excitability.

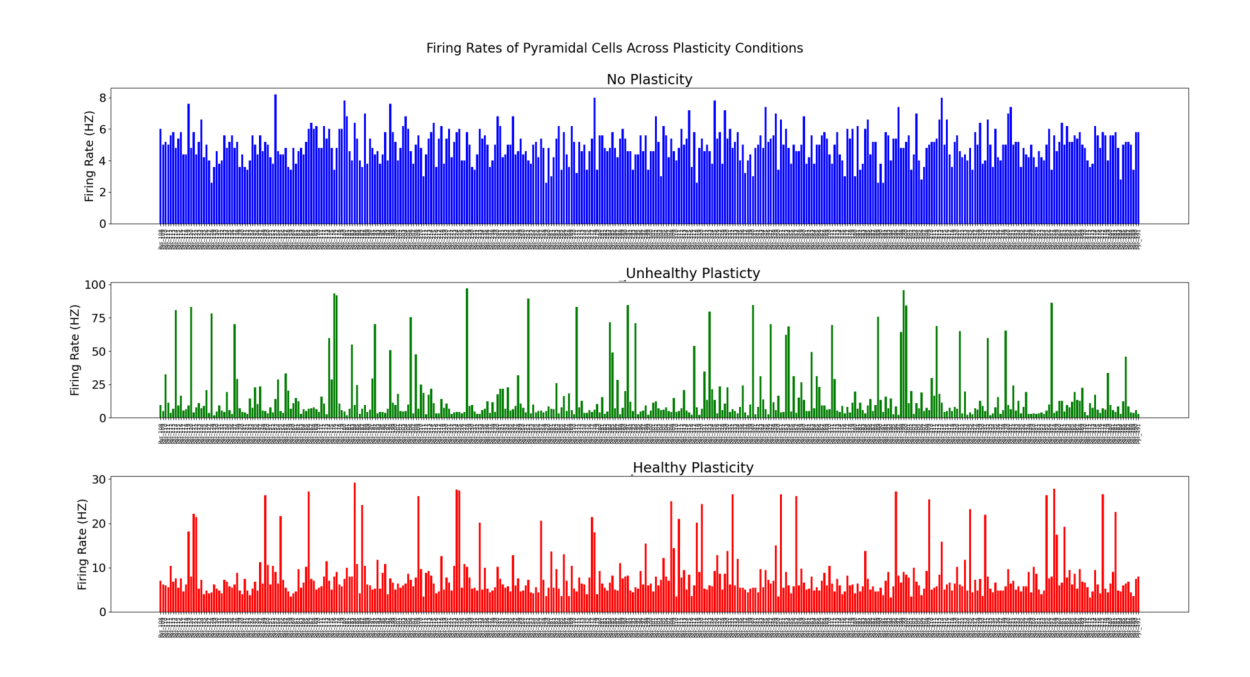


Figure 5.7: Overall firing behavior of pyramidal cells under healthy and pathological Hybrid plasticity. Under pathological conditions, several neurons reach firing rates up to 100 Hz, reflecting severe hyperexcitability.

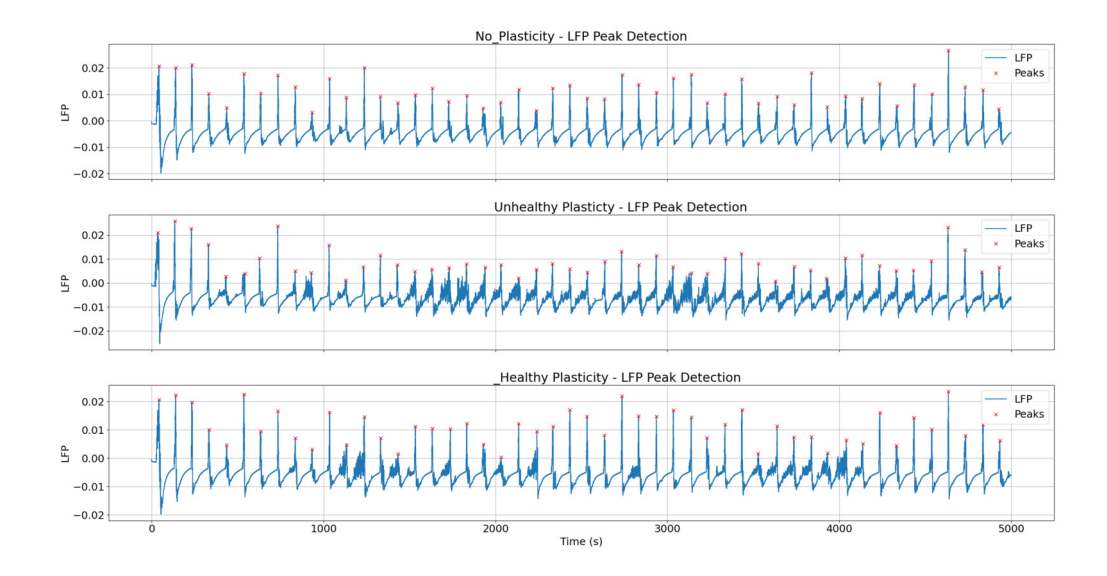


Figure 5.8: Simulated local field potential (LFP) signals under pathological and physiological plasticity compared to baseline. The pathological condition shows increased high-frequency activity and reduced synchrony, resulting in lower interictal event amplitude despite higher firing activity.

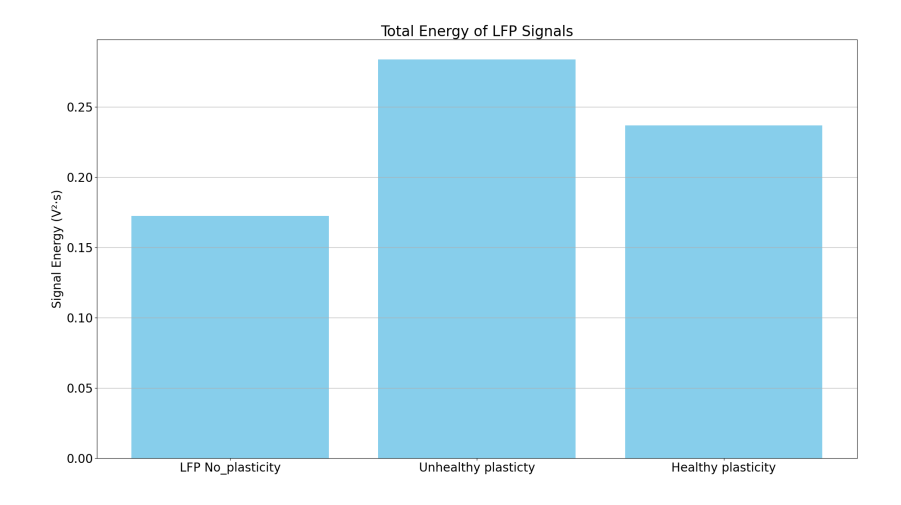


Figure 5.9: Signal energy analysis across conditions. The total energy, computed as the integral of squared signal power, is highest under pathological plasticity, confirming increased hyperactivity and enhanced epileptogenic potential.

Bibliography

- [1] Chen Zhong, Kang Yang, Nianhua Wang, Liang Yang, Zhuanyi Yang, Lixin Xu, Jun Wang, and Longbo Zhang. Advancements in surgical therapies for drug-resistant epilepsy: A paradigm shift towards precision care. *Neurology and Therapy*, 14(2):467–490, April 2025. Epub 2025 Feb 10.
- [2] Eline J. H. van Hugte, Dirk Schubert, and Nael Nadif Kasri. Excitatory/inhibitory balance in epilepsies and neurodevelopmental disorders: Depolarizing γ -aminobutyric acid as a common mechanism. *Epilepsia*, 64(8):1975–1990, 2023.
- [3] Sara Simula, Maëva Daoud, Giulio Ruffini, Christian-G. Bénar, Pascal Benquet, Fabrice Wendling, and Fabrice Bartolomei. Transcranial current stimulation in epilepsy: A systematic review of the fundamental and clinical aspects. *Frontiers in Neuroscience*, 16:909421, 2022.
- [4] Yousef Hawas, Abdallah Abbas, Ibraheem M Alkhawaldeh, Mohamed Abo Zeid, Mohamed Al Diab Al Azzawi, Hamza Khaled Alsalhi, and Ahmed Negida. Efficacy and safety of transcranial direct current stimulation (tdcs) in treatment of refractory epilepsy: an updated systematic review and meta-analysis of randomized shamcontrolled trials. Neurological Sciences, 46(2):671–687, 2025. Epub 2024 Nov 13.
- [5] M. Al Harrach, M. Yochum, G. Ruffini, F. Bartolomei, F. Wendling, and P. Benquet. Neocomm: A neocortical neuroinspired computational model for the reconstruction and simulation of epileptiform events. *Computational Biology and Medicine*, 180:108934, 2024.
- [6] Sophie Demont-Guignard, Pascal Benquet, Urs Gerber, and Fabrice Wendling. Analysis of intracerebral eeg recordings of epileptic spikes: Insights from a neural network model. *IEEE Transactions on Biomedical Engineering*, 56(12):2782–2795, 2009.
- [7] Thomas P Sutula. Mechanisms of epilepsy progression: current theories and perspectives from neuroplasticity in adulthood and development. *Epilepsy Research*, 60(2-3):161–171, 2004.
- [8] H. Z. Shouval, M. F. Bear, and L. N. Cooper. A unified model of nmda receptordependent bidirectional synaptic plasticity. *Proceedings of the National Academy of Sciences*, 97(20):11571–11576, 2000.
- [9] Michael Graupner and Nicolas Brunel. Calcium-based plasticity model explains sensitivity of synaptic changes to spike pattern, rate, and dendritic location. *Proceedings* of the National Academy of Sciences, 109(10):3991–3996, 2012.

- [10] David J. Thurman, Ettore Beghi, Charles E. Begley, Anne T. Berg, Jeffrey R. Buchhalter, Ding Ding, Dale C. Hesdorffer, W. Allen Hauser, Leslie Kazis, Rosemarie Kobau, Barbara Kroner, David M. Labiner, Kai Liow, Béatrice Marin, Joseph Sirven, Michael R. Sperling, Fuhua Tang, Jose F. Tellez-Zenteno, Torbjörn Tomson, and Samuel Wiebe. Epilepsy in adults. The Lancet, 393(10172):689-701, 2019.
- [11] Robert S. Fisher, Carlos Acevedo, Alexis Arzimanoglou, Alicia Bogacz, J. Helen Cross, Christian E. Elger, Jerome Engel, Lars Forsgren, Jacqueline A. French, Mike Glynn, Dale C. Hesdorffer, B. I. Lee, Gary W. Mathern, Solomon L. Moshé, Emilio Perucca, Ingrid E. Scheffer, Torbjörn Tomson, Masako Watanabe, and Samuel Wiebe. Ilae official report: A practical clinical definition of epilepsy. Epilepsia, 55(4):475–482, 2014.
- [12] Kirsten M. Fiest, Khara M. Sauro, Samuel Wiebe, Scott B. Patten, Churl-Su Kwon, Jonathan Dykeman, Tamara Pringsheim, Diane L. Lorenzetti, and Nathalie Jetté. Prevalence and incidence of epilepsy: A systematic review and meta-analysis of international studies. *Neurology*, 88(3):296–303, 2017.
- [13] Roland D. Thijs, Rainer Surges, Terence J. O'Brien, and Josemir W. Sander. Epilepsy in adults. *The Lancet*, 393(10172):689–701, 2019.
- [14] Robert S Fisher, Walter van Emde Boas, Warren Blume, Christian Elger, Pierre Genton, Phillip Lee, and Jerome Engel Jr. Epileptic seizures and epilepsy: Definitions proposed by the international league against epilepsy (ilae) and the international bureau for epilepsy (ibe). *Epilepsia*, 46(4):470–472, 2005.
- [15] Sándor Beniczky, Eugen Trinka, Elaine Wirrell, Fatema Abdulla, Raidah Al Baradie, Mario Alonso Vanegas, and et al. Updated classification of epileptic seizures: Position paper of the international league against epilepsy. *Epilepsia*, 66(6):1804–1823, 2025.
- [16] National Institute of Neurological Disorders and Stroke (NINDS). Epilepsy and seizures. https://www.ninds.nih.gov/health-information/disorders/epilepsy-and-seizures, 2025. Webpage, published online ca. spring 2025.
- [17] A&B Neurology Clinic. Seizures. https://abneurology.com/services/seizures/. Webpage describing what seizures are and their manifestations.
- [18] Haleema Anwar, Qudsia Umaira Khan, Natasha Nadeem, Iqra Pervaiz, Muhammad Ali, and Fatima Fayyaz Cheema. Epileptic seizures. *Discoveries (Craiova)*, 8(2):e110, June 12 2020.
- [19] Jessica J. Falco-Walter, Ingrid E. Scheffer, and Robert S. Fisher. The new definition and classification of seizures and epilepsy. *Epilepsy Research*, 139:73–79, 2018.

- [20] Maria Nataly P. Liman and Abdullah Al Sawaf. *Epilepsy EEG*. StatPearls Publishing, Treasure Island (FL), 2025.
- [21] Emily L. Johnson. Seizures and epilepsy. *Medical Clinics of North America*, 103(2):309–324, March 2019.
- [22] Robert S. Fisher. Ictal, postictal and interictal epileptic discharges. *Clinical Neuro-physiology*, 126(6):1105–1111, 2015.
- [23] Ali A. Asadi-Pooya, Francesco Brigo, Simona Lattanzi, Ingmar Blumcke, et al. Adult epilepsy. *The Lancet*, 402(10399):412–424, 2023.
- [24] Waleed Abood and Susanta Bandyopadhyay. *Postictal Seizure State*. StatPearls Publishing LLC, Treasure Island (FL), internet edition, 2023. Bookshelf ID: NBK526004, accessed via NCBI Bookshelf.
- [25] Rihat Rahman, Shiva Maleki Varnosfaderani, Omar Makke, Nabil J. Sarhan, Eishi Asano, Aimee Luat, and Mohammad Alhawari. Comprehensive analysis of eeg datasets for epileptic seizure prediction. In *Proceedings of the 2021 IEEE International Symposium on Circuits and Systems (ISCAS)*, pages 1–5. IEEE, 2021.
- [26] Hai Chen and Mohamad Z. Koubeissi. Electroencephalography in epilepsy evaluation. Continuum (Minneapollis, Minn.), 25(2):431–453, 2019.
- [27] Marco de Curtis and Giuliano Avanzini. Interictal spikes in focal epileptogenesis. *Progress in Neurobiology*, 63(5):541–567, 2001.
- [28] Fergus Rugg-Gunn, Anna Miserocchi, and Andrew McEvoy. Epilepsy surgery. *Practical Neurology*, 20(1):4–14, 2020.
- [29] Flavia Venetucci Gouveia, Nebras M. Warsi, Hrishikesh Suresh, Rafi Matin, and George M. Ibrahim. Neurostimulation treatments for epilepsy: Deep brain stimulation, responsive neurostimulation and vagus nerve stimulation. *Neurotherapeutics*, 21(3):e00308, 2024. Epub 2024 Jan 4; Received 5 September 2023; Revised 29 November 2023; Accepted 6 December 2023.
- [30] Patrick Kwan, Alexis Arzimanoglou, Anne T. Berg, and et al. Definition of drug resistant epilepsy: Consensus proposal by the ad hoc task force of the ilae commission on therapeutic strategies. *Epilepsia*, 51(6):1069–1077, 2010.
- [31] Patrick Kwan, Martin J. Brodie, and Emilio Perucca. Drug-resistant epilepsy. *The Lancet Neurology*, 2023.
- [32] David J. Thurman, Ettore Beghi, Charles E. Begley, and et al. The burden of epilepsy: a call for action. *The Lancet*, 2023.

- [33] Fatemeh Yavari, Asif Jamil, Mohsen Mosayebi Samani, Liliane Pinto Vidor, and Michael A. Nitsche. Basic and functional effects of transcranial electrical stimulation (tes)—an introduction. Neuroscience and Biobehavioral Reviews, 85:81–92, 2018.
- [34] Filipe Oliveira Barroso, Alejandro Pascual-Valdunciel, Diego Torricelli, Juan C. Moreno, Antonio Del Ama-Espinosa, Jozsef Laczko, and José L. Pons. Noninvasive modalities used in spinal cord injury rehabilitation. In Spinal Cord Injury Therapy. IntechOpen, 2019. Open access.
- [35] Zhihe Zhao, Sina Shirinpour, Harry Tran, Miles Wischnewski, and Alexander Opitz. Intensity-and frequency-specific effects of transcranial alternating current stimulation are explained by network dynamics. *Journal of neural engineering*, 21(2):026024, 2024.
- [36] Michael J. Caire, Vamsi Reddy, and Matthew A. Varacallo. Physiology, synapse. StatPearls [Internet], 2023. Updated 27 March 2023.
- [37] BioRender. Biorender templates, 2025. Accessed: 2025-10-03.
- [38] Suzana Herculano-Houzel. The human brain in numbers: a linearly scaled-up primate brain. Frontiers in Human Neuroscience, 3:31, 2009.
- [39] Dale Purves, George J. Augustine, David Fitzpatrick, William C. Hall, Anthony-Samuel LaMantia, and Leonard E. White. Neuroscience. Oxford University Press, New York, 6th edition, 2018.
- [40] Saul McLeod. Synaptic transmission: A-level psychology, 2025. Accessed: 2025-10-03.
- [41] G. N. Luheshi, J. Allen, A. Harker, D. Brough, and N. J. Rothwell. The transcellular activation of neuronal cytokine receptors by microglial-derived interleukin 1 mirrors the opposite action of il-6 in the induction of cyclooxygenase-2. *Brain, Behavior, and Immunity*, 20(4):536–544, 2006.
- [42] Brian S Meldrum. Glutamate as a neurotransmitter in the brain: review of physiology and pathology. *Journal of Nutrition*, 130(4):1007S–1015S, 2000.
- [43] Pierre Paoletti, Camilla Bellone, and Qiang Zhou. Nmda receptor subunit diversity: impact on receptor properties, synaptic plasticity and disease. *Nature Reviews Neuroscience*, 14(6):383–400, 2013.
- [44] Mark Farrant and Zoltán Nusser. Gabaa receptor function and pharmacology. *Trends in Pharmacological Sciences*, 26(4):156–164, 2005.
- [45] Christopher C. Giza and Mayumi L. Prins. Neuroplasticity. StatPearls Publishing, Treasure Island (FL), 2023. Available from: https://www.ncbi.nlm.nih.gov/books/NBK557811/.

- [46] Eric R. Kandel, John D. Koester, Sarah H. Mack, and Steven A. Siegelbaum. *Principles of Neural Science*. McGraw-Hill Education, New York, 6 edition, 2021.
- [47] Christian Lüscher and Robert C. Malenka. Nmda receptor-dependent long-term potentiation and long-term depression (ltp/ltd). Cold Spring Harbor Perspectives in Biology, 4(6):a005710, 2012.
- [48] Donald O. Hebb. The Organization of Behavior: A Neuropsychological Theory. Wiley, New York, 1949.
- [49] Guo-Qiang Bi and Mu-Ming Poo. Synaptic modifications in cultured hippocampal neurons: dependence on spike timing, synaptic strength, and postsynaptic cell type. Journal of Neuroscience, 18(24):10464–10472, 1998.
- [50] Daniel E. Feldman. The spike-timing dependence of plasticity. *Neuron*, 75(4):556–571, 2012.
- [51] Alan L. Hodgkin and Andrew F. Huxley. A quantitative description of membrane current and its application to conduction and excitation in nerve. *The Journal of Physiology*, 117(4):500–544, 1952.
- [52] Mind the graph. https://mindthegraph.com/. Used under the CC BY-SA license (https://creativecommons.org/licenses/by-sa/4.0/deed.en/), derivative of the original.
- [53] Mariam Al Harrach, Pascal Benquet, and Fabrice Wendling. Long term evolution of fast ripples during epileptogenesis. *Journal of Neural Engineering*, 18(4):046027, 2021.
- [54] S. Demont-Guignard et al. Validation of the ca1 pyramidal neuron model. *Journal of Computational Neuroscience*, 27(2):149–169, 2009.
- [55] Giovanni Berlucchi and Hans A Buchtel. Neuronal plasticity: Historical roots and evolution of meaning. *Experimental Brain Research*, 192(3):307–319, 2009.
- [56] A. B. Author and C. D. Author. Title of the article. Neuroscience, 123(4):567–578, 2020.
- [57] Christoph von der Malsburg. Self-organization of orientation sensitive cells in the striate cortex. *Kybernetik*, 14(2):85–100, 1973.
- [58] Shun-Ichiro Amari. Field theory of self-organizing neural nets. *IEEE Transactions on Systems, Man, and Cybernetics*, SMC-13(3):811–820, 1983.
- [59] David J. Willshaw and Christoph von der Malsburg. How patterned neural connections can be set up by self-organization. *Proceedings of the Royal Society of London. Series B. Biological Sciences*, 194(1117):431–445, 1976.

- [60] Elie L. Bienenstock, Leon N. Cooper, and Paul W. Munro. Theory for the development of neuron selectivity: orientation specificity and binocular interaction in visual cortex. *Journal of Neuroscience*, 2(1):32–48, 1982.
- [61] Claudia Clopath, Lars Büsing, Eleni Vasilaki, and Wulfram Gerstner. Connectivity reflects coding: a model of voltage-based stdp with homeostasis. *Nature Neuroscience*, 13(3):344–352, 2010.
- [62] Elif Köksal-Ersöz, Pascal Benquet, and Fabrice Wendling. Expansion of epileptogenic networks via neuroplasticity in neural mass models. PLOS Computational Biology, 20(12):e1012666, 2024.
- [63] Pablo Marín-Castañeda, Naresh Singh, Natalia Villalobos, Robert Adamec, and Celia Hernández. Interplay of epilepsy and long-term potentiation: implications for memory. Frontiers in Neuroscience, 19:1451740, 2025.
- [64] Gregory Lepeu, Ellen van Maren, Kristina Slabeva, Cecilia Friedrichs-Maeder, Markus Fuchs, Werner J. Z'Graggen, Claudio Pollo, Kaspar A. Schindler, Antoine Adamantidis, Timothée Proix, and Maxime O. Baud. The critical dynamics of hippocampal seizures. *Nature Communications*, 15(1):5656, 2024.
- [65] Gabriel Gaugain, Mariam Al Harrach, Maxime Yochum, Fabrice Wendling, Marom Bikson, Julien Modolo, and Denys Nikolayev. Frequency-dependent phase entrainment of cortical cell types during tacs: Converging modeling evidence. *Journal of neural* engineering, 2024.
- [66] Henry Markram, Eilif Muller, Srikanth Ramaswamy, Michael W Reimann, Marwan Abdellah, Carlos Aguado Sanchez, Anastasia Ailamaki, Lidia Alonso-Nanclares, Nicolas Antille, Selim Arsever, et al. Reconstruction and simulation of neocortical microcircuitry. Cell, 163(2):456–492, 2015.
- [67] M. L. Hines and N. T. Carnevale. The NEURON simulation environment. *Neural Computation*, 9(6):1179–1209, August 1997.
- [68] Marom Bikson, Jacek Dmochowski, and Asif Rahman. The "quasi-uniform" assumption in animal and computational models of non-invasive electrical stimulation. *Brain Stimulation*, 6(4):704–705, July 2013.
- [69] Giulio Ruffini, Fabrice Wendling, Isabelle Merlet, Behnam Molaee-Ardekani, Abeye Mekonnen, Ricardo Salvador, Aureli Soria-Frisch, Carles Grau, Stephen Dunne, and Pedro C. Miranda. Transcranial current brain stimulation (tcs): models and technologies. *IEEE Transactions on Neural Systems and Rehabilitation Engineering*, 21(3):333–345, May 2013.

- [70] Martin Vinck, Marijn van Wingerden, Thilo Womelsdorf, Pascal Fries, and A. Pennartz Cyriel M. The pairwise phase consistency: a bias-free measure of rhythmic neuronal synchronization. *NeuroImage*, 51(1):112–122, 2010.
- [71] John William Strutt (Lord Rayleigh). On the problem of random vibrations, and of random flights in one, two, or three dimensions. *The London, Edinburgh, and Dublin Philosophical Magazine, Series* 6, 37:321–347, 1919.
- [72] Soheila Rezakhani, Mahmood Amiri, Sarah Weckhuysen, and Georgios A. Keliris. Therapeutic efficacy of seizure onset zone-targeting high-definition cathodal tdcs in patients with drug-resistant focal epilepsy. *Clinical Neurophysiology*, 136:219–227, 2022. Epub 2022 Feb 3.
- [73] Greg Kronberg, Morgan Bridi, Ted Abel, Marom Bikson, and Lucas C Parra. Direct current stimulation modulates ltp and ltd: activity dependence and dendritic effects. *Brain stimulation*, 10(1):51–58, 2017.
- [74] André R Brunoni, Michael A Nitsche, Nadia Bolognini, Marom Bikson, Timothy Wagner, Lotfi Merabet, Dylan J Edwards, Antoni Valero-Cabré, Alexander Rotenberg, Alvaro Pascual-Leone, Roberta Ferrucci, Alberto Priori, Paulo S Boggio, and Felipe Fregni. Clinical research with transcranial direct current stimulation (tdcs): Challenges and future directions. *Brain Stimulation*, 5(3):175–195, Jul 2012.
- [75] Marom Bikson, Maki Inoue, Hiroshi Akiyama, Jennifer K Deans, Jane E Fox, Hajime Miyakawa, and John G R Jefferys. Effects of uniform extracellular dc electric fields on excitability in rat hippocampal slices in vitro. The Journal of Physiology, 557(Pt 1):175–190, May 2004.
- [76] Davide Reato, Asif Rahman, Marom Bikson, and Lucas C Parra. Low-intensity electrical stimulation affects network dynamics by modulating population rate and spike timing. *Journal of Neuroscience*, 30(45):15067–15079, Nov 2010.